UNIVERSITÀ DEGLI STUDI DI MILANO

DOCTORAL PROGRAMME IN

TRANSLATIONAL MEDICINE– XXXVII CYCLE

DEPARTMENT OF BIOMEDICAL SCIENCES FOR HEALTH

Scientific Disciplinary Sector ING-INF/06 – Electronic Bioengineering and Informatics

Evaluation of cerebral autoregulation: from the traditional pressure-flow indexes to a directional multivariate analysis

PhD candidate:

Francesca Gelpi

Supervisor: Prof. Alberto Porta

Doctoral Programme Chair: Prof. Chiarella Sforza

Academic Year

2023-2024

UNIVERSITÀ DEGLI STUDI DI MILANO

DOTTORATO DI RICERCA IN

MEDICINA TRASLAZIONALE – CICLO XXXVII

DIPARTIMENTO DI SCIENZE BIOMEDICHE PER LA SALUTE

Settore Scientifico-Disciplinare ING-INF/06 - Bioingegneria Elettronica e Informatica

Valutazione dell'autoregolazione cerebrale: dagli indici tradizionali di pressione-flusso all'analisi direzionale multivariata

Dottoranda:

Francesca Gelpi

Supervisore: Prof. Alberto Porta

Coordinatore del Corso di Dottorato: Prof. Chiarella Sforza

A.A.

2023-2024

Abstract

Cerebrovascular autoregulation (CA) is essential for life, since it guarantees a tight regulation of cerebral blood flow and, consequently, a suitable oxygen delivery to the brain. The cerebrovascular system works in a bidirectional way: mean arterial pressure (MAP) drives changes in mean cerebral blood velocity (MCBv) while situations of hyper/hypoperfusion can induced modifications of MAP. The respiratory system also influences the closed-loop interactions between MAP and MCBv by affecting CA through modifications of partial pressure of gases in the blood and by perturbing mechanically both MAP and MCBv.

Given the complexity of cerebrovascular interactions, there is disagreement between measurement methods to assess the dynamic component of CA. Traditional approaches cannot disentangle the feedforward pathway from pressure to flow from the feedback pathway from flow to pressure.

The aim of this thesis is to study dynamic CA (dCA) via different methods and propose possible complementary approaches to more deeply characterize cerebrovascular control. Traditional methods, namely transfer function analysis (TFA) and autoregulatory index (ARI), will be applied and compared to a causal close-loop approach based on the computation transfer entropy (TE) and TE conditioned on confounding factors (CTE), as to evaluate their ability in characterizing dCA from spontaneous fluctuations of MAP and MCBv.

The cerebrovascular control was evaluated on three protocols: i) healthy young subjects undergoing a head-up tilt test (TILT); ii) subjects suffering from postural orthostatic tachycardia syndrome (POTS) at rest in sitting position, during active standing (STAND) and paced slow breathing (SB); iii) subjects in the acute phase of an ischemic stroke with bilateral recordings from the affected and unaffected hemispheres.

The main results concerning the cerebrovascular interactions are: i) in all the protocols MAP-MCBv dynamic interactions were bidirectional; ii) in healthy subjects, TILT reduced MCBv as a likely consequence of the sympathetic activation, but dCA was not affected; iii) TE and CTE could separate POTS subjects from healthy subjects during SB, unlike traditional non-causal indexes; iv) in subjects with stroke, the causal analysis detected, in both hemispheres, a decrement of the strength along the pressure-to-flow relationship, suggesting an impairment of dCA, and an increment along the flow-to-pressure pathway, supporting the activation of the Cushing reflex.

The present thesis emphasizes the importance of investigating the closed-loop relationship between MAP and MCBv when assessing cerebrovascular control. The findings on healthy and pathological subjects suggest that the autonomic nervous system plays a role in CA, specifically in situations enhancing vagal control. Finally, conditioning on the respiratory signal is particularly important when the respiratory drive is empowered, such as during controlled breathing at slow breathing rates.

Sommario

L'autoregolazione cerebrovascolare (CA) è essenziale per la vita, poiché garantisce una stretta regolazione del flusso ematico cerebrale e, di conseguenza, un adeguato apporto di ossigeno al cervello. Il sistema cerebrovascolare funziona in modo bidirezionale: la pressione arteriosa media (MAP) determina cambiamenti nella velocità media del flusso sanguigno cerebrale (MCBv), mentre situazioni di iper/ipoperfusione possono modificare la MAP. Anche l'apparato respiratorio influenza le interazioni ad anello chiuso tra MAP e MCBv, attraverso modifiche della pressione parziale dei gas nel sangue e perturbando meccanicamente sia MAP che MCBv.

Data la complessità delle interazioni cerebrovascolari, vi è disaccordo tra i metodi di misurazione per valutare la componente dinamica della CA. Gli approcci usati più comunemente non riescono a districare la componente di feedforward dalla pressione al flusso dalla componentte di feedback dal flusso alla pressione.

L'obiettivo di questa tesi è studiare la CA dinamica (dCA) tramite diversi metodi e proporre possibili approcci complementari per caratterizzare più a fondo il controllo cerebrovascolare. Verranno sviluppati metodi tradizionali, quali l'analisi della funzione di trasferimento (TFA) e l'indice di autoregolazione (ARI), confrontati ad un approccio causale ad anello chiuso, quale l'entropia di trasferimento (TE) e l'entropia condizionata di trasferimento (CTE), per valutare dCA da fluttuazioni spontanee di MAP e MCBv.

Il controllo cerebrovascolare è stato valutato su tre protocolli: i) volontari sani sottoposti a test di stimolazione ortostatica passiva (TILT); ii) pazienti affetti da sindrome da tachicardia posturale ortostatica (POTS) durante il riposo supino, durante l'ortostatismo attivo (STAND) e durante la respirazione controllata lenta (SB); iii) soggetti nella fase acuta di un ictus ischemico con registrazioni bilaterali dell'emisfero danneggiato e non danneggiato.

I principali risultati riguardanti le interazioni cerebrovascolari sono: i) in tutti i protocolli, le interazioni dinamiche tra MCBv-MAP sono bidirezionali; ii) nei soggetti sani durante TILT, MCBv si riduce, probabilmente come conseguenza dell'attivazione simpatica, ma dCA non viene modificata; iii) TE and CTE sono riuscite a separare gli individui POTS dai soggetti sani durante SB, a differenza dei tradizionali indici non causali; iv) nei pazienti con ictus, l'analisi causale ha rilevato in modo uniforme in entrambi gli emisferi un decremento dell'interazioni da pressione a flusso, suggerendo una compromissione della dCA, e un incremento da flusso a pressione, supportando l'attivazione del riflesso di Cushing.

Questa tesi sottolinea l'importanza di indagare le interazioni ad anello chiuso tra MAP e MCBv quando si valuta il controllo cerebrovascolare. I risultati sui soggetti sani e patologici suggeriscono che il sistema nervoso autonomo svolge un ruolo nella CA, in particolare in situazioni che rinforzano il controllo vagale. Infine, il condizionamento sul segnale respiratorio è particolarmente importante quando la componente respiratoria è potenziata, come durante la respirazione controllata a ritmi respiratori lenti.

Acknowledgements

I would like to express my gratitude to Prof. Alberto Porta for his scientific mentorship and insightful critiques throughout my doctorate. His commitment to excellence has significantly enhanced the content of this dissertation, enriching my development as a scientist. My appreciation also goes to Prof. Chiarella Sforza, Prof. Daniele Gibelli, and the administrative staff of the PhD program in Translational Medicine at the Department of Biomedical Science for Health at the University of Milan for their support.

I wish to extend my sincere gratitude to Prof. Giuseppe Baselli and Prof. Caroline Rickards for their thorough review of this thesis. Their insightful comments and suggestions have greatly improved the quality of this work.

This endeavor would not have been possible without contributions from clinical collaborations worldwide. I would like to thank Dr. Gianluca Rossato, Dr. Davide Tonon, Prof. Mathias Baumert, Dr. Rachel Wells, Prof. Jatinder Minhas, and Dr. Jonathan Ince for providing the data that led to the results of this thesis.

I am extremely grateful to Prof. Ronney Panerai for the opportunity to do a research visit in his lab. I am particularly thankful to him for sharing his valuable knowledge on cerebrovascular science, for patiently revising my scripts, and for kindly welcoming me to Leicester. His contribution has significantly enhanced the content of this dissertation, and I hope it will lead to more collaborations. A special thanks goes to the entire CHiAMS group at the University of Leicester for the interesting scientific exchanges and for humorously introducing me to British culture.

I would like to express my deepest appreciation to my colleagues at the Laboratory of Complex System Modelling: Dr. Vlasta Bari for her guidance and mentorship; Dr. Beatrice Cairo, Pavandeep Singh, and Dr. Beatrice De Maria for sharing the challenges of being an engineer in medical research. Being part of the team has been a pleasure, both professionally and personally. I would also like to extend my sincere thanks to the researchers at IRCCS Policlinico San Donato for the fulfilling collaborations. I am particularly grateful to all the study coordinators, research nurses, and data managers, including Sara Pugliese, Vittoria Mazzotta, Luca Brischigiaro, Martina Anguissola, Dr. Irene Baroni, Giada De Angeli, Giulia Paglione, and Nathasha Udugampolage, for being the foundation of biomedical research, without whom there would be no research and data to work on.

Lastly, I would like to thank the diverse individuals who crossed my path on the way to this dissertation. Thanks to my multicultural and international friends, teachers, peers, housemates, colleagues, and mountain mates: you inspired me, broadened my horizons, and challenged me to reach higher peaks. Thanks to Dr. Guido Gelpi for reminding me that we are always young enough for everything, even for a PhD. Un ringraziamento speciale a Lina Miotti, per la sua mente brillante che mi ha insegnato a continuare a imparare. Grazie ai miei amici per esserci “quando sono in zona”, alle mie sorelle per la spensieratezza e ai miei genitori per la fiducia incondizionata.

List of Content

List of Figures

List of Tables

List of Abbreviations

AP = arterial pressure

AR = autoregressive

ARI = autoregulatory index

BASELINE = baseline while sitting resting

CA = cerebral autoregulation

CAP = capnography signal

CBF = cerebral blood flow

CBv = cerebral blood velocity

CO_2 = Carbon dioxide

CPP = cerebral perfusion pressure

CTE = conditional transfer entropy

dCA = dynamic cerebral autoregulation

ECG = electrocardiogram

$EtCO_2$ = end tidal carbon dioxide

FFT = fast Fourier transform

HF = high frequency

HP = heart period

ICA = internal carotid arteries

ICP = intra-cranial pressure

IRF = impulse response function

K^2 = squared coherence

LF = low frequency

MAP = mean arterial pressure

MCA = middle cerebral artery

MCBv = mean cerebral blood velocity

O_2 = oxygen

$PaCO_2$ = partial pressure of arterial carbon dioxide

PaO_2 = partial pressure of arterial oxygen

POTS = postural orthostatic tachycardia syndrome

RCM = respiratory chest movements

REST = rest in supine position

SAP = systolic arterial pressure

SB = slow breathing

STAND = active standing

TCD = transcranial Doppler

TE = transfer entropy

TF = transfer function

TFA = transfer function analysis

TFG = transfer function gain

TFP = transfer function phase

TILT = head-up tilt

VLF = very low frequency

CHAPTER 1 - Background

1.1 Introduction

The following chapter begins with a description of the physiological mechanisms governing the cerebrovascular system (Sect.1.2). Mechanisms of cerebral regulation, comprising the pressure-to-flow and the flow-to-pressure links as well as cerebral autoregulation (CA) with its components (i.e., myogenic, metabolic and neurogenic) are explained in Sect.1.3. The assessment of these mechanisms is mainly carried out via analysis of variations of mean cerebral blood velocity (MCBv), derived from transcranial Doppler (TCD) device as an approximation of cerebral blood flow (CBF), in response to variations of mean arterial pressure (MAP). The experimental protocols and time series analysis tools typically exploited to assess pressure-to-flow interactions and closed-loop relationship between MCBv and MAP are described in Sect.1.4. The chapter ends with Sect.1.5, which defines the aims of this doctoral thesis.

1.2 Cerebrovascular system

The brain is an organ with a high metabolic rate but limited nutrient and oxygen (O_2) storage (Willie et al., 2014). To maintain its normal function, it utilizes about 20% of total cardiac output and O_2 consumption despite only accounting for 2% of body weight (McBryde et al., 2017). The brain is only able to endure short periods of lack of blood supply, with ischemic brain tissue stopping working within seconds. Thus, the regulation of CBF is critical for surviving, maintaining constant nutrient and O_2 supply to the brain.

The cerebrovascular system is divided into anterior and posterior circulation. The circle of Willis presented in Figure 1.1.a is the anatomical structure that provides an anastomotic connection between the circulations. It preserves the collateral flow to affected brain regions in the event of arterial incompetency (Rosner et al., 2023). The anterior circulation derives from the internal carotid arteries (ICA) which carries 70% of CBF (Willie et al., 2014). It supplies blood to most of the cerebral hemispheres, including the frontal lobes, parietal lobes, lateral temporal lobes and anterior part of deep cerebral hemispheres (Rosner et al., 2023). At the point of connection between the anterior cerebral arteries and the ICA, the lateral continuation of the ICA becomes the middle cerebral artery (MCA). From the circle of Willis, the intracerebral

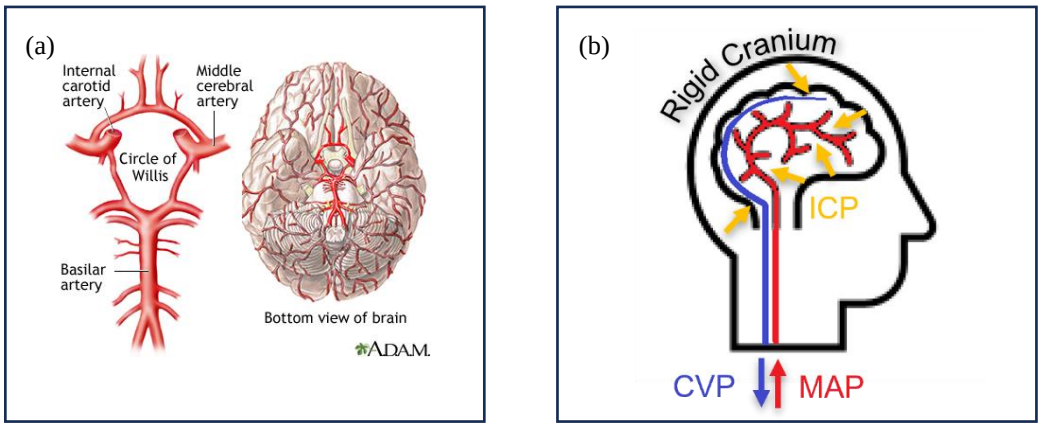

Figure 1.1(a) Joining area of basilar, internal carotid and middle cerebral arteries at the bottom (inferior) side of the brain, known as circle of Wills. Reproduced from A.D.A.M. (b) Driving forces within the rigid cranium are intra-cranial pressure (ICP), mean arterial pressure (MAP) and central venous pressure (CVP).

arteries as MCA branch out, and then ramify to the brain surface where vessels form a dense network of highly vasoactive arterioles.

As shown in Figure 1.1.b, the cranium is a non-expandable case of bone, containing a fixed volume shared between brain tissue, intracranial blood and cerebrospinal fluid (Mokri, 2001). Because of its enclosed nature, the brain is highly vulnerable to changes in intra-cranial pressure (ICP) (Willie et al., 2014). In healthy conditions, resting ICP is low (5–10 mmHg) and largely determined by the cerebrospinal fluid balance between production and drainage through absorption into cervical lymphatics or subarachnoid villi (McBryde et al., 2017). If unopposed, ICP may result in compression of brain vessels, creating a barrier to CBF. MAP opposes ICP to guarantee CBF in the intracerebral arterioles, and consequently to all brain vessels. The driving force that guarantees a CBF is the cerebral perfusion pressure (CPP). CPP is determined by the difference between MAP and ICP and gives a measure of the 'supply pressure' of blood to the brain even though it does not necessarily predict CBF. Being ICP low at rest, CPP is largely determined by the level of MAP when ICP does not vary.

1.3 Cerebrovascular regulation

Cerebrovascular regulation is essential for life, since it guarantees a tight regulation of CBF and, consequently, a suitable O_2 delivery to the brain. The cerebrovascular system works in a bidirectional way: arterial pressure (AP) drives changes of CBF but, in turn, it can be modified in situations of hyper/hypoperfusion. The pressure-to-flow pathway can lead to a variable

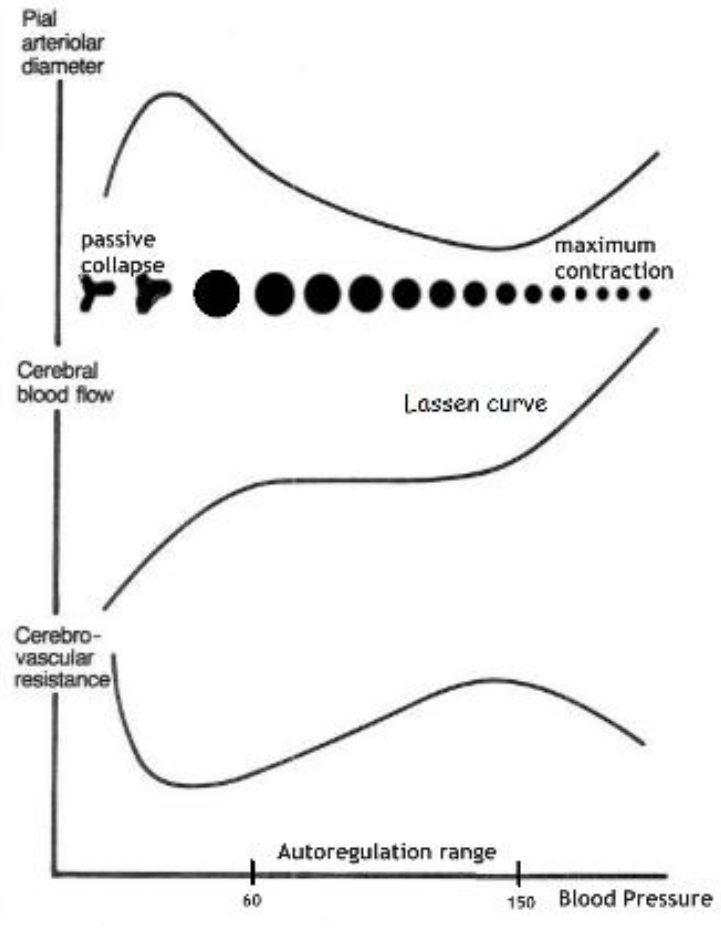

Figure 1.2 Graphical representation of the relationship of pial arteriolar diameter, cerebral blood flow (Lassen curve) and cerebrovascular resistance as a function of arterial blood pressure. Modified from Paulson et al., 1990.

MCBv in response to physiological changes of MAP. If not buffered by the CA, this pathway might even induce hyperaemia with a higher risk of stroke (Joshi et al., 2010), ischemia with insufficient O_2 supply to the brain (Tarumi et al., 2014) or hypoperfusion contributing to postural syncope (Carey et al., 2001). On the reverse pathways, the Cushing reflex modifies MAP in response to hypoperfusion or intracranial pressure rise (Cushing, 1902).

1.3.1 CBF regulation mechanisms

CA is a single concept that simplifies the response of cerebrovascular resistance to maintain a constant CBF despite variation of MAP. CA protects the brain from changes in CPP and keeps MCBv at a stable level, matched to the metabolism needs. CA actively counter-regulates the vessel diameter, and thus cerebrovascular resistance in response to MAP changes, as shown in Figure 1.2. According to (Lassen, 1959), CBF tends to be approximately constant within the pressure range of 60-150 mmHg, so that the Lassen curve reveals a horizontal line with zero slope, known as the "plateau phase". In reality, the MAP and CBF relationship has a "gradient" phase, showing an upward or even a downward slope. Indeed, within the autoregulatory range, CA minimizes the variation to CBF rather than keeping it constant (Claassen, 2016). The range of the autoregulatory gradient also showed a wide interindividual variability. Most studies report a stable CBF whit a slow variation of MAP between approximately −20 and +20 (Claassen et al., 2021) and a lower limit of autoregulation ranging from 40 to 90 mmHg (Vu et al., 2024). Above and below these limits, CA is lost and CBF follows MAP in a linear fashion, as represented by the Lassen curve in Figure 1.2 and Figure 1.3. Below the lower limit of CA, further vasodilation of vessels is impossible resulting in passive collapse. Above the upper limit of CA, the increase of transmural pressure exceeds the ability to constrict leading to passive vasodilatation (Paulson et al., 1990).

Within the autoregulatory range, many responses are established to effectively guarantee the stability of CBF to a sudden change in MAP. The vasodilation and constriction guided by variation in CPP is mainly regulated by the **myogenic** response of the vessel. Following an increase of MAP, the elastic cerebral artery dilates, and their surrounding smooth muscle is stretched. The consequent change in smooth muscle ionic permeability leads to muscle contraction, diameter reduction, and finally vascular resistance increase (Faraci et al., 1989). Variations of partial pressure of arterial carbon dioxide ($PaCO_2$) have a strong impact on CBF dynamics (Halsey Jr & McFarland, 1974; Mitsis et al., 2004; Panerai et al., 2010) referred to as

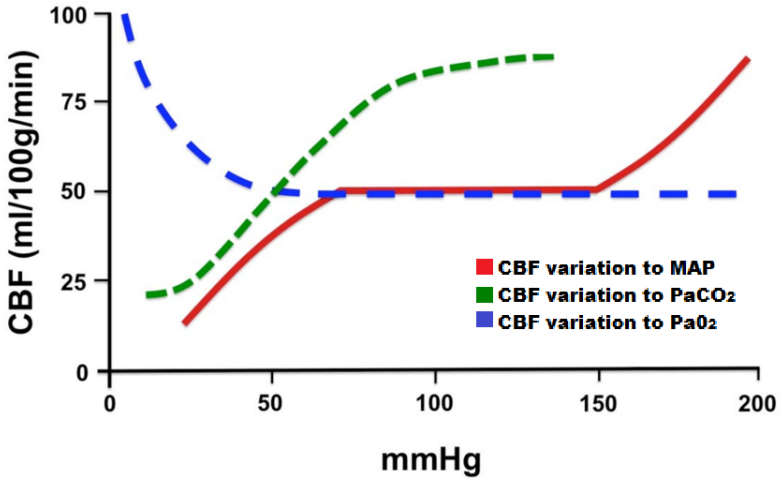

Figure 1.3 Schematic representation of CBF variations associated with changes of MAP (red line), partial pressure of arterial carbon dioxide ($PaCO_2$, short dashed green line) and partial pressure of arterial oxygen (PaO_2, long dashed blue line). Reproduced from Taccone et al., 2013.

the **metabolic** response. A transient increase of CBF promotes an increase of partial pressure of arterial oxygen (PaO_2) and a reduction in $PaCO_2$. The modulation of several metabolites in the arterial endothelium including nitric oxide leads to vasoconstriction to restore the balance between O_2 supply and demand (Hyder et al., 1998; Panerai, 2008). As shown in Figure 1.3, only acute hypoxia (i.e., a decrease of PaO_2 below 50 mmHg) triggers a substantial increase of CBF via dilatation of cerebral microcirculation (Johnston et al., 2003). Vice versa, hypercapnia (i.e., an increase of $PaCO_2$) causes dilatation of the cerebral arterioles to increase MCBv, whereas hypocapnia (i.e., a decrease of $PaCO_2$) causes vasoconstriction to decrease MCBv (Bor-Seng-Shu et al., 2012). Indeed, 5% and 7% inhalation of carbon dioxide (CO_2) leads to a 50% and 100% rise in MCBv, respectively (Kety & Schmidt, 1948).

In addition to the myogenic and metabolic responses, a **neurogenic** response is also taking place. Despite being identified, the effect on CA of the neurogenic regulation performed by the autonomic nervous remains poorly characterized (Gelpi et al., 2022; Gierthmühlen et al., 2011; Hamner et al., 2010; Paulson & Knudsen, 2008; Zhang et al., 2002). The Lassen curve and its limits seem to be modulated by the sympathetic nervous activity (Paulson & Knudsen, 2008), as well CA seems altered by ganglion blockade (Hamner et al., 2010; Zhang et al., 2002). However, some studies have claimed the independence of CA from the sympathetic nervous system (Gierthmühlen et al., 2011), thus establishing the controversial role of sympathetic nerve activity on cerebral vasculature (Ogoh & Tarumi, 2019). The sympathetic nervous system would appear to protect the brain microcirculation against increases in CBF rather than preserve CBF to decreases of MAP (Brassard et al., 2023). This protective role can only explain a third of the cerebral pressure–flow relationship (Hamner & Tan, 2014), thus stressing the relevance of the other mechanisms contributing to the CA.

The previous mechanisms are summarized in Figure 1.4. The neurogenic, myogenic and metabolic responses regulate the vascular bed to protect the brain from rises of CPP due to MAP increment. Particularly, the metabolic response is activated by the maintenance of an O_2 supply matching the metabolic demand, and the neurogenic response is activated by the sympathetic nervous system.

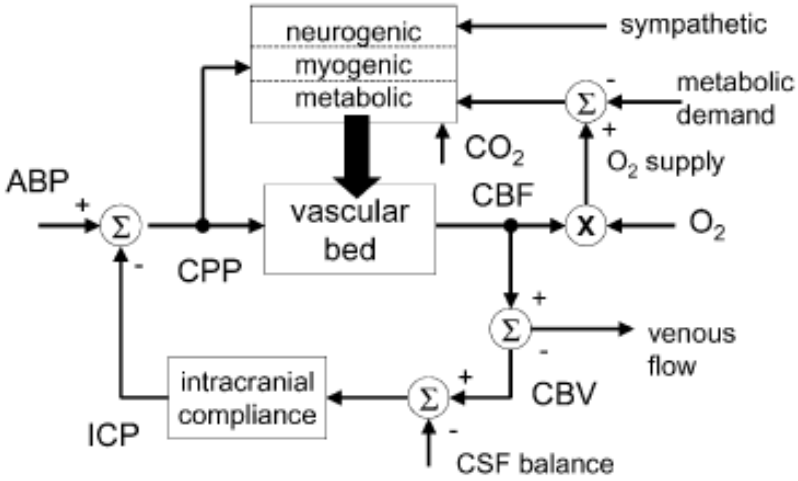

Figure 1.4 Schematic representation of the pressure-to-flow relationship mediated by cerebral perfusion pressure (CPP) defined as the difference between MAP and ICP. The pressure-to-flow relationship is mediated by the neurogenic, myogenic and metabolic response of the vessel. Reproduced from Panerai et al., 2003.

1.3.2 Cushing reflex and vasopressor response

The **Cushing reflex** is the physiological response to drops in CBF. When ICP rises with substantial increases (50–100 mmHg) to the point that it meets and gradually exceeds MAP, cerebral arterioles become compressed (Cushing, 1902). The consequent diminished CBF eventually leads to cerebral ischemia (i.e., insufficient blood supply to a brain area) (Dickinson, 1990). The reflex is believed to be activated in extreme cases, as the terminal stage of acute brain injury, sensing increase of $PaCO_2$ level and decrease of PaO_2. As reported in Figure 1.5, the central chemoreflex fire induces sympathetic activation with an increase of MAP. The consequent baroreceptor fire induces parasympathetic activation resulting into bradycardia. Given the dramatic decrease of brain oxygenation, respiratory cycles change in regularity and rate, with different patterns associated to different location of the brain injury (Grady & Blaumanis, 1988). The combination of hypertension, irregular breathing and bradycardia (known as the Cushing triad) is usually taken as a symptom of severe brain injury (Cushing, 1902; Grady & Blaumanis, 1988; McBryde et al., 2017).

It has been suggested that the Cushing reflex is a near-terminal exaggeration of the **vasopressor** physiological regulation always active in the brain (Dickinson, 1990; McBryde et al., 2017; Saleem et al., 2018). The vasopressor response senses and integrates the information about CPP, playing a central role to regulate the sympathetic drive and basal MAP (Bari et al., 2021; Saleem et al., 2018; Vaini et al., 2019). Indeed, experimental induction of intracranial hypertension can elicit strong vasopressor response within seconds for smaller changes in ICP than the one needed for Cushing reflex activation. MAP showed to be sensitive to small changes in ICP in experiments on animal (20-30 mmHg in dogs and as little as 1 mmHg in rats), and studies on conscious human subjects confirmed these findings (McBryde et al., 2017).

1.3.3 Latent confounders

The respiratory system is one of the mechanisms known to influence cerebrovascular dynamics. By playing a central role in the gas exchange, the respiratory pattern can determine $PaCO_2$, activating the metabolic response. As shown in Figure 1.3, the level of $PaCO_2$ is strongly related to CBF (Taccone et al., 2013). For instance, $PaCO_2$ levels tends to fall slightly during paced respiration, so that control breathing has been exploited to challenge the CA reactivity (Eames et al., 2004; Reinhard et al., 2003). Particularly, slow breathing might enhance the link between MAP and MCBv, as reported by the step response variations in Figure 1.6 (Eames et al., 2004). Beyond the influence on metabolic response, the intrathoracic pressure acting on thoracic and epidural veins lining the spine induces oscillatory respiratory movements of cerebrospinal fluid, and consequent oscillatory changes of ICP (Porta et al., 2021; Yildiz et al., 2017). The

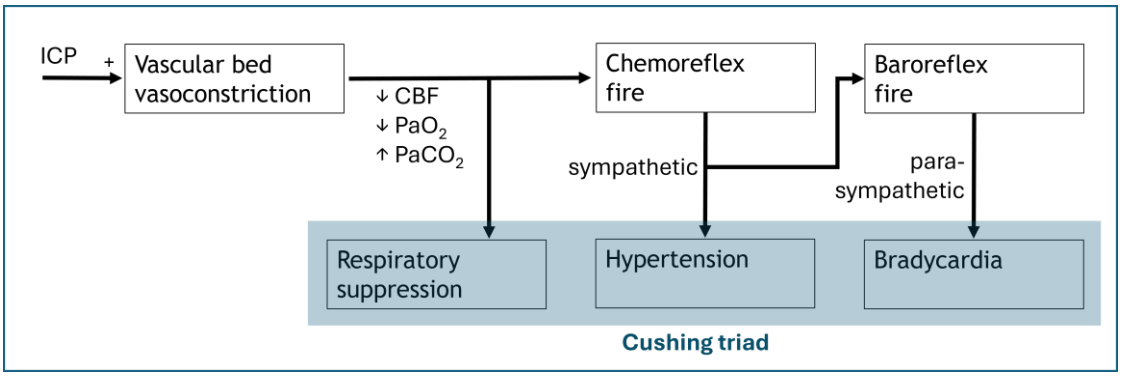

Figure 1.5 Simplified block diagram of the cascade mechanisms induced by an increase of intra-cranial pressure (ICP) leading to a decrease of CBF and PaO_2, and an increase of $PaCO_2$. The consequent respiratory suppression, hypertension and bradycardia is known as the Cushing triad.

oscillatory variations of MAP are also affected by the respiratory stroke volume synchronization (Elstad et al., 2018; Toska & Eriksen, 1993). However, the CBF response to cardiorespiratory oscillations does not seem to affect CA (Holme et al., 2023).

1.4 Interactions between MAP and MCBv

Given the complexity of cerebrovascular interactions, there is disagreement about the consistency between measurement methods to assess them. CA measurement methods are commonly separated into static and dynamic CA. Static CA reports the steady values of CBF, corresponding to slow variations against gradual AP changes over minutes to hours encapsulated by Lassen's curve (Lassen, 1959; Saleem et al., 2015). In contrast, dynamic CA (dCA) describes the response to faster modifications of CBF with transients occurring over seconds usually investigated with continuous recordings of MCBv via TCD to variation of MAP (Zhang, Zuckerman, & Levine, 1998).

Descriptions provided according to the concept of dCA allow an intuitive understanding of directionality in the interactions between MAP and MCBv. Traditional approaches, such as those based on non-parametric transfer function (TF) estimation, do not have the possibility to disentangle feedforward pressure-to-flow pathway from the feedback flow-to-pressure. Conversely, some approaches (Bari et al., 2017, 2021; Saleem et al., 2018; Vaini et al., 2019) account specifically for the feedback flow-to-pressure pathway. Mathematical methods such as Granger causality can be exploited to estimate the causal dynamics accounting for the directionality of the interactions and confounding factors.

1.4.1 Static CA and dCA

The traditional approach of assessing CA investigates the steady value of CBF observed in association with a given level of MAP. The analysis provides a curve, the Lassen curve, referred to as static CA. This curve gives information about the range of MAP in which CA is active (Lassen, 1959). Historically, steady values of CBF were assessed after the inhalation of nitrous

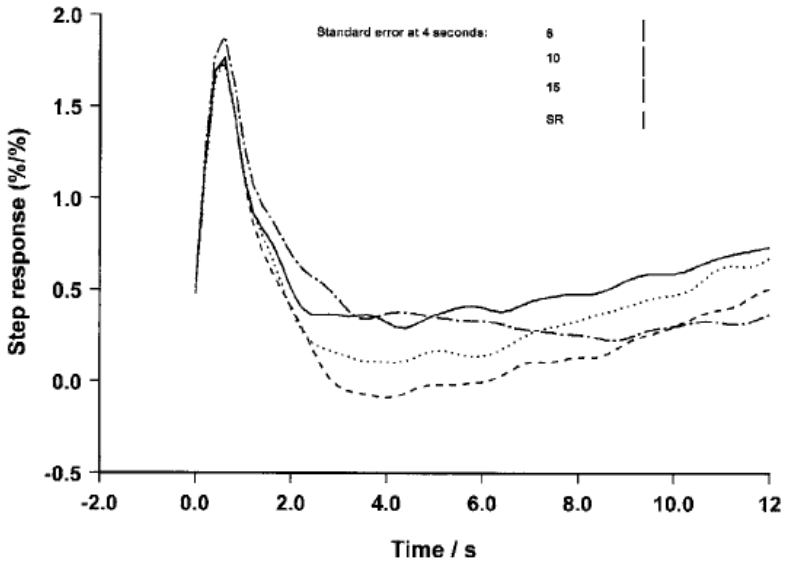

Figure 1.6 Mean response of CBv to step change in MAP for respiratory rates of 6 breaths/min (solid line), 10 breaths/min (dotted line), 15 breaths/min (dashed line) and spontaneous respiration (dashed-dotted line). Reproduced from Eames et al., 2004.

oxide (Kety & Schmidt, 1948). or Xenon 133 (Obrist et al., 1998) through the application of the Fick principle. The Lassen curve is usually computed in humans on several groups of subjects, including pathological subjects under treatment with vasoactive agents, to span a range of MAP values adequately large (Figure 1.2 and Figure 1.3).

The steady-state assessment of CA (Lassen, 1959) was overcome with the development of TCD (Aaslid et al., 1989). TCD provides a sufficient time resolution to continuously record cerebral blood velocity (CBv) and track its quick adjustments. Moreover, the intracranial CBv measured via TCD can be considered an adequate surrogate of the actual CBF when the MCA cross-sectional area remains constant (Panerai et al., 2001). dCA complemented static CA by indicating the efficiency of faster CA mechanisms, as the rapidity to return to basal MCBv value after perturbing MAP. Thus, it is mainly described based on transient changes in CBF in response to experimentally induced AP changes (J. A. Claassen et al., 2015).

1.4.2 Assessment of the pressure-to-flow pathway

The dCA assessment was originally associated to interventions necessary to provoke a sudden and important modification of MAP. The first attempt to quantify dCA was based on an interventional method using the thigh cuff technique to evoke transient adjustment of MCBv response to the rapid reduction in MAP induced by deflation of the thigh cuffs (Aaslid et al., 1989). Lower body negative pressure, cold pressor test, handgrip, Valsalva manoeuvre (Panerai et al., 2001) and sit-to-stand (Sorond et al., 2009) were among the protocols applied to force changes in MAP. Since the manoeuvres induce larger AP oscillations, they augment the signal-to-noise ratio and challenge dCA more powerfully (Brassard et al., 2023).

In the context of interventional dCA, the assessment method was originally developed by (Tiecks et al., 1995). The functioning of dCA was approximated by a second-order linear differential equation set describing the dynamical response of MCBv to changes of MAP (Tiecks et al., 1995). The model provides a set of responses graded according to an autoregulation index (ARI) ranking the dCA efficiency from 0, i.e. absent dCA, to 9, i.e. excellent dCA. A low value of ARI (i.e., ARI<4) corresponds to impaired dCA since a variation of MAP corresponds to a variation in MCBv. The higher the value of ARI the faster the MCBv returns to its baseline level. In Figure 1.7, the set of MCBv responses to a sudden raise of MAP is shown.

In the attempt to enlarge the assessment of dCA in subjects that might be at risk when relevant (around 20mmHg) MAP changes were induced, (Panerai et al., 1998) firstly estimated a MCBv

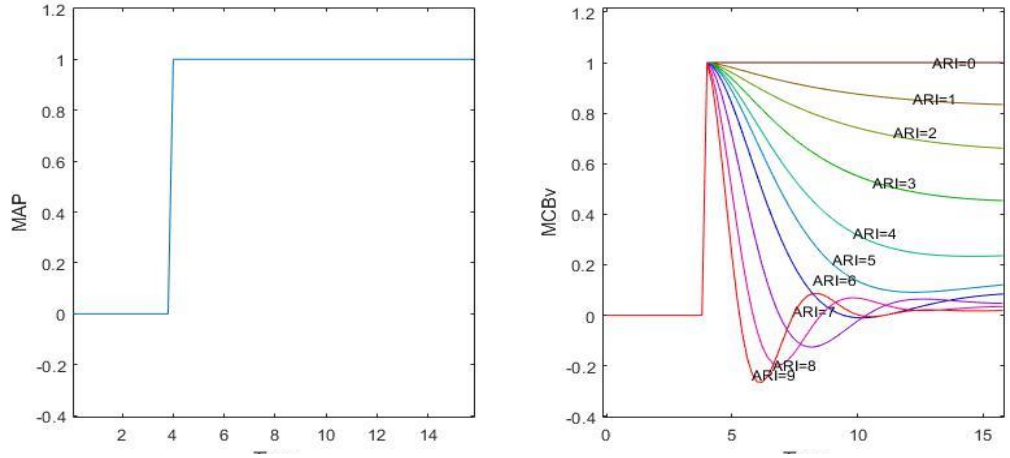

Figure 1.7 MAP unit step positive variation and the ten responses of MCBv as a function of ARI based on the Tiecks model.

step response from spontaneous fluctuations of MAP. Successively, other ARI assessment methods were developed and established exploiting spontaneous fluctuations (Bari et al., 2022; Carey et al., 2001; Gelpi et al., 2022; Mahdi et al., 2017; Panerai et al., 1998; D. M. Simpson et al., 2001). The impulse and step responses can be estimated after the estimation of the TF from MAP to MCBv via a non-parametric method based on Fourier transform (Panerai et al., 1998, 2001) or parametric method via modelling approach (D. M. Simpson et al., 2001). The similarity between the response estimated via non-parametric or parametric techniques and the one derived from the Tiecks' model are evaluated via suitable metrics to select the ARI corresponding to the best agreement (Panerai et al., 1998, 2001). A simpler time domain method has been introduced to directly feed the differential equations of the Tiecks' model with the spontaneous variations of MAP. It lets the MAP dynamics evolve over time and identifies the model response that best fits the measured MCBv (Gelpi et al., 2022; Mahdi et al., 2017).

While the experimental evidence is well established and ARI is commonly used, methods for dCA assessment in individual patients remain an open challenge, with no gold-standard having emerged (Brassard et al., 2023; Liu et al., 2015; Mahdi et al., 2017; Sanders et al., 2019; D. Simpson & Claassen, 2018). Over the years, different approaches have been developed to quantify dCA from spontaneous fluctuation of MAP. Correlation coefficient-like methods have been extensively tested in the clinical setting from recording of CBv or signals such as cerebral oxygenation and hemoglobin volume (Caicedo et al., 2016; Czosnyka et al., 1996). The most common linear approach examines the correlation between MCBv and MAP series and the resulting function is averaged over consecutive sequences to improve robustness (Czosnyka et al., 1996). Other time-domain methods may also account for non-linearity, non-stationarity, and influence of additional physiological variable (Brassard et al., 2023). These methods include Laguerre expansion of first-order Volterra kernels or finite infinite impulse response methods (Mitsis et al., 2004; Sanders et al., 2019) and multiple-input models to clarify the influence of other variables, such as CO_2 concentration and heart rate (Brassard et al., 2023).

Frequency-domain analysis techniques have also been applied to spontaneous MAP and MCBv variability series. These methods include transfer function analysis (TFA) (Claassen et al. 2016; Elting et al. 2020; Gommer et al. 2010; Liu, J., Simpson, Panerai 2022; Panerai et al. 2018; Sanders et al. 2019; Watanabe et al. 2022), projection pursuit analysis, wavelet decomposition analysis (Holme et al., 2023; Latka et al., 2005; Peng et al., 2010), principal dynamic mode analysis (Brassard et al., 2023) and spectral causality approaches (Pernice et al., 2022; Porta et al., 2023). Given the concept that dCA represents the dynamic relationship between MAP (stimulus or input) and MCBv (response or output), TFA has become a popular approach adopted in studies based on spontaneous fluctuations of MAP and MCBv (J. A. Claassen et al., 2015; Panerai et al., 2023; Zhang, Zuckerman, Giller, et al., 1998). TFA investigates the dCA from the perspective of linear response theory in the spectral domain from 0.02 to 0.50 Hz. This spectral domain is usually divided into frequency bands of very low frequency (VLF, 0.02-0.07 Hz), low frequency (LF, 0.07-0.20 Hz) and high frequency (HF, 0.20-0.50 Hz) (Claassen et al., 2015). AP oscillations in the HF band are primarily induced by respiration (Diehl et al., 1995; Elstad et al., 2018) and VLF oscillations reflects multiple physiological mechanisms that confound interpretation (Ogoh et al., 2005). Whereas, MAP changes detected in the LF band are independent of the respiratory frequency and showed to be related to changes in MCBv (Watanabe et al., 2022), being specifically linked to physiological mechanisms associated with sympathetic control (Marchi et al., 2013). TFA indicated that dCA can be described as a high-pass filter that readily transmits rapid changes in MAP to MCBv, but progressively attenuates the transmission of slower MAP perturbations to MCBv as a function of the period of the oscillation (Zhang, Zuckerman, Giller, et al., 1998). Parameters derived from TFA include phase shift and gain in the LF band. Specifically, the gain quantifies the damping effect of CA (i.e., the relative changes in the amplitude of MCBv to MAP) and the phase indicates the time

lag at a given frequency between MAP and MCBv (Zhang, Zuckerman, Giller, et al., 1998). TFA allows the computation of coherence as well measuring the strength of the MCBv-MAP relationship and utilized to identify conditions where estimates of gain and phase may not be reliable. Coherence represents the fraction of output variance that can be explained by the corresponding input power at the specific frequency according to a linear description of the interactions.

1.4.3 Bidirectional MCBv-MAP assessment

Fewer studies have overcome the traditional pressure-to-flow methodologies, and introduced the closed-loop approach, considering the bidirectional interaction of CBF and AP. A seminal work applied a model-free method to assess directionality of closed-loop relationship to cerebrovascular interactions (Faes et al., 2015). A time-domain causality index was also used to determine whether spontaneous cerebral pressure-flow fluctuations exhibit closed-loop dynamics that are consistent with the Cushing reflex mechanism (Saleem et al., 2018). The authors found that a significant amount of the interaction, around 40%, are bidirectional, as shown in Figure 1.8. Similarly, the same authors found that both forward and backward interactions between MAP and MCBv are influenced by spinal cord injury, which may be associated with impaired cerebrovascular buffering and widespread of AP instability (Saleem et al., 2019).

Since cerebrovascular variability interactions result from closed-loop mechanisms, causality analysis accounting for the directionality of the influences seems to be a valid tool. Within the biomedical research, causality methods are widely used in cardiovascular and neuroscience studies as a tool for establishing pathways of brain connectivity (Porta & Faes, 2013). Granger causality approach has already been successfully used to estimate the strength of time interaction from systolic arterial pressure to heart period (HP) to address cardiovascular control and baroreflex (Charleston-Villalobos et al., 2023; Porta et al., 2002; Porta & Faes, 2013).

Similarly, this method can be applied to cerebrovascular regulation. Indeed, the causality tools can provide spectral profiles of the causal coupling between MAP and MCBv, specifically addressing the flow-to-pressure pathway (Pernice et al., 2022; Porta et al., 2023). These authors use spectral measures of directed causal coupling derived from linear parametric models to investigate the cerebrovascular interaction in healthy subjects and subjects suffering of postural syncope. Causal squared coherence was exploited by (Bari et al., 2023) to characterize the cerebrovascular control in subjects undergoing surgical aortic valve replacement during a three-

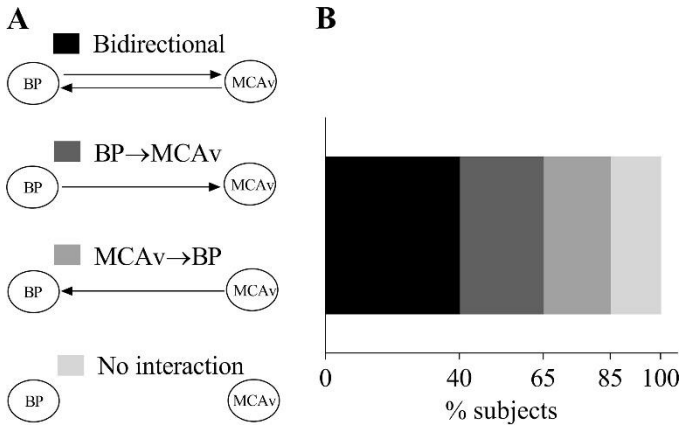

Figure 1.8 Graphical representation of bidirectional, unidirectional, and no Granger-causal trends between time series of MAP, here indicated as BP, and MCBv here indicated as MCAv (A), and the proportions of 20 baseline recordings having these Granger-causal associations under the supine position (B). Reproduced from Saleem et al., 2018.

month follow-up. A spectral representation of the self-dependencies has also been proposed by (Sparacino et al., 2023) and applied to the cerebrovascular system to investigate the oscillatory processes in response to postural stress. However, spectral causality approaches are not the sole directional methods utilized in the literature. Information domain directional metrics, such as transfer entropy (TE), have also been used to quantify the degree of MCBv dependence on MAP and vice versa in subject undergoing cardiopulmonary bypass (Vaini et al., 2019) and to identify subjects at risk of postural syncope (Bari et al., 2017). While Granger-causality is framed in terms of prediction, TE is framed in terms of resolution of uncertainty. However, for Gaussian variables, the two frameworks have been proven to be equivalent (Barnett et al., 2009).

The causality approach can account for disturbances that might mix up causal relationship. When investigating the MAP and MCBv coupling, respiration seems to play a confounding effect on the cerebrovascular interactions (Porta et al., 2021). According to this conjecture, conditional TE (CTE) identifies cerebrovascular impairment in subjects prone to develop postural syncope when respiratory signal was conditioned out (Bari et al., 2017). Similarly, the same method, using as conditioning signal the respiratory chest movements (RCM) from a thoracic belt and end-tidal carbon dioxide ($EtCO_2$) variability detected from the capnography signal (CAP), was fruitfully applied in subjects with dysautonomia (Gelpi et al., 2023).

1.5 Aim of the thesis

The aim of this thesis is to study dCA via different methods and propose possible complementary approaches to more deeply characterize cerebrovascular control. Traditional methods, namely TFA and ARI, a closed-loop causal approach, namely TE, and a closed-loop approach accounting for conditioning variables, namely CTE, will be developed to assess dCA from spontaneous fluctuations of MAP and MCBv. These approaches will be employed with the goal of investigating the directionality of the interactions and the impact of conditioning factors, namely respiration (Gelpi et al., 2023). The cerebrovascular control will be evaluated during three protocols: i) healthy subjects undergoing a head-up tilt test; ii) subjects suffering from postural orthostatic tachycardia syndrome (POTS) during supine resting, while performing active standing and under control breathing conditions; iii) subjects in the acute phase of ischemic stroke with bilateral recordings from the affected and unaffected hemisphere. The orthostatic challenges of head-up tilt and active standing were exploited to induce an autonomic response via a sympathetic activation and vagal withdrawn. Subjects with POTS were selected due to the exacerbated sympathetic activation that affects baroreflex control (Barbic et al., 2020; Farquhar et al., 2000), whose effect on dCA is unknown (Wells et al., 2020). Finally, subjects with moderate ischemic stroke were investigated to test the ability of the proposed method to detect the dCA impairment that has been reported to affect the stroke hemisphere (Nogueira et al., 2022).

CHAPTER 2 - Methods

2.1 Introduction

The following chapter describes the methods employed in this thesis to characterize cerebrovascular control in different populations and experimental conditions. Sect.2.2 describes the traditional non-causal methods of TFA and ARI. dCA is evaluated via TFA as the dynamic relationship between MAP and MCBv via estimation of TF gain (TFG), TF phase (TFP), and square coherence (K^2), and via the estimation of the response to a unit step variation of MAP. Sect.2.3 describes the directional model-based causal approach utilized in this thesis. In Sect. 2.3.1, the TE assessing the degree of association between MAP and MCBv in a specific time direction (i.e., from MAP to MCBv and *vice versa*) is defined. The TE is extended in Sect.2.3.2, to compute the CTE accounting for the conditioning effect of series of respiratory origin (i.e., RCM and $EtCO_2$). Finally, Sect. 2.4 describes the surrogate approach that will be used to test the null hypothesis of uncoupling.

2.2 Traditional non-causal methods

2.2.1 Transfer function analysis

The TFA approach for dCA assessment estimates the traditional input-output relation of MAP and MCBv via the cross-spectral approach between the two series. Figure 2.1 summarizes the main stages of TFA. The starting point is the estimation of the fast Fourier transform (FFT) of MAP and MCBv as

$$FFT_{MAP}(f) = \sum_{n=0}^{N-1} MAP_n \cdot e^{\frac{-j \cdot 2\pi \cdot f \cdot n}{N}} \quad (2.1)$$

and

$$FFT_{MCBv}(f) = \sum_{n=0}^{N-1} MCBv_n \cdot e^{\frac{-j \cdot 2\pi \cdot f \cdot n}{N}} \quad (2.2)$$

where N is the frame length, e is the exponential function, j is imaginary unit of the complex plane, MAP_n and $MCBv_n$ are the nth MAP and MCBv value. The auto-spectral density function of MAP and MCBv are given by

$$S_{MAP}(f) = \Delta T \cdot \frac{FFT_{MAP}(f) \cdot FFT^*_{MAP}(f)}{N} \quad (2.3)$$

and

$$S_{MAP}(f) = \Delta T \cdot \frac{FFT_{MCBv}(f) \cdot FFT^*_{MCBv}(f)}{N} \quad (2.4)$$

respectively, and the cross-spectral density function from MAP to MCBv as

$$C_{MCBv-MAP}(f) = \Delta T \cdot \frac{FFT_{MCBv}(f) \cdot FFT^*_{MAP}(f)}{N} \quad (2.5)$$

where Δt is the mean heart period, * is the complex conjugation operator, and f=0,…, f_N with $f_N = \frac{0.5}{\Delta T}$ is the Nyquist frequency. Long sequences of MAP and MCBv variability series can be broken down in smaller overlapped sequences matching the constraints for the applications of FFT. The Welch's method is utilized to improve the consistency of the auto- and cross-spectral densities via averaging (Claassen et al., 2015). The Hanning window was applied prior to each FFT to smooth the edges of the signal and thus minimize spectral leakage, a distortion of energy spreading from one frequency to the others (Bendat & Piersol, 1986). Superposition between frames is usually set to 50% (Panerai et al., 2023; D. Simpson & Claassen, 2018).

The auto- and cross-spectral density functions are utilized to estimate the TF and to derive TFG, TFP and K^2 (J. A. Claassen et al., 2015). The TF is estimated as the ratio of the $C_{MCBv-MAP}$ to S_{MAP} (Porta et al., 2000) as

$$TF(f) = \frac{C_{MCBv-MAP}(f)}{S_{MAP}(f)}. \qquad (2.6)$$

The TFG is computed as the modulus of the TF and quantifies the relative changes in the amplitude of MCBv to MAP oscillations. A reduction in gain indicates that there is a weaker response of MCBv to changes in AP, and may imply that dCA is more effective, giving a more robust dampening effect. The TFP is intended as the phase of TF. TFP indicates the time lag at a specific frequency between MAP and MCBv. Positive TFP values suggest that MCBv modifications lead MAP changes. The more positive the TFP, the more efficient the CA (J. A. Claassen et al., 2015). Negative phase values indicate that MCBv lags passively behind MAP and suggest an impaired CA. Similarly, a decrease of TFP when compared across group, over time or in response to an intervention may also suggest an impaired dCA.

The K^2 is computed as the ratio between the squared modulus of $C_{MCBv-MAP}$ by the product of S_{MAP} and S_{MCBv} as

$$K^2(f) = \frac{|C_{MAP-MCBv}(f)|^2}{S_{MAP}(f) \cdot S_{MCBv}(f)} \qquad (2.7)$$

$K^2(f)$ ranges from 0 to 1, indicating, respectively, null and full linear association between the MCBv and MAP series. Low values of K^2 are considered not-physiological, and are usually excluded if below a computed threshold around 0.30 (Claassen et al., 2015). Nevertheless, these excluded values might be due to non-linear mechanisms involving dCA (Panerai et al., 2006).

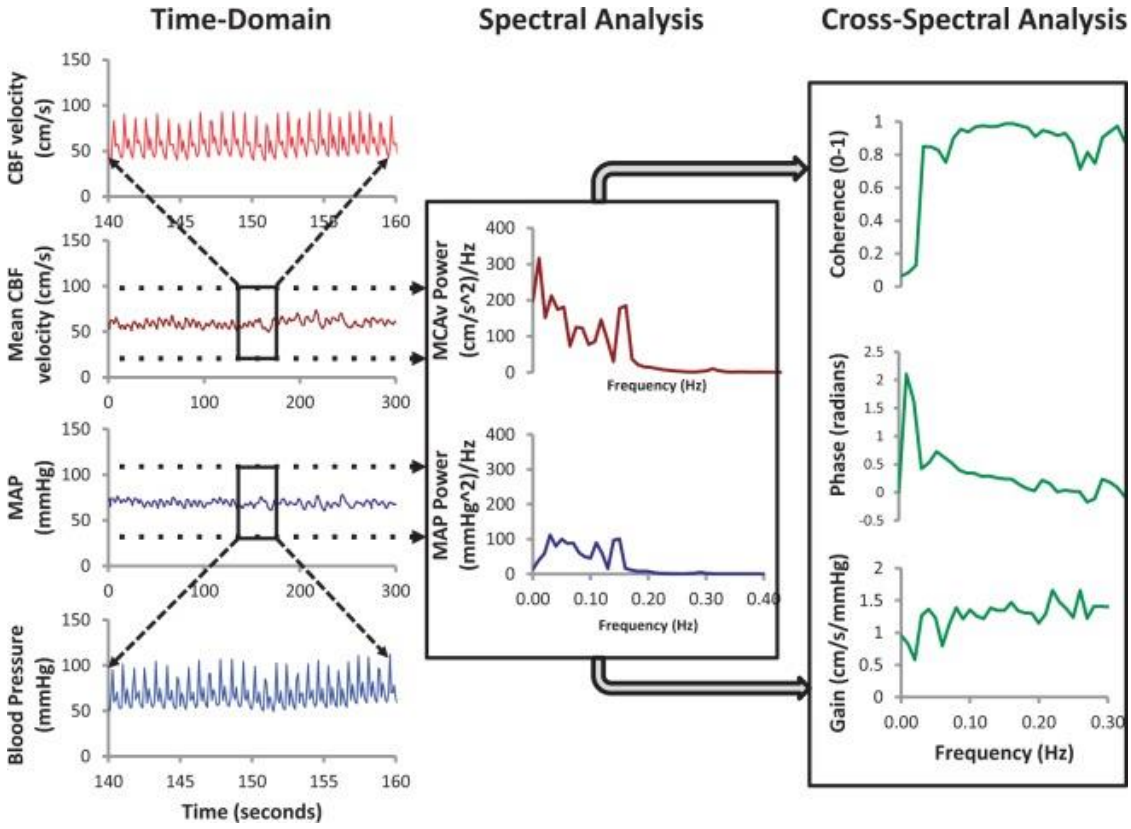

Figure 2.1 Main steps of TFA. In the time domain, mean values of AP and CBv in each cardiac cycle are obtained on a beat-to-beat basis. FFT approach is applied to MAP and MCBv series to obtain spectral estimates in the frequency domain. The auto- and cross-spectral densities are then used to obtain TFG, TFP, and K^2. Reproduced from Claassen et al., 2015.

2.2.2 Autoregulatory index

The derivative filter originally developed in (Tiecks et al., 1995) describing the dynamical link from MAP to MCBv was applied to spontaneous fluctuations in (Panerai et al., 1998). The Tiecks' model was discretized according to the equations

$$x_{1,k} = x_{1,k-1} + \frac{P_k - x_{2,k-1}}{f \cdot T} \qquad (2.8)$$

$$x_{2,k} = x_{2,k-1} + \frac{x_{1,k-1} - 2 \cdot D \cdot x_{2,k-1}}{f \cdot T} \qquad (2.9)$$

where x_1 and x_2 are state variables, k is the time instance, P_k is the MAP series taken as the input of the filter, f is the resampling frequency, D is the damping coefficient, and T is the time constant. The estimated velocity (V) is

$$V_k = V_{mean} \cdot (1 + P_k + K \cdot x_{2,k}) \qquad (2.10)$$

where V_k is the MCBv at the time instance k, V_{mean} is the mean of V over the selected sequence input and K is the gain. The initial conditions (i.e., at $k = 0$) are set as

$$x_{1,0} = 2 \cdot D \cdot P_0 \qquad (2.11)$$

$$x_{2,0} = P_0 \qquad (2.12)$$

Ten combinations of the triplet K, T and D reported in Table 2.1 are defined according to (Tiecks et al., 1995) with each combination corresponding to value of ARI ranging from absent CA (i.e. ARI = 0) to excellent CA (ARI = 9).

ARI is selected by comparing the step response to the theoretical step responses (Panerai et al., 1998). Firstly, the impulse response function (IRF) is estimated via the inverse FFT applied to the TF from MAP and MCBv as computed in Sect.2.2.1 (Panerai et al., 1998). A numerical estimate of the step response is obtained by integration of the IRF. Secondly, the theoretical step responses are derived by fitting the Tiecks' model response to a unity sustained step as shown in Figure 1.7. Theoretical and predicted step responses are rescaled by dividing each sample by their own maximum absolute value. The ARI is selected to the one corresponding to the theoretical curve with the minimum normalized mean square error (NMSE) from the estimated curve. Examples of the step responses predicted from the data and the corresponding step response estimated from the Tiecks' model are shown in Figure 2.2.

Table 2.1 Parameters for the computation of the 10 levels of ARI according to the second-order differential equation given in (Tiecks et al., 1995).

ARI	T	D	K
0	2	0	0
1	2	1.60	0.20
2	2	1.50	0.40
3	2	1.15	0.60
4	2	0.90	0.80
5	1.9	0.75	0.90
6	1.6	0.65	0.94
7	1.2	0.55	0.96
8	0.87	0.52	0.97
9	0.65	0.50	0.98

2.3 Directional causal multivariate approach

In 1956, Norbert Wiener introduced the notion that one stochastic variable (or process) could be called 'causal' to another if the ability to predict the second variable is improved by incorporating information about the first (Bressler & Seth, 2011). This concept was made operational by (Granger, 1969) via linear vector autoregressive (AR) models in the context of multivariate stochastic process. Defined two stochastic processes X and Y, if the prediction of the stochastic variable Y_n at time n using past states of X and Y (*i.e.*, X_{n-i} and Y_{n-i} with i=1,…,m). is better than the prediction of Y_n using only past states of Y (*i.e.*, Y_{n-i} with i=1,…,m), X is said to Granger-cause Y. In other words, X Granger-causes Y if it carries unique information about the future evolution of Y that cannot be derived from Y itself.

Symmetrically, TE from X to Y represents the degree to which X disambiguates the future of Y beyond the degree to which Y already disambiguates its own future. Under the Gaussian assumption, "disambiguates" and "predicts" correspond, given that the reduction of uncertainty equals the predictability improvement (Barnett et al., 2009). Thus, despite the difference in metrics, TE parallels Granger's causality.

2.3.1 Transfer entropy

TE assesses the degree of association from a cause system X, whose dynamical behavior is described by the process X, to an effect system Y, whose dynamical behavior is described by the process Y, as the amount of information genuinely transferred from X to Y, namely the amount of information carried by Y that can be derived solely from X, above and beyond the amount of information carried by past states of Y (Porta, Maestri, et al., 2018).

Defined the multidimensional vectors $\boldsymbol{Y}^- = \{\boldsymbol{Y}_n^- = [Y_{n-1} \cdots Y_{n-m}], n = m+1, \cdots, N\}$, $\boldsymbol{X}^- = \{\boldsymbol{X}_n^- = \left[X_{n-\tau_{Y,X}} \cdots Y_{n-m-\tau_{Y,X}+1}\right], n = m+\tau_{Y,X}+1, \cdots, N\}$ and $\boldsymbol{Y}^- \oplus \boldsymbol{X}^- = \{\boldsymbol{Y}_n^- \oplus \boldsymbol{X}_n^-, n = m+\tau_{Y,X}+1, \cdots, N\}$, where $\tau_{Y,X}$ is the latency of the action of X on Y and $\boldsymbol{Y}_n^- \oplus \boldsymbol{X}_n^-$ is the vector concatenating $\boldsymbol{Y}_n^-$ and $\boldsymbol{X}_n^-$, the conditional entropy of Y given $\boldsymbol{Y}^-$, namely $H(Y|\boldsymbol{Y}^-)$ and the conditional entropy of Y given $\boldsymbol{Y}^-$ and $\boldsymbol{X}^-$, namely $H(Y|\boldsymbol{Y}^- \oplus \boldsymbol{X}^-)$ measure the amount of information carried by Y that cannot be derived, respectively, from past states of Y alone, and that cannot be derived from past states of Y and X. The TE from X to Y is given by (Schreiber, 2000)

$$TE_{X\to Y} = H(Y|\boldsymbol{Y}^-) - H(Y|\boldsymbol{Y}^- \oplus \boldsymbol{X}^-)\,. \qquad (2.13)$$

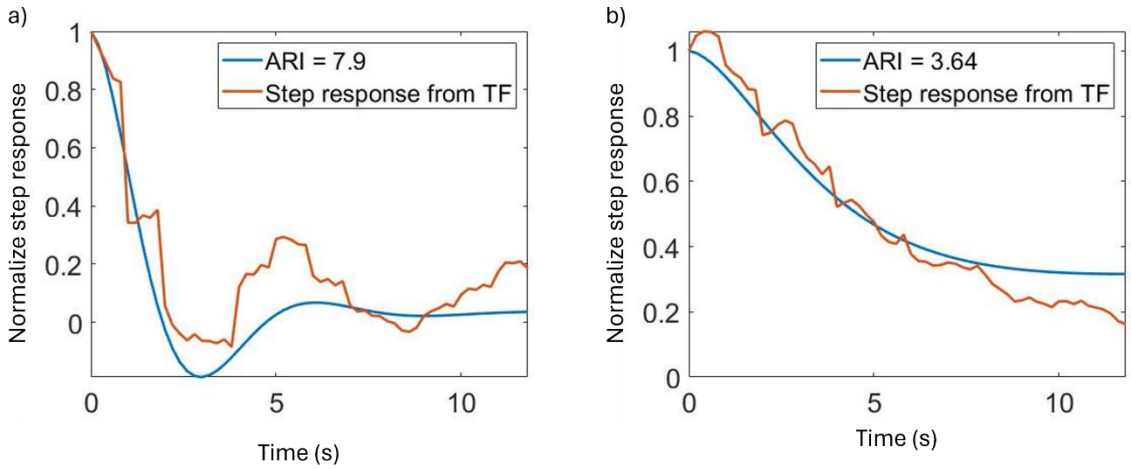

Figure 2.2. Step responses (orange) derived from TF and the response derived from the Tiecks' model that best fit to the estimated response from two subjects from the POTS Protocol.

$TE_{X\to Y}$ represents the information about *Y* genuinely transferred from *X*. Under the hypothesis of Gaussianity of the distributions of *m*-dimensional patterns derived from *X* and *Y* and linear interactions in the causal direction from X to Y, $H(Y|\boldsymbol{Y}^-)$ and $H(Y|\boldsymbol{Y}^- \oplus \boldsymbol{X}^-)$ can be estimated via vector autoregressive (AR) model approach (Barnett et al., 2009).

After defining the full universe of knowledge $\Omega = \{X, Y\}$, an AR model with exogenous (X) input (ARX) (Porta et al., 2000) can be utilized to describe the current state of Y_n of the process *Y* as a linear combination of past states of *Y* and *X* corrupted by the current state W_n^{YX} of zero mean white Gaussian noise W^{YX} with variance λ_{YX}^2 as

$$Y_n = \boldsymbol{Y}_n^- \cdot \boldsymbol{a}^{YX} + \boldsymbol{X}_n^- \cdot \boldsymbol{b}^{YX} + W_n^{YX} \qquad (2.14)$$

where $\boldsymbol{a}^{YX} = |a_1^{YX} \cdots a_m^{YX}|^T$ and $\boldsymbol{b}^{YX} = |b_{\tau_{Y,X}}^{YX} \cdots b_{m+\tau_{Y,X}}^{YX}|^T$ are vectors of *m* constant coefficients and T is the transpose operator. After defining a restricted universe of knowledge $\Omega/X = \{Y\}$, an AR model can be exploited to describe the current state of Y_n of the process *Y* as a linear combination of past states corrupted by the current state W_n^Y of zero mean white Gaussian noise W^Y with variance λ_Y^2 as

$$Y_n = \boldsymbol{Y}_n^- \cdot \boldsymbol{a}^Y + W_n^Y \qquad (2.15)$$

where $\boldsymbol{a}^Y = |a_1^Y \cdots a_m^Y|^T$ is a vector of *m* constant coefficients. Indicated the variances of W^{YX} in (2.14) and of W^Y in (2.15) with $\sigma^2_{Y|\boldsymbol{Y}^-\oplus\boldsymbol{X}^-}$ and $\sigma^2_{Y|\boldsymbol{Y}^-}$ respectively, they can be estimated as the variance of the prediction error after identifying the coefficients $\boldsymbol{a}^{YX}$, $\boldsymbol{b}^{YX}$ in (2.14) and $\boldsymbol{a}^Y$ in (2.15) and optimizing the model order *m* through an assigned figure of merit (Akaike, 1974). Given that, under the above mentioned hypotheses, $H(Y|\boldsymbol{Y}^- \oplus \boldsymbol{X}^-) = 0.5 \cdot \log(2\pi\sigma^2_{Y|\boldsymbol{Y}^-\oplus\boldsymbol{X}^-})$ and $H(Y|\boldsymbol{Y}^-) = 0.5 \cdot \log(2\pi\sigma^2_{Y|\boldsymbol{Y}^-})$, the $TE_{x\to y}$, can be computed as the natural logarithm of the ratio between prediction error variance in $\Omega\backslash x$ and that Ω (Barnett et al., 2009; Porta, Bari, et al., 2018)

$$TE_{X\to Y} = \frac{1}{2} log \frac{\sigma^2_{Y|\boldsymbol{Y}^-}}{\sigma^2_{Y|\boldsymbol{Y}^-\oplus\boldsymbol{X}^-}}. \qquad (2.16)$$

$TE_{X\to Y}$ is dimensionless and directional (i.e., $TE_{X\to Y}$ is different from $TE_{Y\to X}$). Higher values of TE represent a greater strength from X to Y. A graphical representation of these information quantities involved in TE calculation is reported in Figure 2.3. In this thesis, TE was computed from the beat-to-beat series of MCBv and MAP in a specific time direction, thus assessing $TE_{MAP\to MCBv}$ along the pressure-to-flow pathway and $TE_{MCBv\to MAP}$ along the flow-to-pressure link.

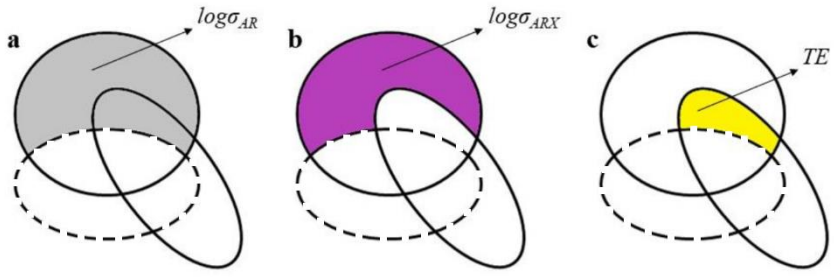

Figure 2.3. Venn diagrams of the information-theoretic quantities involved in TE computation. The ellipses represent the amount of information carried by Y (solid circle), past states of Y (dotted oval) and past states of X (solid oval). (a) the logarithm of the standard deviation of the prediction error of the AR model. (b) the logarithm of the standard deviation of the prediction error of the ARX model. (c) the TE from X to Y.

2.3.2 Conditional transfer entropy

In a fully multivariate approach, conditioning traces can also be included in the universes of knowledge to compute CTE (Porta, Faes, Marchi, et al., 2015). More specifically, in a trivariate application, a third system Z, whose conditioning behaviour is described by the process *Z*, is considered with the target Y and the driver X. While $TE_{X\to Y}$ presents the information transfer from X to Y above and beyond the past of *Y*, $CTE_{X\to Y|Z}$ represents the information transfer from *X* to Y above and beyond the past states of *Y* and *Z* (Barnett et al., 2009; Porta, Faes, Marchi, et al., 2015).

Defined the multidimensional vectors, $\boldsymbol{Z}^- = \{\boldsymbol{Z}_n^- = [Z_{n-\tau_{Y,Z}} \cdots Z_{n-m-\tau_{Y,Z}+1}], n = m + \tau_{Y,Z} + 1, \cdots, N\}$, $\boldsymbol{Y}^- \oplus \boldsymbol{Z}^- = \{\boldsymbol{Y}_n^- \oplus \boldsymbol{Z}_n^-, n = m + \tau_{Y,Z} + 1, \cdots, N\}$ and $\boldsymbol{Y}^- \oplus \boldsymbol{X}^- \oplus \boldsymbol{Z}^- = \{\boldsymbol{Y}_n^- \oplus \boldsymbol{X}_n^- \oplus \boldsymbol{Z}_n^-, n = m + \max(\tau_{Y,X}, \tau_{Y,Z}) + 1, \cdots, N\}$, where $\tau_{Y,Z}$ is the latency of the action of Z on Y, $\boldsymbol{Y}_n^- \oplus \boldsymbol{Z}_n^-$ is the vector concatenating $\boldsymbol{Y}_n^-$ and $\boldsymbol{Z}_n^-$ and $\boldsymbol{Y}_n^- \oplus \boldsymbol{X}_n^- \oplus \boldsymbol{Z}_n^-$ is the vector concatenating $\boldsymbol{Y}_n^-$, $\boldsymbol{X}_n^-$ and $\boldsymbol{Z}_n^-$, the conditional entropy of Y given $\boldsymbol{Y}^-$ and $\boldsymbol{Z}^-$, namely $H(Y|\boldsymbol{Y}^- \oplus \boldsymbol{Z}^-)$ and the conditional entropy of Y given $\boldsymbol{Y}^-$, $\boldsymbol{X}^-$, and $\boldsymbol{Z}^-$, namely $H(Y|\boldsymbol{Y}^- \oplus \boldsymbol{X}^- \oplus \boldsymbol{Z}^-)$ measure the amount of information carried by Y that cannot be derived, respectively, from past states of Y and Z and that cannot be derived from past states of Y, X and Z. The TE from X to Y conditioned on Z is given by (Barnett et al., 2009; Porta, Faes, Marchi, et al., 2015)

$$CTE_{X\to Y|Z} = H(Y|\boldsymbol{Y}^- \oplus \boldsymbol{Z}^-) - H(Y|\boldsymbol{Y}^- \oplus \boldsymbol{X}^- \oplus \boldsymbol{Z}^-)\,. \quad (2.17)$$

$CTE_{X\to Y|Z}$ represents the information about *Y* genuinely transferred from *X* when *Z* is conditioned out. Again under the hypothesis of Gaussianity of the distributions of *m*-dimensional patterns derived from *X*, *Y*, and *Z* and linear interactions in the causal direction from X to Y, and from Z to Y, $H(Y|\boldsymbol{Y}^- \oplus \boldsymbol{Z}^-)$ and $H(Y|\boldsymbol{Y}^- \oplus \boldsymbol{X}^- \oplus \mathbf{Z}^-)$ can be estimated via vector AR model approach (Barnett et al., 2009).

After defining the full and restricted universe of knowledge as $\Omega = \{X, Y, Z\}$, an AR model with double X (XX) inputs (ARXX) can be utilized to fit *Y* in Ω as

$$Y_n = \boldsymbol{Y}_n^- \cdot \boldsymbol{a}^{YXZ} + \boldsymbol{X}_n^- \cdot \boldsymbol{b}^{YXZ} + \boldsymbol{Z}_n^- \cdot \boldsymbol{c}^{YXZ} + W_n^{YXZ} \quad (2.18)$$

where $\boldsymbol{a}^{YXZ} = |a_1^{YXZ} \cdots a_m^{YXZ}|^T$, $\boldsymbol{b}^{YXZ} = |b_{\tau_{Y,X}}^{YXZ} \cdots b_{m+\tau_{Y,X}}^{YXZ}|^T$ and $\boldsymbol{c}^{YXZ} = |c_{\tau_{Y,Z}}^{YXZ} \cdots c_{m+\tau_{Y,Z}}^{YXZ}|^T$ are vectors of m constant coefficients, and W_n^{YXZ} is the current state of a zero mean white Gaussian noise W^{YXZ}. Analogously, after defining the restricted universe of knowledge as $\Omega\backslash X = \{Y, Z\}$ an ARX model can be utilized to fit Y in $\Omega\backslash X$ as

$$Y_n = \boldsymbol{Y}_n^- \cdot \boldsymbol{a}^{XZ} + \boldsymbol{Z}_n^- \cdot \boldsymbol{c}^{XZ} + W_n^{XZ} \quad (2.19)$$

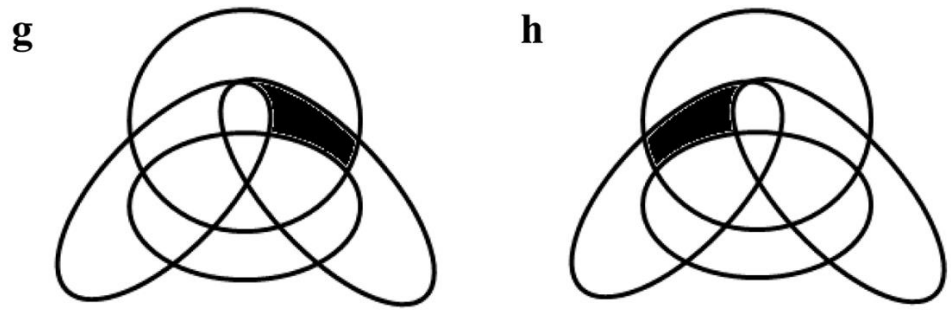

Figure 2.4 Venn diagrams of the information-theoretic quantities involved in CTE computation. The ellipses represent the amount of information carried by Y, past states of Y, past states of X, and past states of Z. The solid black areas are relevant to CTE from X to Y conditioned on Z (g) and CTE from Z to Y conditioned on X (h). Redrawn from Porta et al., 2015.

where $\boldsymbol{a}^{XZ} = |a_1^{YZ} \cdots a_m^{YZ}|^T$, and $\boldsymbol{c}^{YZ} = |c_{\tau_{Y,Z}}^{YZ} \cdots c_{m+\tau_{Y,Z}}^{YZ}|^T$ are vectors of m constant coefficients, and W_n^{YZ} is the current state of a zero mean white Gaussian noise W^{YZ}. Both the ARXX and ARX models can be identified and the model order m can be optimized as previously indicated. Given that, under the above mentioned hypotheses, $H(Y|\boldsymbol{Y}^- \oplus \boldsymbol{Z}^-) = 0.5 \cdot \log(2\pi\sigma^2_{Y|\boldsymbol{Y}^- \oplus \boldsymbol{Z}^-})$ and $H(Y|\boldsymbol{Y}^- \oplus \boldsymbol{X}^- \oplus \boldsymbol{Z}^-) = 0.5 \cdot \log(2\pi\sigma^2_{Y|\boldsymbol{Y}^- \oplus \boldsymbol{X}^- \oplus \boldsymbol{Z}^-})$, where $\sigma^2_{Y|\boldsymbol{Y}^- \oplus \boldsymbol{Z}^-}$ is the variance of the prediction error of the ARX model in $\Omega \backslash X$ and $\sigma^2_{Y|\boldsymbol{Y}^- \oplus \boldsymbol{X}^- \oplus \boldsymbol{Z}^-}$ is the variance of the predictor error of the ARXX model in Ω, the CTE from X to Y given Z is computed as

$$CTE_{X \to Y|Z} = \frac{1}{2} log \frac{\sigma^2_{Y|\boldsymbol{Y}^- \oplus \boldsymbol{X}^-}}{\sigma^2_{Y|\boldsymbol{Y}^- \oplus \boldsymbol{X}^- \oplus \boldsymbol{Z}^-}}. \qquad (2.20)$$

This trivariate approach can be exploited to investigate the confounding effects of respiration on cerebrovascular control. In this thesis, the CTE is computed along the pressure-to-flow pathway and along the flow-to-pressure link. Respiratory series (i.e., RCM and $EtCO_2$) are taken as confounding factors, thus computing $CTE_{MAP \to MCBv|RCM}$, $CTE_{MCBv \to MAP|RCM}$, $CTE_{MAP \to MCBv|EtCO_2}$, $CTE_{MCBv \to MAP|EtCO_2}$. A graphical representation of these information quantities is shown in Figure 1.1Figure 2.4.

2.4 Testing null hypotheses of uncoupling

Since values of TE and CTE might be different from 0 even in presence of full uncoupling due to noise and artifacts, the significance of the TE and CTE values is tested using the method of surrogates. The null hypothesis of absence of dynamic interactions among series (H_0) is tested by assessing TE and CTE over surrogate series built from their original versions with the aim at destroying all possible links among series, while preserving amplitude distribution and power spectral density (Porta & Faes, 2016). Uncoupled pairs and triplets are generated via time-shifting method (Andrzejak et al., 2003; Quian Quiroga et al., 2002). The method shifts in time the presumed cause and confounding series with random different latencies while the effect series is left unaltered (Andrzejak et al., 2003). The values at the end of the cause and confounding series are wrapped on their onsets. By construction, distributions of values, power spectral densities and nonlinear dynamics are preserved because temporal dynamics are preserved. Conversely, if a sufficiently long latency was selected, the series are fully uncoupled.

In the bivariate approach, for each subject in each experimental condition, one surrogate pair is generated by associating the original unaltered effect series with the cause series shifted by a latency randomly selected from 45 to 79 beats. In the trivariate approach, one surrogate triplet is generated by associating the original unaltered effect series with the cause and confounding series shifted by two different latencies randomly selected from 45 to 79 beats. Giving that the same number of original and surrogate pairs is generated, paired t-test, or a Wilcoxon signed rank test when appropriate, was applied to check the difference between the original and surrogate group. In surrogate pairs and triplets, the coupling between cause and effect and between confounding series and effect is lost and the computed values of CE and CTE provide an estimate of zero level of information transfer. Thus, if TE and CTE computed over the original pairs and triplets are significantly above that derived from the surrogates, the null hypothesis of uncoupling is rejected, thus indicating that a significant information transfer is detected.

CHAPTER 3 - Experimental protocols and data analysis

3.1 Introduction

In the following sections (i.e., Sect.3.2, 3.3 and 3.4), the three different experimental protocols exploited in the present thesis are described. The protocols are applied to: i) healthy (HEALTHY) subjects with no overt pathologies undergoing a head-up tilt (TILT) test (HEALTHY protocol); ii) subjects affected by a form of dysautonomia, namely POTS, recorded at rest in supine position (REST), during active standing (STAND) and under slow breathing (SB) contrasted against control (CONTROL) individuals (POTS protocol); iii) subjects in the acute phase of ischemic stroke (STROKE) with bilateral recordings from the affected and unaffected hemisphere contrasted against CONTROL individuals (STROKE protocol). Following, Sect.3.5 is dedicated to the extraction of the physiological variables and construction of the variability series according to rigorously defined conventions of measurement allowing the association of a physiological variable to a specific cardiac beat. The two following sections, namely Sect.3.6 and Sect.3.7, describe the computation of cardiovascular and cerebrovascular dynamic markers from the variability series. Finally, the chapter ends with Sect.3.8 describing the statistical analysis performed for each experimental protocol.

3.2 HEALTHY protocol

The data were selected from the historical database originally designed to assess the impact of postural challenge on cerebrovascular control markers in HEALTHY individuals (Bari et al., 2017; Faes et al., 2013). Data were collected at the Neurology Division of Sacro Cuore Hospital, Negrar, Italy. The experimental protocol was approved by the local institutional human research ethics committee and adhered to the principles of the Declaration of Helsinki for medical research involving humans. Each subjects gave written informed consent before performing the experimental session.

Fourteen young subjects (age: 27 ± 8 yrs.; 5 males) with no overt pathology underwent a physical examination and full neurological assessment to confirm their healthy status. None of the individuals were taking any medication affecting cardiovascular control. Before participating to the experiment, subjects refrained from heavy exercise and the intake of nicotine, caffeine or alcohol-beverage for 24 h. All the sessions of the protocol took place in a climate controlled environment, with subjects laying on a tilt table supported by two belts at the level of thigh and waist, and with both feet in contact with the footrest of the table.

Subjects were instrumented to continuously monitor the electrocardiogram (ECG) from the lead II and AP via photoplethysmography volume-clamp device from the middle finger (Finapres Medical Systems, Enschede, The Netherlands). CBv was measured from the MCA through a TCD device (Multi-Dop T, DWL, 2 MHz, Compumedics, San Juan Capistrano, CA, USA), and was taken as a proxy of CBF (Figure 3.1). The probe was fixed in place over the temporal window, and MCA was insonated by selecting the velocity toward the probe with depth between 30 and 60 mm. The CBv signal was low-pass filtered with a sixth-order Butterworth filter with cut-off frequency of 10 Hz. RCM signal was obtained via a thoracic impedance belt. All signals were acquired synchronously via an analog-to-digital board at a sampling rate of 1000 Hz.

After having instrumented the subject, a period of 5 minutes was left for stabilization of the physiological variables. Signal acquisition was performed for 10 minutes at REST, followed by TILT obtained by passive transition to 60° upright position. The three minutes of TILT session after the change of the inclination of the tilt table was excluded to avoid transitory adjustments of the variables. TILT session was prolonged up to 40 minutes, but analysis was carried out within the first ten minutes after the TILT onset. All subjects responded TILT with tachycardia and reduced respiratory sinus arrhythmia. No one presented presyncope signs during TILT and all subjects exhibited spontaneous recovery when returned to REST.

3.3 POTS protocol

Two age- and gender-matched groups of 19 CONTROL subjects (age: 28 ± 13 yrs.; 5 males) and 15 individuals with POTS (age: 29 ± 11 yrs.; 3 males) were enrolled at the Centre for Heart Rhythm Disorders, The University of Adelaide, Adelaide, Australia. The data were selected from the historical database originally designed to assess the impact of sustained cognitive stress on cerebrovascular hemodynamic in POTS (Wells et al., 2020). The protocol adhered to the principles of the Declaration of Helsinki for medical research involving human subjects and all participants provided written informed consent before their inclusion in the protocol. The experimental protocol was approved by the local institutional human research ethics committee.

Individuals with POTS were enrolled if specific clinical criteria were met during upright postural challenge with resolution when recumbent, namely a documentation of a sustained increment of heart rate greater the 30 beats-per-minutes during orthostatic challenge within 10 minutes after the onset of the stimulus without a postural drop of BP greater than 20 mmHg (Wells et al., 2020). Symptoms of POTS included light-headedness, headache, fatigue, neurocognitive deficits, palpitations, nausea, altered vision, or shortness of breath while upright. No other medical explanation was identified to justify the symptoms. The CONTROL group consisted of subjects with no known cardiac or autonomic symptoms. Their healthy status was confirmed by clinical evaluation and by checking their cardiovascular response to active standing. Questionnaires to rate POTS symptoms and assess quality of life clearly differentiate between POTS and CONTROL subjects, confirming that CONTROL individuals did not have orthostatic intolerance.

All testing sessions were performed in the morning, in a climate-controlled facility (22°C). Before participating to the experiment, all subjects were asked to abstain from heavy exercise and the intake of nicotine, caffeine or alcohol-beverage over the preceding 24 hours. All participants with POTS were on treatment in accordance with current guidelines without any

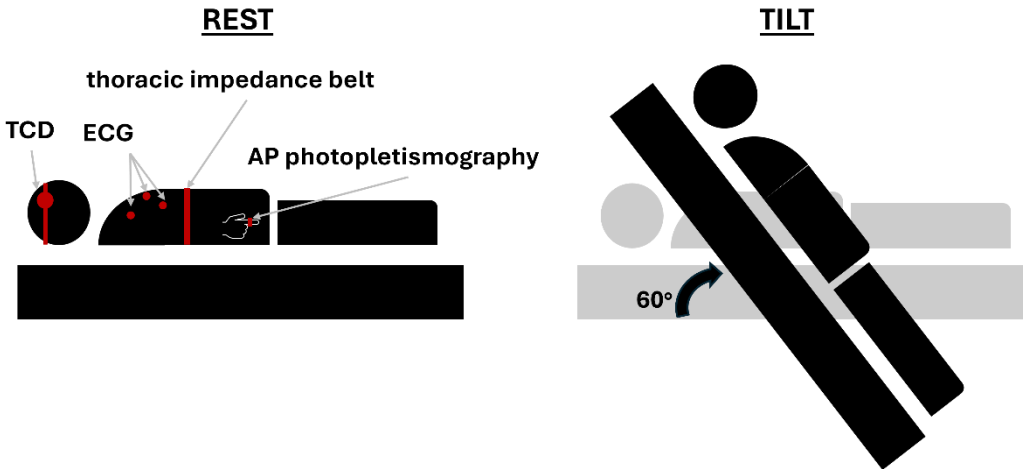

Figure 3.1 In HEALTHY protocol, subjects without signs of overt pathology undergo sessions at REST and during TILT with tilt table inclination of 60° while recording ECG, CBv via TCD, noninvasive AP, and RCM via a thoracic belt.

modification of the therapy in the previous month. Participants were permitted to continue all their usual medications except for vasopressors. Subjects who usually took midodrine (α-adrenergic agonist, half-life of 3 hours) in the morning were asked to delay this dose until after completing the study to avoid exogenous vasopressor therapy confounding interpretation of the results.

As shown in Figure 3.2, subjects were instrumented to continuously monitor the ECG via a commercial bio amplifier (FE132 Bioamp, ADInstruments Pty Ltd) and non-invasive AP using a cuff placed on the middle finger of the right hand via a volume clamp device (Finapres Medical Systems BV). The CBv was measured from the MCA through a TCD device (Doppler-BoxX, Compumedics DWL) from the temporal window as in HEALTHY protocol. A chest wall strain gauge (MLT 1132/D Piezo Respiratory Belt Transducer, ADInstruments) was used to record the RCM. Lastly, capnography was exploited to monitor partial pressure of CO_2 in the respiratory gases during inspiration and expiration, thus producing a CAP. This equates $PaCO_2$ in the blood only at the end of expiration. CAP was measured (Capnostream 20P, Medtronic, Minneapolis, MN, USA) via nasal prongs with mouth scoop (Smart CapnoLine Plus, Microstream, Medtronic). All signals were sampled simultaneously and continuously through a data acquisition device (Powerlab PL35/16, ADInstruments Pty Ltd, NSW, Australia) at a sampling rate of 1000 Hz.

Signals were recorded for 10 minutes at baseline (BASELINE) while sitting resting with back support at a desk, followed by 10 minutes during active standing (STAND). The three minutes of STAND session was excluded to avoid sequences featuring transitory adjustments of the variables. After STAND a period of 5 minutes of resting was allowed and afterward subjects were asked to perform 5 respiratory cycles at slow breathing (SB) with a frequency of 8 breaths per minute (breaths/min), namely with a period close to 10 s.

3.4 STROKE protocol

Two age- and gender-matched groups were considered with 33 CONTROL subjects (age: 66 ± 7 yrs.) and 48 individuals with ischemic STROKE (age: 66 ± 12 yrs.) in the 48 hours of symptoms onset. Subjects with stroke were enrolled at the Stroke Unit ward at the Leicester Royal Infirmary (Leicester, UK) within a study promoted by the Department of Cardiovascular Science at University of Leicester (Leicester, UK). For the CONTROL group, volunteers able and willing to comply with all the study requirements were recruited from the hospital and university staff, and among patients' relatives. Concerning the STROKE group, only conscious subjects able to give their written informed consent were enrolled. All subjects gave their written

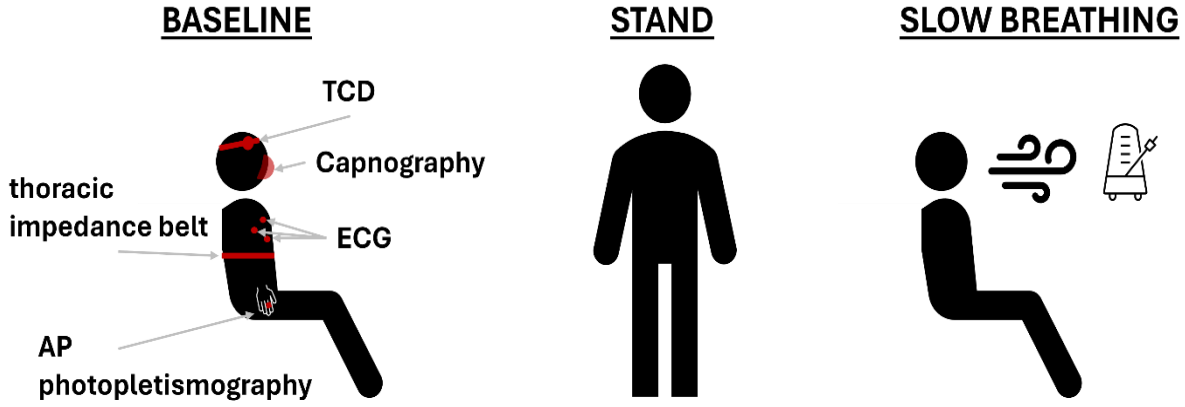

Figure 3.2 In POTS protocol, CONTROL subjects and POTS individuals undergo sessions at BASELINE, STAND and SB while recording ECG, CBv via TCD, noninvasive AP, RCM via a thoracic impedance belt, and CAP.

informed consent. The local institutional human research ethics committee approved the experimental protocol which adhered to the principles of the Declaration of Helsinki.

Experiments were performed at the University of Leicester's Cerebral Haemodynamics in Ageing and Stroke Medicine research laboratory, with minimal auditory or visual distraction, following the standard protocol for recordings at rest (Minhas et al., 2018; Patel et al., 2016). Healthy subjects were asked to avoid heavy exercise, caffeine, alcohol and nicotine for at least 12 hours before attending the measurements.

As shown in Figure 3.3, subjects were instrumented to continuously monitor non-invasive AP using a cuff placed on the middle finger of the right hand via a volume-clamped device (Finapres Medical Systems BV). The CBv was measured from the MCA through a TCD device (Doppler-BoxX, Compumedics DWL). MCA was isonated from the temporal as in HEALTHY protocol and an auditory check was performed to confirm the selection of the correct vessel. The measurements were performed bilaterally with 2-MHz probes supported by a headframe. In STROKE, the hemisphere in which the lesion occurred was defined as AFFECTED, while the other one as UNAFFECTED. The CAP was acquired via capnography (Capnocheck Plus, IcuMedical) using nasal prongs with a mouth scoop. Data were continuously recorded through a data acquisition system (PHYSIDAS, Department of Medical Physics, University Hospitals of Leicester) for subsequent off-line analysis using a sampling rate of 500 Hz. In the CBv signals, any narrow spikes were removed by linear interpolation and high-frequency noise was removed with a median filter. All signals were then low-pass filtered with an eighth-order, zero-phase Butterworth filter with a cutoff frequency of 20 Hz.

A 5-minute baseline recording was obtained with the subject breathing normally in the supine position with the head supported by one or two pillows.

3.5 Variability series extraction

Conventions of the measurements are reported in Figure 3.4. From the ECG, the R-wave peaks were detected using a threshold applied to the first derivative. The *n*th HP was derived as the time distance between the (*n*–1)th and the *n*th R-wave detected over the ECG. The *n*th systolic arterial pressure (SAP) and diastolic arterial pressure (DAP) were located, respectively, at the timing of the maximum arterial pressure within the *n*th HP, and at the timing of the minimum following the *n*th SAP. The *n*th MAP was computed as the ratio of the definite integral of AP between the (*n*–1)th and *n*th DAP occurrences to the inter-diastolic interval. Similarly, the *n*th MCBv was obtained as the integral of CBv between the (*n*-1)th and *n*th minima detected over

Figure 3.3 Experimental setup for TCD, capnography, ECG and BP recordings at the University of Leicester's Cerebral Haemodynamic in Ageing and Stroke Medicine research laboratory. Courtesy of Lauren Walker.

CBv and closest in time to (*n*-1)th and nth DAP fiducial points and by dividing the result by the time distance between the two minima (Bari et al., 2017).

The CAP signal was filtered via a four-order low-pass Butterworth filter with a cutoff frequency of 0.5 Hz. The $EtCO_2$ was computed as the CAP at the end of exhalation. $EtCO_2$ derived on a breath-to-beath basis was interpolated to provide values for every cardiac beat. The RCM and $EtCO_2$ signals were sampled in correspondence to the second R-wave peak delimiting the *n*th HP to define the corresponding beat-to-beat series.

For the STROKE protocol in Sect.3.4, all the original series present in database were spline interpolated and resampled at 5 Hz. The original series were down sampled at 1 Hz because frequency content of vascular and cerebrovascular control mechanisms was below 0.5 Hz.

The resulting series were manually corrected in case of missing beats or misdetections. The effect of ectopic beats or isolated arrhythmic events were mitigated via linear interpolation between the closest values unaffected by arrhythmic beat. Corrections did not exceed 5% of the total sequence length. Sequences of 250 consecutive beats were selected for each experimental condition with the onset of the sequence randomly selected within the session. Representative examples of variability series extracted from the recorded signals are reported in Figure 3.4 and Figure 3.5 for a CONTROL subject at REST from POTS.

3.6 Computation of variability markers

As for the cardiovascular control, in the time domain, mean and variance of the HP and SAP series, namely μ_{HP}, σ^2_{HP}, μ_{SAP}, and σ^2_{SAP}, were computed and expressed in ms, ms^2, mmHg and $mmHg^2$, respectively. In the frequency domain, parametric power spectral analysis was carried out according to an AR representation of the series (Task Force of the European Society of Cardiology and the North American Society of Pacing and Electrophysiology, 1996). The power of HP in the high frequency (HF) band (i.e., from 0.20 to 0.40 Hz) and the power of SAP in the low frequency (LF) band (i.e., from 0.04 to 0.20 Hz), denoted, respectively, as HF_{HP} and LF_{SAP} and expressed in absolute units (i.e., ms^2 and $mmHg^2$, respectively). HF_{HP} and

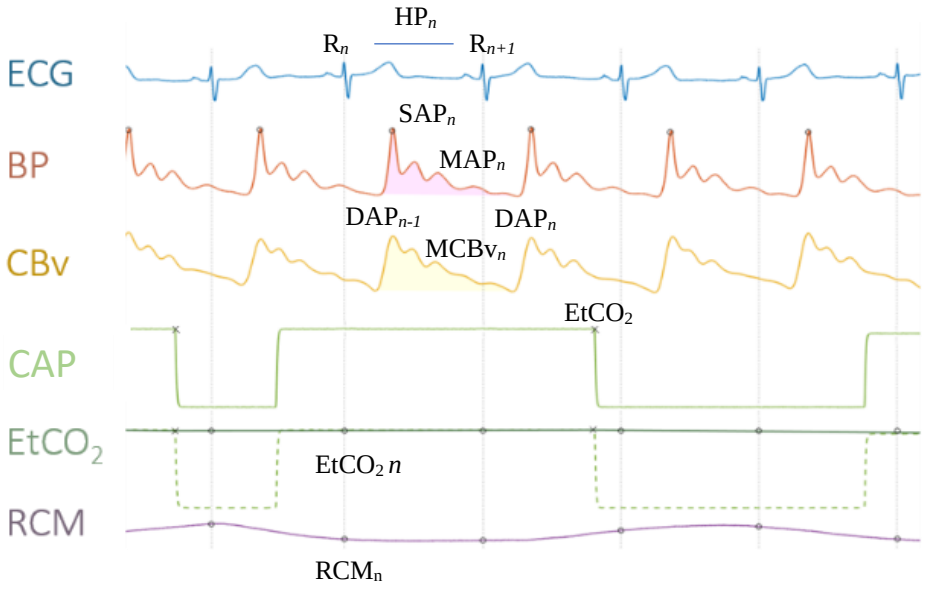

Figure 3.4 Example from a CONTROL subject at REST from POTS protocol. The signals recorded are ECG, non-invasive arterial pressure (AP), cerebral blood velocity (CBv), capnography (CAP) and respiratory chest movements (RCM). The extracted variables heart period (HP), mean arterial pressure (MAP), mean cerebral blood velocity (MCBv), end-tidal carbon dioxide ($EtCO_2$) and respiratory chest movement (RCM) are associated to a specific cardiac beat (n) according to the conventions of measurement.

LF_{SAP} were taken, respectively, as a marker of vagal modulation directed to the heart (Task Force of the European Society of Cardiology and the North American Society of Pacing and Electrophysiology, 1996) and sympathetic modulation directed to the vessels (Marchi et al., 2016; Pagani et al., 1997).

Respiratory indexes were extracted from RCM, and $EtCO_2$ series. The frequency of the dominant oscillation of the RCM series within the HF band was taken as the respiratory frequency (f_{Resp}). The dominant oscillation within the LF was also calculated to identify subjects where the respiratory rate fall below 0.20 Hz. In these cases, the value of the dominant oscillation in the LF band was utilized. f_{Resp} was expressed in breaths/min. In the STROKE protocol, RCM was not recorded thus the respiratory indexes were extracted via the analysis of the dominant frequency of MAP in HF and LF as for RCM (Nemati et al., 2010). The mean and variance of $EtCO_2$, denoted with μ_{EtCO2} and σ^2_{EtCO2}, and expressed in mmHg and $mmHg^2$, respectively, were taken as a parameter describing the CO_2 level and its variability.

Cerebrovascular indexes were computed similarly to cardiovascular indexes. For MCBv and MAP, mean and variance, namely μ_{MAP}, σ^2_{MAP}, μ_{MCBv}, and σ^2_{MCBv}, were computed and expressed in mmHg, $mmHg^2$, $cm \cdot s^{-1}$ and $cm^2 \cdot s^{-2}$, respectively. Spectral indexes in the LF band were computed via AR approach (Bari et al., 2017; J. A. Claassen et al., 2015). The powers of the MAP and MCBv series were expressed in absolute units, namely $mmHg^2$ and $cm^2 \cdot s^{-2}$ respectively, and labelled LF_{MAP} and HF_{MCBv}.

3.7 Computation of CA indexes

The TFA parameters (i.e., TFG, TFP and K^2) were calculated in the LF band given the strict relation detected in the specific band between MAP and MCBv changes (J. A. Claassen et al., 2015; Panerai et al., 2023; Watanabe et al., 2022; Zhang, Zuckerman, & Levine, 1998). Previous studies have shown that the VLF range reflects multiple physiological mechanisms that confound interpretation (Ogoh et al., 2005), while arterial AP oscillations in the HF are primarily induced by the respiratory frequency (Diehl et al., 1995; Elstad et al., 2018). Thus, TFA was carried out only in the LF band and the values of TFG, TFP and K^2 were averaged

Figure 3.5 Example of series extracted from a CONTROL subject at REST from POTS protocol. The variability series are heart period (HP), mean arterial pressure (MAP), mean cerebral blood velocity (MCBv), end-tidal carbon dioxide ($EtCO_2$) and respiratory chest movement (RCM).

within the LF band. TFG was expressed in cm·s^{-1}·mmHg^{-1}, TFP ranged from $-\pi$ and $+\pi$ and expressed in radians (rad), while K^2 ranged from 0 to 1 and it was dimensionless.

For the ARI computation, the beat-to-beat MAP and MCBv variability series were resampled at f=5 Hz. MCBv was normalized by its mean value, while MAP was normalized as:

$$dMAP_k = \frac{MAP_k - \mu_{mean}}{MAP_k - P_{cr}}$$

where μ_{mean} is the mean of MAP over the selected sequence, P_{cr} is the is the critical closing pressure set to 12 mmHg and k is the current time index. Since dCA effects should be exhausted by a few seconds (Zhang, Zuckerman, Giller, et al., 1998), comparison between predicted and theoretical step responses was carried out over 8 s (Panerai et al., 1998) as reported in Sect.2.2.2. Linear interpolation between discrete values of ARI was used to obtain a scale to the second decimal (Chacon et al., 2008). The percentage of subjects with an effective dCA (i.e., ARI>4) was calculated for each population and experimental condition.

As for the causal bivariate approach, on the pressure-to-flow pathway TE was computed with MAP as the driver and MCBv as the target, namely $TE_{MAP\rightarrow MCBv}$. Vice versa on the flow-to-pressure pathway, TE was computed with MAP as the driver and MCBv as the target, namely $TE_{MCBv\rightarrow MAP}$. As for the multivariate approach, CTE is computed with MAP and MCBv as the driver and target, while RCM or $EtCO_2$ as the conditioning variable. CTE was labelled as $CTE_{MAP\rightarrow MCBv|RCM}$ and $CTE_{MAP\rightarrow MCBv|EtCO2}$ along the pressure-to-flow pathway and $CTE_{MCBv\rightarrow MAP|RCM}$ and $CTE_{MCBv\rightarrow MAP|EtCO2}$ along the flow-to-pressure pathway.

3.7.1 Latencies' optimization

When computing causality analysis, the latency of the driver and confounding factors on the target signal should be set according to physiological and methodological considerations. Indeed, when considering closed-loop interactions, some delay is present in the closed-loop between the drive and the target. While the pressure-to-flow pathway has capacitive and inertial properties, the fast responses on the flow-to-pressure link is rapidly driven by the barosensitive areas in the brain stem (Bari et al., 2021; Vaini et al., 2019). The delay along the pressure-flow interactions has also been found on experimental data. A cross-correlation analysis on subjects undergoing cardiopulmonary bypass has shown a latency of 2 beats on the pathway describing the pressure-to-flow relationship and a much faster effect on the reverse pathway with a latency of 0 beats (Vaini et al., 2019). Similar results were found on the CONTROL group in the STROKE protocol.

Given the physiological consideration on the response speed, the delay of 2 beats was attributed to the pathway describing the pressure-to-flow relationship, while the latency from MCBv was set to 0 beats. As for CTE, the latency from respiratory signals to MAP and MCBv was set to 0 beats according to fast mechanical action of RCM onto MAP and MCBv (Porta et al., 2021; Porta, Faes, Nollo, et al., 2015) and rapid influences of $EtCO_2$ via cerebrovascular reactivity.

3.8 Statistical analysis

Statistical analysis was carried out using a commercial statistical program (Sigmaplot, v.14.0, Systat Software, Inc., Chicago, IL, USA). Regardless of the type of statistical test the level of significance was set to 0.05.

3.8.1 Statistical analysis of data relevant to HEALTHY protocol

The Shapiro-Wilk normality test was utilized to test normality of the distributions. A paired t-test, or a Wilcoxon signed rank test when appropriate, was applied to check the effect of TILT on time-domain variability and traditional cerebrovascular markers. For each experimental condition (i.e., REST or TILT) a paired t-test, or a Wilcoxon signed rank test when appropriate, was applied to check the difference between information transfer markers (i.e., TE or CTE) computed over ORIGINAL and SURROGATE series. Two-way analysis of variance repeated measures (Holm-Sidak test for multiple comparisons) was used to compare TE and CTE indexes within the same experimental condition and differences across experimental conditions using the same type of information transfer index (i.e., TE or CTE).

3.8.2 Statistical analysis of data relevant to POTS protocol

The Shapiro-Wilk normality test was utilized to test normality of the distributions. Two-way analysis of variance (Holm-Sidak test for multiple comparisons) was used on time-domain variability, traditional cerebrovascular markers and information transfer indexes to assess the impact of the experimental condition within the same populations (i.e., CONTROL or POTS) and to compare populations within the same challenge (i.e., BASELINE, STAND and SB). For each population for each experimental condition, a paired t-test, or a Wilcoxon signed rank test when appropriate, was applied to check the difference between information transfer markers computed over ORIGINAL and SURROGATE series. For each population, two-way analysis of variance (Holm-Sidak test for multiple comparisons) was used to compare information transfer indexes (i.e., TE versus CTE) within the same experimental condition and to assess the effect of the experimental condition within the same type of index.

3.8.3 Statistical analysis of data relevant to STROKE protocol

The Shapiro-Wilk normality test was utilized to test normality of the distributions. A unpaired t-test, or a Mann-Whitney rank sum test when appropriate, was applied to check the difference between CONTROL and STROKE over time-domain markers. One-way repeated measures analysis of variance (Dunnett's test for multiple comparisons), or Friedman repeated measures analysis of variance on ranks if appropriate (Dunnett's test for multiple comparisons), was utilized to compare the cerebrovascular markers across groups (i.e., CONTROL, UNAFFECTED, and AFFECTED). For each group a paired t-test, or a Wilcoxon signed rank test when appropriate, was applied to check the difference between information transfer markers (i.e., TE or CTE) computed over ORIGINAL and SURROGATE series. Two-way analysis of variance (Holm-Sidak test for multiple comparisons) was used to compare TE and CTE indexes within the same group and differences across groups using the same type of information transfer index (i.e., TE or CTE).

CHAPTER 4 - Results

4.1 Introduction

The following chapter introduces the results of cardiovascular, respiratory and cerebrovascular variability indexes, and TE and CTE parameters for each of the three experimental datasets described in CHAPTER 3 -. The following Sections list the results obtained from HEALTHY (Sect.4.2), POTS (Sect.4.3) and STROKE (Sect.4.4) protocols.

4.2 Results of the HEALTHY protocol

Two recordings during TILT were discarded for the poor quality of the CBv signal. Therefore, the beat-to-beat variability series relevant to these subjects were discarded both at REST and during TILT to allow the application of repeated measures analysis of variance.

4.2.1 Variability markers

Table 4.1 reports the cardiovascular and respiratory parameters at REST and during TILT in the HEALTHY protocol. The orthostatic challenge induces a significant decrease of μ_{HP} and HF_{HP} and an increase of LF_{SAP}. No variations were observed in the respiratory frequency.

Similarly, Table 4.2 reports the cerebrovascular parameters at REST and during TILT. The orthostatic challenge induces a significant increase of σ^2_{MAP}, LF_{MAP}, and LF_{MCBv} in association with a decrease in μ_{MCBv}.

4.2.2 CA indexes

Table 4.3 reports the indexes derived from TFA analysis in the HEALTHY protocol. They remained stable during TILT.

Table 4.4 and Table 4.5 summarize the information transfer indexes computed over the ORIGINAL and SURROGATE pairs. Regardless of the experimental condition (i.e., REST and TILT), the directionality (i.e., MAP→MCBv and MCBv→MAP) or the type of parameters (i.e., TE and CTE), information transfer indexes computed over the ORIGINAL pairs were significantly higher than those over SURROGATE series.

The grouped error bar graphs in Figure 4.1 show the comparison of TE (black bars) and CTE|RCM (grey bars) at REST and during TILT. On the pressure-to-flow pathway (i.e., MAP→MCBv, Figure 4.1.a) conditioning on RCM had no effect on the interactions estimation and this result held regardless of the experimental condition. Regardless of the information domain marker, the impact of TILT was negligible. On the flow-to-pressure pathway (i.e., MCBv→MAP, Figure 4.1.b) TILT did not modify both TE and CTE|RCM. Conversely, regardless of the experimental condition, CTE|ECM was significantly smaller than TE.

Table 4.1 Cardiovascular and respiratory parameters at REST and during TILT in the HEALTHY protocol.

	REST	**TILT**
μ_{HP} [ms]	876.8 ± 181.1	708.1 ± 93.6 *
σ^2_{HP}[ms^2]	2534.4 ± 2700.3	1643.5 ± 960
HF_{HP} [ms^2]	464.4 ± 555.4	182.6 ± 241.1 *
μ_{SAP} [mmHg]	136.2 ± 28.6	132.6 ± 16.7
σ^2_{SAP} [mmHg^2]	29 ± 21.6	32.7 ± 17.3
LF_{SAP} [mmHg^2]	4.8 ± 5.2	13.7 ± 14 *
f_{Resp} [breaths/min]	19.1 ± 3.2	20.2 ± 3.3

HP = heart period; μ_{HP} = HP mean; σ^2_{HP} = HP variance; SAP = systolic arterial pressure; μ_{SAP} = SAP mean; σ^2_{SAP} = SAP variance; LF = low frequency; HF = high frequency; HF_{HP} = power of the HP series in the HF band; LF_{SAP} = power of the SAP series in the LF band; RCM = respiratory chest movement; f_{Resp} = respiratory frequency computed from RCM. Results are reported as mean ± standard deviation. The symbol * indicates a $p<0.05$ versus REST.

Table 4.2. Cerebrovascular parameters at REST and during TILT in the HEALTHY protocol.

	REST	**TILT**
μ_{MAP} [mmHg]	94.6 ± 14	93.4 ± 13
σ^2_{MAP} [mmHg^2]	13 ± 9.6	17 ± 10.1 *
LF_{MAP} [mmHg^2]	3.1 ± 3	8.8 ± 8.4 *
μ_{MCBv} [cm s^{-1}]	71.7 ± 21.6	61.8 ± 17.3 *
σ^2_{MCBv} [cm^2·s^{-2}]	16.7 ± 6.6	31.1 ± 27.2
LF_{MCBv} [cm^2·s^{-2}]	3 ± 3.9	9.2 ± 9.4 *

MCBv = mean cerebral blood velocity; μ_{MCBv} = MCBv mean; σ^2_{MCBv} = MCBv variance; MAP = mean arterial pressure; μ_{MAP} = MAP mean; σ^2_{MAP} = MAP variance; LF = low frequency; LF_{MCBv} = power of the MCBv series in the LF band; LF_{MAP} = power of the MAP series in the LF band. Results are reported as mean ± standard deviation. The symbol * indicates a $p<0.05$ versus REST.

Table 4.3. Transfer function indexes at REST and during TILT in the HEALTHY protocol.

	REST	**TILT**
TFG [cm·s^{-1}·mmHg^{-1}]	0.58 ± 0.24	0.77 ± 0.77
TFP [rad]	0.14 ± 0.36	0.06 ± 0.29
K^2	0.25 ± 0.15	0.32 ± 0.19
ARI	3.40 ± 1.15	3.62 ± 1.6
ARI > 4	25%	29%

TFG = transfer function gain in the LF band; TFP = transfer function phase in the LF band; K^2 = squared coherence in the LF band; ARI= cerebral autoregulation index. Results are reported as mean ± standard deviation and as percentage for ARI>4. The symbol * indicates a $p<0.05$ versus REST.

Table 4.4. Information transfer indexes computed over ORIGINAL and SURROGATE pairs at REST in the HEALTHY protocol.

REST	**ORIGINAL**	**SURROGATE**
$TE_{MAP \rightarrow MCBv}$	0.07±0.04	0.02±0.01 *
$CTE_{MAP \rightarrow MCBv\|RCM}$	0.07±0.04	0.02±0.01 *
$TE_{MCBv \rightarrow MAP}$	0.13±0.08	0.02±0.01 *
$CTE_{MCBv \rightarrow MAP\|RCM}$	0.11±0.08	0.03±0.01 *

MAP = mean arterial pressure; MCBv = mean cerebral blood velocity; RCM = respiratory chest movement; TE = transfer entropy; CTE = conditional TE; $TE_{MAP \rightarrow MCBv}$ = TE from MAP to MCBv; $CTE_{MAP \rightarrow MCBv|RCM}$ = CTE from MAP to MCBv when RCM is conditioned out; $TE_{MCBv \rightarrow MAP}$ = TE from MCBv to MAP; $CTE_{MCBv \rightarrow MAP|RCM}$ = CTE from MCBv to MAP when RCM is conditioned out. Results are reported as mean ± standard deviation. The symbol * indicates a $p<0.05$ versus ORIGINAL.

Table 4.5. Information transfer indexes computed over ORIGINAL and SURROGATE pairs during TILT in the HEALTHY protocol.

TILT	**ORIGINAL**	**SURROGATE**
$TE_{MAP \rightarrow MCBv}$	0.09±0.03	0.02±0.02 *
$CTE_{MAP \rightarrow MCBv\|RCM}$	0.08±0.03	0.02±0.01 *
$TE_{MCBv \rightarrow MAP}$	0.2±0.07	0.03±0.02 *
$CTE_{MCBv \rightarrow MAP\|RCM}$	0.17±0.07	0.03±0.02 *

MAP = mean arterial pressure; MCBv = mean cerebral blood velocity; RCM = respiratory chest movement; TE = transfer entropy; CTE = conditional TE; $TE_{MAP \rightarrow MCBv}$ = TE from MAP to MCBv; $CTE_{MAP \rightarrow MCBv|RCM}$ = CTE from MAP to MCBv when RCM is conditioned out; $TE_{MCBv \rightarrow MAP}$ = TE from MCBv to MAP; $CTE_{MCBv \rightarrow MAP|RCM}$ = CTE from MCBv to MAP when RCM is conditioned out. Results are reported as mean ± standard deviation. The symbol * indicates a $p<0.05$ versus ORIGINAL.

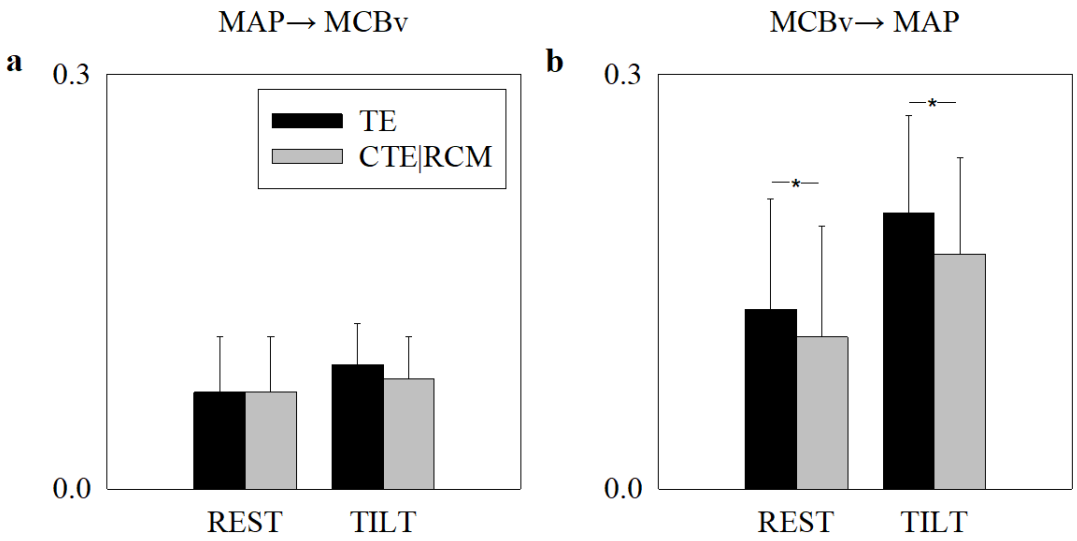

*Figure 4.1 Comparison of information transfer indexes(i.e., TE and CTE|RCM) computed at REST and during TILT on the pressure-to-flow (a) and on the flow-to-pressure (b) pathways in the HEALTHY protocol. The symbol * indicates a $p<0.05$ versus TE within the same experimental condition (i.e., REST or TILT).*

4.3 Results of the POTS protocol

One recording at BASELINE and 4 recordings at STAND were discarded for the poor quality of at least one of the signals in the CONTROL group. One recording at BASELINE and STAND was discarded for the poor quality of the CBv signal in POTS population. A reliable estimation of variability and cerebrovascular markers was carried out only in 11 POTS and 10 CONTROL subjects. Therefore, repeated measures analysis of variance could not be applied, and a traditional two-way analysis of variance approach was carried out. This high rate of discarded recordings was due to the complexity of the experimental set-up, which included five simultaneous signals.

4.3.1 Variability markers

Table 4.6 reports the cardiovascular and respiratory parameters at BASELINE, during STAND and SB in CONTROL and POTS groups. Standing did not induce any significant modification of the markers. In the CONTROL group SB induced an increase of σ^2_{HP}, σ^2_{SAP} and LF_{SAP} compared to BASELINE. Similar trends of σ^2_{HP} and LF_{SAP} were observed in POTS subjects. In the CONTROL group the increase observed in σ^2_{HP} and LF_{SAP} during SB was significant compared STAND as well. As expected f_{RMC} during SB was about 8 breaths/min and this value was smaller than that detected at BASELINE and STAND. In both CONTROL and POTS individuals, experimental condition did not influence μ_{EtCO2} nor σ^2_{EtCO2}. When compared to CONTROL subjects, POTS individual presents lower μ_{HP} at BASELINE and smaller values of σ^2_{HP} and HF_{HP} during SB.

Table 4.7 reports the cerebrovascular parameters at BASELINE, during STAND and SB in the CONTROL and POTS groups. STAND induced an increase in the LF_{MAP} compared to BASELINE, but this modification was detected only in POTS. Only in the CONTROL group an increase of σ^2_{MAP} and a decrease of μ_{MAP} during SB compared to BASELINE were significant. Regardless of the experimental condition, differences between CONTROL and POTS were not significant.

4.3.2 CA indexes

Table 4.8 reports the indexes derived from TFA. Regardless of the group, markers remained stable despite the orthostatic challenge (i.e., STAND) and respiratory frequency variation induced by SB. In addition, no significant between-group differences were detected and this result held regardless of the experimental condition.

Table 4.9, Table 4.10 and Table 4.11 report the information transfer indexes computed on ORIGINAL and SURROGATE pairs in POTS group at BASELINE, during STAND and during SB, respectively. Similarly, Table 4.12, Table 4.13 and Table 4.14 report the data for CONTROL subjects. Regardless of the population (i.e., POTS and CONTROL) and the directionality (i.e., MAP→MCBv and MCBv→MAP), at BASELINE and during STAND

information transfer indexes computed over the ORIGINAL series featured significantly higher values than those calculated over SURROGATE series. This result held for both TE and CTE markers regardless of the conditioning signal. During SB, TE was significant over the original data compared to SURROGATE, while CTE indexes were similar along the pressure-to-flow pathway. This finding was detected in both the groups and held regardless of the conditioning signal (Table 4.11 and Table 4.14). Conversely, along the reverse pathway the CTE markers computed over ORIGINAL data were significantly higher than those over the SURROGATE series with the notable exception of $CTE_{MCBv \rightarrow MAP|RCM}$ in the CONTROL group.

The grouped error bar graphs in Figure 4.2 show the comparison of TE (black bars), $CTE|EtCO_2$ (light grey bars) and CTE|RCM (dark grey bars) at BASELINE, during STAND and during SB in POTS (Figure 4.2.a and Figure 4.2.b) and in CONTROL (Figure 4.2.c and Figure 4.2.d). On the pressure-to-flow pathway (i.e., MAP→MCBv), SB increases the information transfer compared to BASELINE and STAND. This increase was more evident in CONTROL group (Figure 4.2.c) than in POTS one (Figure 4.2.a). On the pressure-to-flow pathway, conditioning has no effect at BASELINE and during STAND but increased the information transfer during SB. In POTS $CTE_{MAP \rightarrow MCBv|EtCO2}$ was larger than TE and $CTE_{MAP \rightarrow MCBv|RCM}$ (Figure 4.2.a), while in CONTROL $CTE_{MAP \rightarrow MCBv|RCM}$ was above TE and $CTE_{MAP \rightarrow MCBv|EtCO2}$ (Figure 4.2.c). On the flow-to-pressure pathway (i.e., MCBv→MAP), the increment induced by SB is statistically significant in CONTROL for CTE but not for TE (Figure 4.2.d). Indeed, at SB $TE_{MCBv \rightarrow MAP}$ is statistically lower than $CTE_{MCBv \rightarrow MAP|RCM}$ and $CTE_{MCBv \rightarrow MAP|EtCO2}$. In POTS, an increment of information transfer is detected in SB when compared to STAND via $CTE_{MCBv \rightarrow MAP|RCM}$ (Figure 4.2.b). Moreover, $CTE_{MCBv \rightarrow MAP|RCM}$ is lower than $TE_{MCBv \rightarrow MAP}$ and $CTE_{MCBv \rightarrow MAP|RCM}$ at BASELINE and STAND.

The grouped error bar graphs in Figure 4.3 compare the information transfer indexes computed in the different groups, namely CONTROL (black bars) and POTS (grey bars) as a function of the experimental condition. On both pathways (i.e., MAP→MCBv and MCBv→MAP), an increase is observed during SB compared to BASELINE and STAND regardless of the information transfer index with the notable exception of $TE_{MCBv \rightarrow MAP}$ in POTS (Figure 4.2.b). At BASELINE and during STAND information transfer indexes computed over CONTROL and POTS were not different and these results held regardless of the direction of the interactions. POTS group featured a lower information transfer compared to CONTROL individuals during SB and this difference was statistically significant for $TE_{MAP \rightarrow MCBv}$ (Figure 4.2.a), $CTE_{MAP \rightarrow MCBv|RCM}$ (Figure 4.2.c), $CTE_{MCBv \rightarrow MAP|RCM}$ (Figure 4.2.d), and $CTE_{MCBv \rightarrow MAP|EtCO2}$ (Figure 4.2.f).

Table 4.6. Cardiovascular and respiratory parameters in CONTROL and POTS group at BASELINE, during STAND and SB in the POTS protocol.

	CONTROL			POTS		
	BASELINE	**STAND**	**SB**	**BASELINE**	**STAND**	**SB**
μ_{HP} [ms]	808.4 ± 114.1	726.2 ± 95.7	822.2 ± 87.9	704.4 ± 122.1 °	679.9 ± 172.4	756.6 ± 193.3
σ^2_{HP} [ms^2]	3484.3 ± 3024.7	2241.5 ± 1753.6	9282.7 ± 6938.7 *#	1465.5 ± 1190.5	1769.3 ± 1717.7	4858.1 ± 4343.5 *°
HF_{HP} [ms^2]	714.3 ± 938.9	404.7 ± 607.7	1204.8 ± 1665.5	246.3 ± 295.9	262.3 ± 444.8	414.1 ± 482.8 °
μ_{SAP} [mmHg]	108.5 ± 19.7	120.6 ± 20.8	121 ± 17.7	118.5 ± 14.5	130.9 ± 15.4	117.7 ± 16.9
σ^2_{SAP} [$mmHg^2$]	14.3 ± 7.9	20.4 ± 12	32.5 ± 26.2 *	14.6 ± 13.8	18.9 ± 13.4	27.1 ± 18.1
LF_{SAP} [$mmHg^2$]	3.3 ± 3.9	7.5 ± 6.4	22.7 ± 18.7 *#	4.3 ± 4.7	9.3 ± 9.3	18.4 ± 15.8 *
f_{Resp} [breaths/min]	14 ± 3.7	12.2 ± 5.4	8.4 ± 1.2 *#	14.2 ± 3.9	13.5 ± 3.5	8.6 ± 2.1 *#
μ_{EtCO2} [mmHg]	39.4 ± 3.2	38.3 ± 4.6	36.8 ± 4.3	38.7 ± 3.2	37.7 ± 3	37.9 ± 2.6
σ^2_{EtCO2} [mmHg2]	0.8 ± 0.7	1.4 ± 0.8	1.1 ± 1.2	0.7 ± 0.6	1 ± 0.5	1.4 ± 1.4

HP = heart period; μ_{HP} = HP mean; σ^2_{HP} = HP variance; SAP = systolic arterial pressure; μ_{SAP} = SAP mean; $\sigma 2_{SAP}$ = SAP variance; LF = low frequency; HF = high frequency; HF_{HP} = power of the HP series in the HF band; LF_{SAP} = power of the SAP series in the LF band; RCM = respiratory chest movement; f_{Resp} = respiratory frequency computed from RCM; CO_2 = carbon dioxide; $EtCO_2$ = partial pressure of the CO_2 at the end of exhalation; μ_{EtCO2} = $EtCO_2$ mean; σ^2_{EtCO2} = $EtCO_2$ variance. Results are reported as mean ± standard deviation. The symbols * and # indicate a $p<0.05$ versus BASELINE and STAND, respectively, within the same group (i.e., CONTROL or POTS). The symbol ° indicates a $p<0.05$ versus CONTROL within the same experimental condition (i.e., BASELINE, STAND or SB).

Table 4.7. Cerebrovascular parameters in CONTROL and POTS groups at BASELINE, during STAND and SB in the POTS protocol.

	CONTROL			POTS		
	BASELINE	**STAND**	**SB**	**BASELINE**	**STAND**	**SB**
μ_{MAP} [mmHg]	82.2 ± 17.3	94.8 ± 16.7	90.7 ± 12	91.2 ± 12.7	103.7 ± 15	90 ± 16.1
σ^2_{MAP} [mmHg^2]	6.6 ± 4.1	8.2 ± 4.5	13.6 ± 11.1 *	5.9 ± 2.1	8.8 ± 5.2	12 ± 10
LF_{MAP} [mmHg^2]	1.8 ± 2.2	4.2 ± 5.4	4.3 ± 2.9	1.9 ± 1.8	5.7 ± 5 *	4 ± 4
μ_{MCBv} [cm s^{-1}]	55.3 ± 15	52.2 ± 14.3	40.7 ± 8.9 *	56.8 ± 14.9	54.6 ± 17.1	44.2 ± 14.9
σ^2_{MCBv} [cm^2·s^{-2}]	30.2 ± 20.5	33.2 ± 22.8	45.8 ± 28.2	31.6 ± 17.5	45.8 ± 25.7	44.7 ± 29.1
LF_{MCBv} [cm^2·s^{-2}]	7 ± 6.9	7.3 ± 8.1	15 ± 16.3	8.3 ± 7.9	9.9 ± 9.4	14.3 ± 10.9

MCBv = mean cerebral blood velocity; μ_{MCBv} = MCBv mean; σ^2_{MCBv} = MCBv variance; MAP = mean arterial pressure; μ_{MAP} = MAP mean; σ^2_{MAP} = MAP variance; LF = low frequency; LF_{MCBv} = power of the MCBv series in the LF band; LF_{MAP} = power of the MAP series in the LF band. Results are reported as mean ± standard deviation. The symbol * indicates a $p<0.05$ versus BASELINE within the same group (i.e., CONTROL or POTS).

Table 4.8. Transfer function indexes in CONTROL and POTS groups at BASELINE, during STAND and SB in the POTS protocol.

	CONTROL			POTS		
	BASELINE	**STAND**	**SB**	**BASELINE**	**STAND**	**SB**
TFG [cm·s^{-1}·mmHg^{-1}]	2.6 ± 0.3	3.1 ± 0.3	2.6 ± 0.4	2.5 ± 0.3	3.1 ± 0.3	2.1 ± 0.6
TFP [rad]	0.6 ± 0.1	0.3 ± 0.1	0.6 ± 0.1	0.5 ± 0.1	0.6 ± 0.1	0.5 ± 0.2
K^2	0.84 ± 0.04	0.79 ± 0.05	0.77 ± 0.06	0.87 ± 0.05	0.85 ± 0.05	0.77 ± 0.09
ARI	5.6 ± 0.5	5.4 ± 0.5	6.1 ± 0.6	5.5 ± 0.5	6.0 ± 0.5	4.3 ± 1.0
ARI > 4	93%	79%	90%	85%	86%	50%

TFG = transfer function gain in the LF band; TFP = transfer function phase in the LF band; K^2 = squared coherence in the LF band; ARI= cerebral autoregulation index. Results are reported as mean ± standard deviation and as percentage for ARI>4.

Table 4.9 Information transfer indexes computed on ORIGINAL and SURROGATE pairs at BASELINE in POTS group in the POTS protocol.

POTS at BASELINE	**ORIGINAL**	**SURROGATE**
$TE_{MAP→MCBv}$	0.08±0.04	0.02±0.01 *
$CTE_{MAP→MCBv\|RCM}$	0.07±0.03	0.01±0.01 *
$CTE_{MAP→MCBv\|EtCO2}$	0.09±0.05	0.02±0.01 *
$TE_{MCBv→MAP}$	0.24±0.1	0.03±0.02 *
$CTE_{MCBv→MAP\|RCM}$	0.18±0.09	0.03±0.01 *
$CTE_{MCBv→MAP\|EtCO2}$	0.23±0.1	0.03±0.01 *

MAP = mean arterial pressure; MCBv = mean cerebral blood velocity; RCM = respiratory chest movement; CO_2 = carbon dioxide; $EtCO_2$ = partial pressure of the CO_2 at the end of exhalation; TE = transfer entropy; CTE = conditional TE; $TE_{MAP→MCBv}$ = TE from MAP to MCBv; $CTE_{MAP→MCBv|RCM}$ = CTE from MAP to MCBv when RCM is conditioned out; $CTE_{MAP→MCBv|EtCO2}$ = CTE from MAP to MCBv when $EtCO_2$ is conditioned out; $TE_{MCBv→MAP}$ = TE from MCBv to MAP; $CTE_{MCBv→MAP|RCM}$ = CTE from MCBv to MAP when RCM is conditioned out; $CTE_{MCBv→MAP|EtCO2}$ = CTE from MCBv to MAP when $EtCO_2$ is conditioned out. Results are reported as mean ± standard deviation. The symbol * indicates a $p<0.05$ versus ORIGINAL.

Table 4.10 Information transfer indexes computed on ORIGINAL and SURROGATE pairs at STAND in POTS group in the POTS protocol.

POTS during STAND	**ORIGINAL**	**SURROGATE**
$TE_{MAP→MCBv}$	0.09±0.04	0.02±0.01 *
$CTE_{MAP→MCBv\|RCM}$	0.07±0.03	0.02±0.01 *
$CTE_{MAP→MCBv\|EtCO2}$	0.09±0.04	0.02±0.02 *
$TE_{MCBv→MAP}$	0.23±0.14	0.03±0.02 *
$CTE_{MCBv→MAP\|RCM}$	0.18±0.12	0.02±0.01 *
$CTE_{MCBv→MAP\|EtCO2}$	0.23±0.13	0.03±0.01 *

MAP = mean arterial pressure; MCBv = mean cerebral blood velocity; RCM = respiratory chest movement; CO_2 = carbon dioxide; $EtCO_2$ = partial pressure of the CO_2 at the end of exhalation; TE = transfer entropy; CTE = conditional TE; $TE_{MAP→MCBv}$ = TE from MAP to MCBv; $CTE_{MAP→MCBv|RCM}$ = CTE from MAP to MCBv when RCM is conditioned out; $CTE_{MAP→MCBv|EtCO2}$ = CTE from MAP to MCBv when $EtCO_2$ is conditioned out; $TE_{MCBv→MAP}$ = TE from MCBv to MAP; $CTE_{MCBv→MAP|RCM}$ = CTE from MCBv to MAP when RCM is conditioned out; $CTE_{MCBv→MAP|EtCO2}$ = CTE from MCBv to MAP when $EtCO_2$ is conditioned out. Results are reported as mean ± standard deviation. The symbol * indicates a $p<0.05$ versus ORIGINAL.

Table 4.11 Information transfer indexes computed on ORIGINAL and SURROGATE pairs at SB in POTS group in the POTS protocol.

POTS during SB	**ORIGINAL**	**SURROGATE**
$TE_{MAP→MCBv}$	0.21±0.15	0.07±0.03 *
$CTE_{MAP→MCBv\|RCM}$	0.28±0.25	0.10±0.08
$CTE_{MAP→MCBv\|EtCO2}$	0.33±0.28	0.16±0.17
$TE_{MCBv→MAP}$	0.37±0.22	0.08±0.05 *
$CTE_{MCBv→MAP\|RCM}$	0.52±0.32	0.06±0.02 *
$CTE_{MCBv→MAP\|EtCO2}$	0.51±0.27	0.08±0.06 *

MAP = mean arterial pressure; MCBv = mean cerebral blood velocity; RCM = respiratory chest movement; CO_2 = carbon dioxide; $EtCO_2$ = partial pressure of the CO_2 at the end of exhalation; TE = transfer entropy; CTE = conditional TE; $TE_{MAP→MCBv}$ = TE from MAP to MCBv; $CTE_{MAP→MCBv|RCM}$ = CTE from MAP to MCBv when RCM is conditioned out; $CTE_{MAP→MCBv|EtCO2}$ = CTE from MAP to MCBv when $EtCO_2$ is conditioned out; $TE_{MCBv→MAP}$ = TE from MCBv to MAP; $CTE_{MCBv→MAP|RCM}$ = CTE from MCBv to MAP when RCM is conditioned out; $CTE_{MCBv→MAP|EtCO2}$ = CTE from MCBv to MAP when $EtCO_2$ is conditioned out. Results are reported as mean ± standard deviation. The symbol * indicates a $p<0.05$ versus ORIGINAL.

Table 4.12 Information transfer indexes computed on ORIGINAL and SURROGATE pairs at BASELINE in CONTROL group in the POTS protocol.

CONTROL at BASELINE	**ORIGINAL**	**SURROGATE**
$TE_{MAP→MCBv}$	0.07±0.05	0.02±0.01 *
$CTE_{MAP→MCBv\|RCM}$	0.06±0.03	0.01±0.01 *
$CTE_{MAP→MCBv\|EtCO2}$	0.07±0.05	0.01±0.01 *
$TE_{MCBv→MAP}$	0.28±0.22	0.02±0.02 *
$CTE_{MCBv→MAP\|RCM}$	0.24±0.21	0.03±0.02 *
$CTE_{MCBv→MAP\|EtCO2}$	0.28±0.22	0.03±0.01 *

MAP = mean arterial pressure; MCBv = mean cerebral blood velocity; RCM = respiratory chest movement; CO_2 = carbon dioxide; $EtCO_2$ = partial pressure of the CO_2 at the end of exhalation; TE = transfer entropy; CTE = conditional TE; $TE_{MAP→MCBv}$ = TE from MAP to MCBv; $CTE_{MAP→MCBv|RCM}$ = CTE from MAP to MCBv when RCM is conditioned out; $CTE_{MAP→MCBv|EtCO2}$ = CTE from MAP to MCBv when $EtCO_2$ is conditioned out; $TE_{MCBv→MAP}$ = TE from MCBv to MAP; $CTE_{MCBv→MAP|RCM}$ = CTE from MCBv to MAP when RCM is conditioned out; $CTE_{MCBv→MAP|EtCO2}$ = CTE from MCBv to MAP when $EtCO_2$ is conditioned out. Results are reported as mean±standard deviation. The symbol * indicates a $p<0.05$ versus ORIGINAL.

Table 4.13 Information transfer indexes computed on ORIGINAL and SURROGATE pairs at STAND in CONTROL group in the POTS protocol.

CONTROL during STAND	**ORIGINAL**	**SURROGATE**
$TE_{MAP→MCBv}$	0.11±0.05	0.03±0.01 *
$CTE_{MAP→MCBv\|RCM}$	0.09±0.06	0.03±0.02 *
$CTE_{MAP→MCBv\|EtCO2}$	0.12±0.06	0.04±0.01 *
$TE_{MCBv→MAP}$	0.28±0.3	0.03±0.02 *
$CTE_{MCBv→MAP\|RCM}$	0.25±0.25	0.03±0.01 *
$CTE_{MCBv→MAP\|EtCO2}$	0.3±0.3	0.03±0.01 *

MAP = mean arterial pressure; MCBv = mean cerebral blood velocity; RCM = respiratory chest movement; CO_2 = carbon dioxide; $EtCO_2$ = partial pressure of the CO_2 at the end of exhalation; TE = transfer entropy; CTE = conditional TE; $TE_{MAP→MCBv}$ = TE from MAP to MCBv; $CTE_{MAP→MCBv|RCM}$ = CTE from MAP to MCBv when RCM is conditioned out; $CTE_{MAP→MCBv|EtCO2}$ = CTE from MAP to MCBv when $EtCO_2$ is conditioned out; $TE_{MCBv→MAP}$ = TE from MCBv to MAP; $CTE_{MCBv→MAP|RCM}$ = CTE from MCBv to MAP when RCM is conditioned out; $CTE_{MCBv→MAP|EtCO2}$ = CTE from MCBv to MAP when $EtCO_2$ is conditioned out. Results are reported as mean ± standard deviation. The symbol * indicates a $p<0.05$ versus ORIGINAL.

Table 4.14 Information transfer indexes computed on ORIGINAL and SURROGATE pairs at SB in CONTROL group in the POTS protocol.

CONTROL during SB	**ORIGINAL**	**SURROGATE**
$TE_{MAP→MCBv}$	0.33±0.15	0.16±0.10 *
$CTE_{MAP→MCBv\|RCM}$	0.52±0.29	0.50±0.25
$CTE_{MAP→MCBv\|EtCO2}$	0.38±0.22	0.29±0.17
$TE_{MCBv→MAP}$	0.49±0.21	0.28±0.15 *
$CTE_{MCBv→MAP\|RCM}$	0.94±0.49	0.67±0.31
$CTE_{MCBv→MAP\|EtCO2}$	0.91±0.41	0.56±0.28 *

MAP = mean arterial pressure; MCBv = mean cerebral blood velocity; RCM = respiratory chest movement; CO_2 = carbon dioxide; $EtCO_2$ = partial pressure of the CO_2 at the end of exhalation; TE = transfer entropy; CTE = conditional TE; $TE_{MAP→MCBv}$ = TE from MAP to MCBv; $CTE_{MAP→MCBv|RCM}$ = CTE from MAP to MCBv when RCM is conditioned out; $CTE_{MAP→MCBv|EtCO2}$ = CTE from MAP to MCBv when $EtCO_2$ is conditioned out; $TE_{MCBv→MAP}$ = TE from MCBv to MAP; $CTE_{MCBv→MAP|RCM}$ = CTE from MCBv to MAP when RCM is conditioned out; $CTE_{MCBv→MAP|EtCO2}$ = CTE from MCBv to MAP when $EtCO_2$ is conditioned out. Results are reported as mean ± standard deviation. The symbol * indicates a $p<0.05$ versus ORIGINAL.

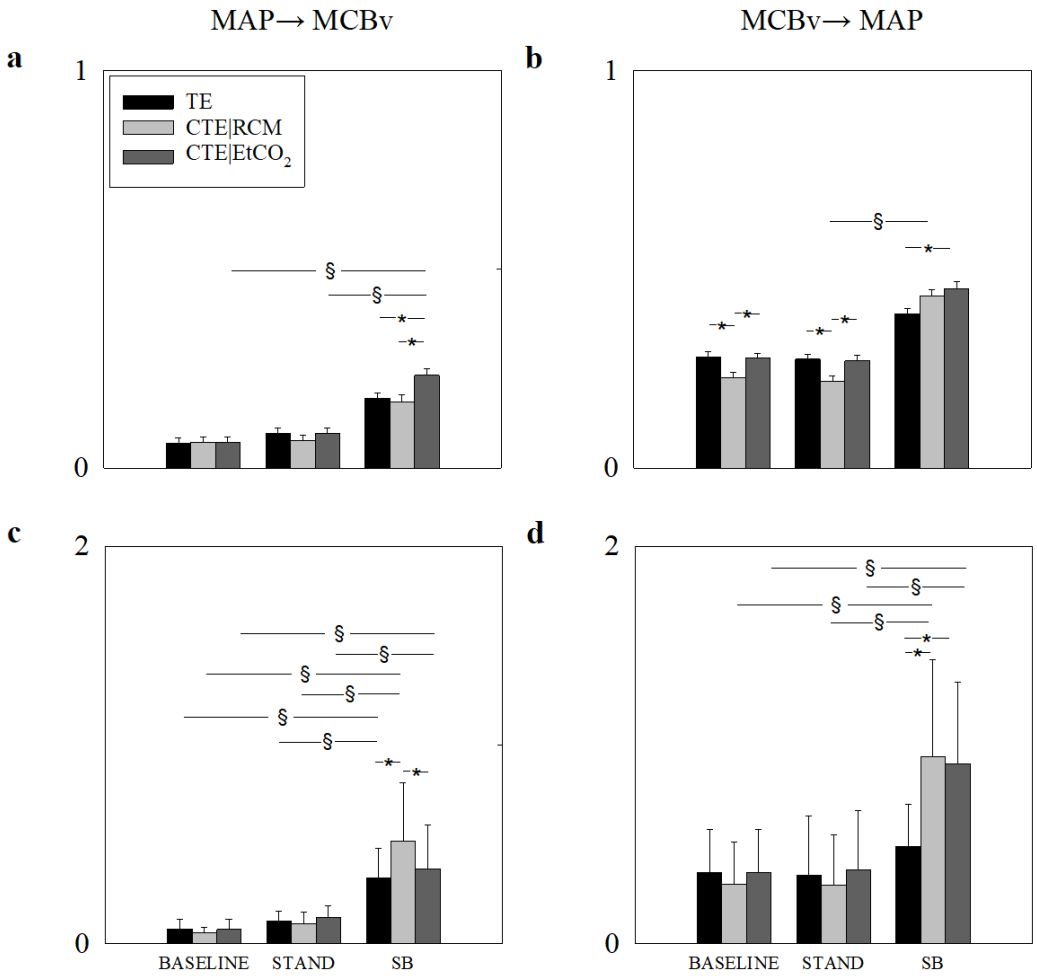

*Figure 4.2 Comparison of information transfer indexes (i.e., TE, CTE|RCM and CTE|EtCO₂) computed at BASELINE, during STAND and SB in POTS (a,b) and in CONTROL (c,d) on the pressure-to-flow (a,c) and on the flow-to-pressure (b,d) pathways in the POTS protocol. The symbol * indicates significant differences between markers within the same experimental condition (i.e., BASELINE, STAND and SB), while the symbol § indicates a significant difference between experimental condition withing the same type of information transfer indexes.*

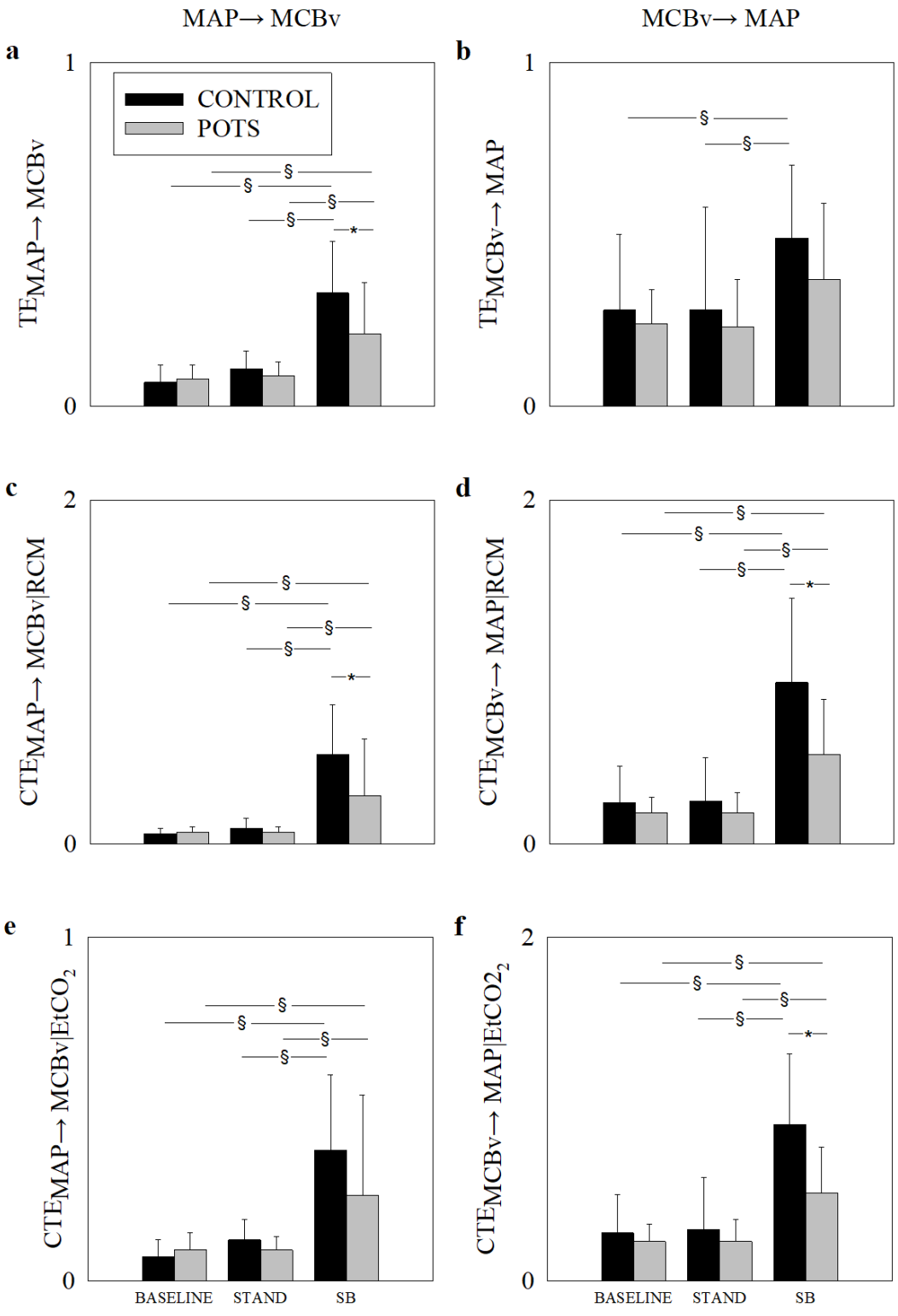

*Figure 4.3 TE (a,b), CTE|RCM (c,d) and CTE|$EtCO_2$ (e,f) computed at BASELINE, during STAND and SB in POTS and in CONTROL on the pressure-to-flow (a,c,e) and on the flow-to-pressure (b,d,f) pathways in the POTS protocol. The symbol * indicates significant differences between groups (i.e., CONTROL and POTS) within the same experimental condition (i.e., BASELINE, STAND and SB), while the symbol § indicates a significant difference between experimental condition withing the same group.*

4.4 Results of the STROKE protocol

One subject was discarded in CONTROL for poor quality of the signals. One subject was discarded in the STROKE for poor quality of the CBv signal recorded from the UNAFFECTED hemisphere.

4.4.1 Variability markers

Table 4.15 compares the cardiovascular and respiratory parameters in CONTROL and STROKE populations. A higher μ_{MAP} and σ^2_{MAP} concomitant with a mild hypocapnia, as indicated by a lower μ_{EtCO2}, and an increased σ^2_{EtCO2} were detected in the STROKE group when compared to the CONTROL one. The mild hypocapnia was independent on the f*resp*, which was similar in the two groups.

Table 4.16 compares the cerebrovascular parameters in CONTROL and STROKE populations. In the STROKE group a mild hypoperfusion was detected, as indicated by a lower μ_{MCBv}, compared to CONTROL subjects. The decrease was significantly in the AFFECTED hemisphere.

4.4.2 CA indexes

Table 4.17 reports the indexes derived from TFA. No differences were detected between STROKE and CONTROL and this result held regardless of the hemisphere.

Table 4.18, Table 4.19 and Table 4.20 summarize the information transfer indexes computed on ORIGINAL and SURROGATE pairs. Regardless of the group, namely CONTROL (Table 4.18), STROKE in the UNAFFECTED hemisphere (Table 4.19) and STROKE in the

Table 4.15. Cardiovascular and respiratory parameters in CONTROL and STROKE subjects in the STROKE protocol.

	CONTROL	**STROKE**
μ_{MAP} [mmHg]	90.2±8.4	103.1±17.7 *
σ^2_{MAP} [mmHg^2]	6±4.2	19.4±17.3 *
LF_{MAP} [mmHg^2]	0.7±0.8	2.8±5.3
μ_{EtCO2} [mmHg]	38.3±2.3	33.7±3.9 *
σ^2_{EtCO2} [mmHg^2]	2.4±9.3	4.9±12.3 *
f_{Resp} [breaths/min]	17.6±4.2	16.6±5.2

MAP = mean arterial pressure; μ_{MAP} = MAP mean; σ^2_{MAP} = MAP variance; LF = low frequency; LF_{MAP} = power of the MAP series in the LF band; CO_2 = carbon dioxide; $EtCO_2$ = partial pressure of the CO_2 at the end of exhalation; μ_{EtCO2} = $EtCO_2$ mean; σ^2_{EtCO2} = $EtCO_2$ variance; f*resp* = respiratory frequency. Results are reported as mean ± standard deviation. The symbol * indicates a $p<0.05$ versus CONTROL.

Table 4.16. Cerebrovascular and respiratory parameters in CONTROL and STROKE subjects in the UNAFFECED and AFFECTED hemisphere in the STROKE protocol.

	CONTROL	**STROKE Unaffected**	**STROKE Affected**
μ_{MCBv} [cm s^{-1}]	52.3±13	45.5±14.7	41.7±15.9 *
σ^2_{MCBv} [cm^2·s^{-2}]	7.2±6.3	9.7±9.9	6.4±5.6
LF_{MCBv} [cm^2·s^{-2}]	0.7±0.65	0.85±1.21	1.03±1.77

MCBv = mean cerebral blood velocity; μ_{MCBv} = MCBv mean; σ^2_{MCBv} = MCBv variance; LF = low frequency; LF_{MCBv} = power of the MCBv series in the LF band. Results are reported as mean ± standard deviation. The symbol * indicates a

AFFECTED hemisphere (Table 4.20), directionality (i.e., MAP→MCBv and MCBv→MAP) or the information domain parameters (i.e., TE and CTE|$EtCO_2$), markers computed over the ORIGINAL series featured significantly higher values than those calculated over the SURROGATE pairs.

Figure 4.4 compares the information transfer indexes, namely TE (black bars) and CTE|$EtCO_2$ (grey bars), computed in the different groups, namely CONTROL, STROKE in the UNAFFECTED hemisphere and STROKE in the AFFECTED hemisphere. On both pathways (i.e., MAP→MCBv and MCBv→MAP), no significant differences are observed between TE and CTE|$EtCO_2$ and this finding was detected regardless of the group. On the pressure-to-flow pathway (i.e., MAP→MCBv), the indexes detect a significant decrease in the STROKE population and this result held regardless of the hemisphere (Figure 4.4.a). Conversely, along the flow-to-pressure pathway (i.e., MCBv→MAP), STROKE group exhibited a tendency toward higher values of TE and CTE|$EtCO_2$ than CONTROL subjects in both hemispheres (Figure 4.4.b).

Table 4.17. Transfer function indexes in CONTROL and STROKE subjects in the UNAFFECTED and AFFECTED hemisphere in the STROKE protcol.

	CONTROL	**STROKE Unaffected**	**STROKE Affected**
TFG [$cm \cdot s^{-1} \cdot mmHg^{-1}$]	1.4 ± 0.49	1.28 ± 0.77	1.36 ± 0.82
TFP [rad]	0.6 ± 0.24	0.56 ± 0.38	0.57 ± 0.36
K^2	0.84 ± 0.13	0.8 ± 0.16	0.77 ± 0.16
ARI	4.87 ± 1.47	4.8 ± 2.18	4.65 ± 1.88
ARI > 4	72%	68%	69%

TFG = transfer function gain in the LF band; TFP = transfer function phase in the LF band; K^2 = squared coherence in the LF band; ARI= cerebral autoregulation index. Results are reported as mean ± standard deviation and as percentage for ARI>4.

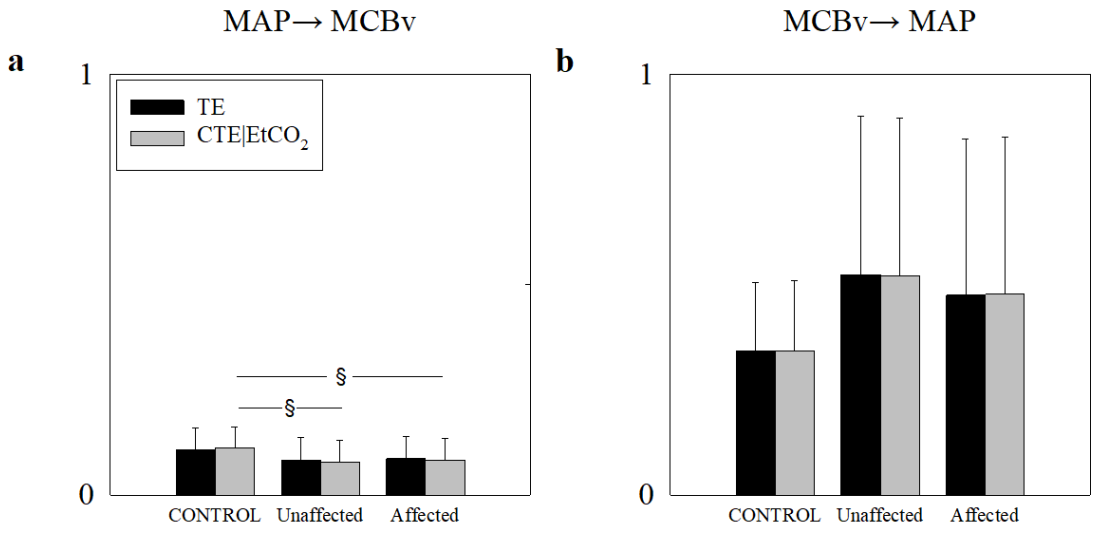

Figure 4.4 Comparison of information transfer indexes (i.e., TE, CTE|RCM and CTE|$EtCO_2$) computed over CONTROL, STROKE in the UNAFFECTED hemisphere and STROKE in the AFFECTED hemisphere along the pressure-to-flow (a) and on the flow-to-pressure (b) pathways in the STROKE protocol. The symbol § indicates a $p<0.05$ versus CONTROL within the same information domain marker (i.e., TE or CTE|$EtCO_2$).

Table 4.18. Information transfer indexes computed over ORIGINAL and SURROGATE pairs in CONTROL subjects of the STROKE protocol.

CONTROL	**ORIGINAL**	**SURROGATE**
$TE_{MAP \rightarrow MCBv}$	0.11±0.05	0.02±0.01 *
$CTE_{MAP \rightarrow MCBv \mid EtCO2}$	0.12±0.05	0.01±0.01 *
$TE_{MCBv \rightarrow MAP}$	0.34±0.16	0.03±0.01 *
$CTE_{MCBv \rightarrow MAP \mid EtCO2}$	0.34±0.16	0.03±0.01 *

MAP = mean arterial pressure; MCBv = mean cerebral blood velocity; CO_2 = carbon dioxide; $EtCO_2$ = partial pressure of the CO_2 at the end of exhalation; TE = transfer entropy; CTE = conditional TE; $TE_{MAP \rightarrow MCBv}$ = TE from MAP to MCBv; $CTE_{MAP \rightarrow MCBv \mid EtCO2}$ = CTE from MAP to MCBv when $EtCO_2$ is conditioned out; $TE_{MCBv \rightarrow MAP}$ = TE from MCBv to MAP; $CTE_{MCBv \rightarrow MAP \mid EtCO2}$ = CTE from MCBv to MAP when $EtCO_2$ is conditioned out. Results are reported as mean ± standard deviation. The symbol * indicates a $p<0.05$ versus ORIGINAL.

Table 4.19. Information transfer indexes computed over ORIGINAL and SURROGATE pairs in STROKE subjects in the UNAFFECTED hemisphere in the STROKE protocol.

STROKE Unaffected	**ORIGINAL**	**SURROGATE**
$TE_{MAP \rightarrow MCBv}$	0.08±0.05	0.02±0.01 *
$CTE_{MAP \rightarrow MCBv \mid EtCO2}$	0.08±0.02	0.02±0.01 *
$TE_{MCBv \rightarrow MAP}$	0.52±0.37	0.02±0.01 *
$CTE_{MCBv \rightarrow MAP \mid EtCO2}$	0.52±0.37	0.02±0.01 *

MAP = mean arterial pressure; MCBv = mean cerebral blood velocity; CO_2 = carbon dioxide; $EtCO_2$ = partial pressure of the CO_2 at the end of exhalation; TE = transfer entropy; CTE = conditional TE; $TE_{MAP \rightarrow MCBv}$ = TE from MAP to MCBv; $CTE_{MAP \rightarrow MCBv \mid EtCO2}$ = CTE from MAP to MCBv when $EtCO_2$ is conditioned out; $TE_{MCBv \rightarrow MAP}$ = TE from MCBv to MAP; $CTE_{MCBv \rightarrow MAP \mid EtCO2}$ = CTE from MCBv to MAP when $EtCO_2$ is conditioned out. Results are reported as mean ± standard deviation. The symbol * indicates a $p<0.05$ versus ORIGINAL.

Table 4.20. Information transfer indexes computed over ORIGINAL and SURROGATE pairs in STROKE subjects in the AFFECTED hemisphere in the STROKE protocol.

STROKE Affected	**ORIGINAL**	**SURROGATE**
$TE_{MAP \rightarrow MCBv}$	0.09±0.05	0.02±0.01 *
$CTE_{MAP \rightarrow MCBv \mid EtCO2}$	0.08±0.05	0.02±0.01 *
$TE_{MCBv \rightarrow MAP}$	0.48±0.37	0.03±0.01 *
$CTE_{MCBv \rightarrow MAP \mid EtCO2}$	0.47±0.38	0.02±0.01 *

MAP = mean arterial pressure; MCBv = mean cerebral blood velocity; CO_2 = carbon dioxide; $EtCO_2$ = partial pressure of the CO_2 at the end of exhalation; TE = transfer entropy; CTE = conditional TE; $TE_{MAP \rightarrow MCBv}$ = TE from MAP to MCBv; $CTE_{MAP \rightarrow MCBv \mid EtCO2}$ = CTE from MAP to MCBv when $EtCO_2$ is conditioned out; $TE_{MCBv \rightarrow MAP}$ = TE from MCBv to MAP; $CTE_{MCBv \rightarrow MAP \mid EtCO2}$ = CTE from MCBv to MAP when $EtCO_2$ is conditioned out. Results are reported as mean ± standard deviation. The symbol * indicates a $p<0.05$ versus ORIGINAL.

CHAPTER 5 - Discussion

5.1 Introduction

The following chapter discusses the results obtained from the three experimental protocols and their significance in the study of directional cerebrovascular interactions. In Sect.5.2 the findings derived from the surrogate analysis are discussed with a focus on the necessity of a directional approaches for a more complete understanding of dCA. In Sect.5.3 the relevance of a closed-loop approach to the evaluation of dCA is highlighted. Sect.5.4 analyses the methodological findings about conditioning the information transfer compared to traditional bivariate TE and differentiates results according to the type of respiratory signal. Sect.5.5 and Sect.5.7 discuss, respectively, the effects of orthostatic challenge in healthy individuals and in POTS. The impact of SB on cerebrovascular information transfer was evaluated in Sect.5.7. In Sect.5.8 the most relevant results of STROKE protocol are analysed in relation to cerebrovascular impairment. Finally, Sect.5.9 addresses the main limitations of the methodologies and experimental protocols included in the thesis.

5.2 The strength of the interaction between MAP and MCBv is significant along both the causal directions

In the present thesis, a causal multivariate approach has been exploited to investigate bidirectional cerebrovascular information transfer. On one direction, the pathway from MAP to MCBv is usually exploited when assessing dCA (Tiecks et al., 1995). On the other direction, the reverse causal pathway, namely from MCBv to MAP, describes the response of the cerebrovascular system to an increase in ICP, usually referred to as the Cushing reflex (Cushing, 1902; Grady & Blaumanis, 1988; McBryde et al., 2017).

The causal approach requires an assessment of the significance of the information transfer, estimated from real data. Indeed, non-null values of the causality metrics (i.e., TE and CTE) do not *per se* mean a significant level of coupling (Porta & Faes, 2016). Therefore, the null hypothesis of absence of dynamic interactions among series was tested by assessing the markers over surrogate series. The null hypothesis was rejected whether the markers computed over the original series were above the values computed over a set of surrogate pairs constructed according to the null hypothesis. Surrogate series were built by imposing a random, sufficiently long, latency from MAP to MCBv variability series (Andrzejak et al., 2003). So that, in surrogate pairs, the temporal dynamics of MAP and MCBv were not modified, but the coupling between MAP and MCBv was destroyed.

Both TE and CTE could differentiate original and surrogate pairs, and this result held regardless of the protocol, experimental condition and type of information domain markers. Only in POTS protocol, during SB the CTE, mainly from MAP to MCBv, featured a much more limited statistical power in separating original from surrogate pairs. This result was evident in both CONTROL and POTS groups and held regardless of the conditioning signal as a likely result of the more limited length of SB featuring a few cycles of paced breathing compared to the analysis at BASELINE and during STAND.

The surrogate analysis highlights the significant presence of interactions between cerebrovascular variability series in both causal directions, stressing the necessity of a closed-loop approach (Bari et al., 2017; Saleem et al., 2018; Vaini et al., 2019). Non-causal traditional methods, such as those based on non-parametric TF estimation, hypothesize an open-loop pressure-to-flow relationship, disregarding the feedback pathway. In this thesis, TE and CTE could differentiate on both pathways between physiological cerebrovascular interactions in real

data and the absence of dynamic interaction in surrogate pairs. Remarkably, the relevance of the closed-loop interactions held regardless of the type of information domain indexes, suggesting that the inclusion of confounding factors was not able to explain the presence of feedback. This result confirms previous findings (Gelpi et al., 2023; Saleem et al., 2018) which identified a significant level of bidirectional interactions and stressed the importance of assessing the reverse causal pathway along the flow-to-pressure direction.

Future works could exploit this finding by investigating beyond the mere information transformation transfer. Indeed, the causal bivariate approach allows for estimation of directional step responses that could be investigated and integrated into the cerebrovascular step response model first introduced by Tiecks (Gelpi et al., 2022).

5.3 On the relevance of estimating bidirectional causal interactions

The information transfer indexes highlighted significant variations between experimental conditions and populations that were not detected by traditional approach indexes. Given their open-loop approach, traditional non-causal metrics based on TFA are much less powerful in separating experimental conditions and populations. Therefore, a directional approach can give better insights on dCA functioning and impairment than non-causal methods.

One of the most impressive differences between information transfer markers computed along the different causal directions is detected in the STROKE protocol. In STROKE, both TE and CTE|$EtCO_2$ decreased along the pressure-to-flow, while they increased along the flow-to-pressure. This result is the likely consequence of the impairment of dCA reducing the strength of the relation from MAP to MCBv, and the activation of the Cushing reflex along the flow-to-pressure pathway in relation to the cerebral hypoperfusion. Remarkably, TFA markers and ARI were not able to distinguish CONTROL subjects from STOKE subjects.

Additional evidence supporting the relevance of causality analysis is the possibility offered by both TE and CTE|RCM to separate CONTROL individuals from POTS subjects during SB. Indeed, SB is known to increase respiratory sinus arrhythmia and likely evoked a vagal activation. This separation was not achieved via more traditional indexes of dCA characterization such as TFA markers and ARI.

5.4 Effects of conditioning respiratory signals on closed-loop cerebrovascular interactions

This thesis assessed the information transferred from MAP to MCBv and vice versa via TE and CTE conditioning out RCM and $EtCO_2$. TE and CTE were explicitly compared in each protocol for each specific experimental condition and population to help identify the respiratory disturbances that might mix up causal relationships between MAP and MCBv.

5.4.1 Effects of conditioning out RCM

The impact of conditioning out RCM over the pathway from MAP to MCBv is very limited during free breathing. Indeed, $TE_{MAP\rightarrow MCBv}$ and $CTE_{MAP\rightarrow MCBv|RCM}$ were similar, and this conclusion held regardless of the protocol in experimental conditions under natural breathing conditions. An increase in $CTE_{MAP\rightarrow MCBv|RCM}$ compared to $TE_{MAP\rightarrow MCBv}$ was observed only during SB, thus suggesting modelling respiratory influences might be useful only when respiratory fluctuations of AP are more important.

The impact of RCM is much more important on the pathway from MCBv to MAP during spontaneous breathing. Indeed, in both HEALTHY and POTS protocols, $CTE_{MCBv\rightarrow MAP|RCM}$ was lower than $TE_{MCBv\rightarrow MAP}$ at resting conditions and during orthostatic challenge. Conversely, during SB the information transfer conditioned on RCM increased compared to TE. RCM signal

is usually considered to be a surrogate of the intrathoracic pressure inducing respiratory oscillations of MCBv, mediated by changes in intracranial pressure driven by respiratory movements of cerebrospinal fluid (Porta et al., 2022; Yildiz et al., 2017) and modifications of MAP because of the respiratory synchronization of right and left stroke volumes (Elstad et al., 2018; Toska & Eriksen, 1993).

The different impact of RCM on the pressure-to-flow pathway compared to the flow-to-pressure one suggests that when modelling dCA accounting for RCM might be important only during controlled breathing at a slow breathing rate. Conversely, describing mechanical respiratory influences is much more important when assessing the reverse pathway. Indeed, the intracranial pressure can change on a breath-to-breath basis, and this modification might have a confounding effect on causality estimation along the Cushing reflex. Remarkably, accounting RCM might increase or decrease information transfer compared to TE, thus making less predictable the impact of RCM over the strength of the interactions.

5.4.2 Effects of conditioning out $EtCO_2$

The impact of conditioning out $EtCO_2$ was negligible during experimental conditions featuring spontaneous breathing. Indeed, in both the directions of the interactions no differences were detected between TE and CTE|$EtCO_2$ in CONTROL and POTS subjects while resting and during postural challenge. Since $EtCO_2$ can be taken as an indicator of $PaCO_2$, $EtCO_2$ is an important confounding factor for the pressure-to-flow relationship given that alterations of $PaCO_2$ change MCBv regardless of MAP variations via modulations of CA (Ogoh, 2019). In this thesis, the effect of $PaCO_2$ on the closed-loop interactions between MAP and MCBv was not evidently detected using $EtCO_2$ as a conditioning signal. We hypothesize that the oscillations of $EtCO_2$ are too slow to have an impact on the dynamic component of the CA (Gelpi et al., 2023). Conversely, the impact of $EtCO_2$ was much more evident during SB in which CTE|$EtCO_2$ was higher than TE on both the pathways of the closed-loop.

5.5 Cerebrovascular response to the orthostatic challenge in healthy individuals

Orthostatic challenges such as TILT are valuable tests to assess cardiovascular autonomic regulation and dCA, especially in populations with suspected dysautonomia (Bari et al., 2017; Carey et al., 2001; Kenny et al., 1986; Wells et al., 2020). TILT rapidly and passively moves the subject from a supine to an upright position. It induces a gravitational shift in blood volume in the lower extremities, thus producing a baroreflex unloading and consequent sympathetic activation. As a result, TILT can evaluate the integrity of the autonomic response and the ability of peripheral microcirculation to constrict appropriately to maintain CPP (Kenny et al., 1986).

In the HEALTHY protocol, the subject during TILT responded with the expected autonomic response (Marchi et al., 2013; Pomeranz et al., 1985). Interestingly, at REST elevated AP pressure (i.e., SAP > 120 mmHg) was observed in these young subjects, without any overt hypertension. This might be attributed to the “white coat effect” or the emotions related to the TILT test. Nevertheless, during TILT, the decrease of μ_{HP} and HF_{HP} indicates the vagal withdrawal, while the increase of LF_{SAP} suggests sympathetic activation. These modifications were observed in the CONTROL population of the POTS protocol during STAND but they were not significant because active standing is a much less powerful postural stimulus compared to TILT. Moreover, the statistical power was weaker considering that three experimental conditions were included in the analysis.

The orthostatic challenge also induced the well-known decrease in μ_{MCBv} (Carey et al., 2001; Grubb et al., 1991; Wells et al., 2020; Zhang, Zuckerman, & Levine, 1998). This result is the likely consequence of the sympathetic activation associated with TILT increasing

cerebrovascular resistance, rather than indicating an impairment in dCA (Carey et al., 2001; Gelpi et al., 2022). The rise of the spectral indexes of MCBv variability computed in a range of frequencies under autonomic control observed during TILT (Hamner et al., 2010), namely LF_{MCBv}, can be explained by the increase of the LF_{MAP}, leaving unmodified the MCBv variation per unit variation of MAP, as indicated by the TFG and consequently the dCA (Gelpi et al., 2022). Similar considerations were held in the CONTROL population of the POTS protocol during STAND.

A decrease in μ_{MCBv} may be linked to hypotension and hypocapnia (Minhas et al., 2019). In both the HEALTHY and POTS protocols, we did not observe any reduction in AP during the TILT and STAND phases, respectively, suggesting that hypotension is not a direct factor. In the POTS protocol, we can exclude the effect of hypocapnia since the subjects performed the STAND phase under normocapnic conditions. While in the HEALTHY protocol, we cannot rule out the possibility that the decrease in μ_{MCBv} was a result of hypocapnia, as carbon dioxide levels were not recorded.

Surprisingly, the percentage of ARI below the threshold of dCA impairment (i.e., ARI<4) in the HEALTHY protocol was high at REST, and it did not increase during TILT. This result could be related to the low values of K^2 suggesting a limited significance of the MCBv-MAP relationship in this protocol. Indeed, a coherence around 0.30 has been indicated as the minimum level of association between MAP and MCBv for reliable cerebrovascular measurements (J. A. Claassen et al., 2015; Gommer et al., 2010). Another possible explanation for the high percentage of subjects with ARI below the impairment threshold in the HEALTHY protocol could be the constant bias related to ARI computation (Gelpi et al., 2022). While ARI methods were first developed to model the response of CA to induced sudden changes of BP up to 20 mmHg (Panerai et al., 2001), the application of the Tiecks' model on spontaneous fluctuations has been widely applied. However, these estimates highly depend on the method utilized for the computation, being estimates in the time domain (Mahdi et al., 2017), via non-parametric method based on Fourier transform (Panerai et al., 1998, 2001) or via parametric modelling approach (D. M. Simpson et al., 2001). In a previous study (Gelpi et al., 2022), it was reported that ARI estimates computed according to different methods might be uncorrelated and, even when correlated, might exhibit a significant bias. In the present thesis, it was preferred an historical method for ARI computation from the spontaneous variability of MAP and MCBv, namely the non-parametric method based on FFT (Panerai et al., 1998, 2001). This method was selected because it follows directly from the TF estimate via a fully non-causal technique, and this makes the comparison with the proposed causal approach more evident. This method was successful in detecting a significant number of subjects with ARI>4 in the CONTROL population of the POTS protocol at BASELINE and during STAND and in the CONTROL population of the STROKE protocol, likely due to the high K^2 compared to values in the HEALTHY protocol.

Despite the possible bias in ARI computation, all dCA indexes, including information transfer markers, agreed in detecting an effective response of dCA to the orthostatic challenge in the HEALTHY protocol. Indeed, both TFA indexes and information transfer markers, remained stable from REST to TILT. The results relevant to causality analysis held regardless of the pathway of the closed-loop, thus stressing the ability of dCA to cope with the challenge and making unnecessary a stronger intervention of the feedback. The negligible impact of postural challenge in healthy individuals was supported by the findings during STAND in the CONTROL population of the POTS protocol as well.

5.6 Cerebrovascular response to STAND in POTS subjects

The hyperadrenergic state in POTS appears to be evident at BASELINE compared to CONTROL subjects (Furlan et al., 1998). Indeed, at BASELINE, a significantly lower value of μ_{HP}, indicating tachycardia, and smaller HF_{HP} in POTS subjects than in CONTROL subjects suggest a reduced vagal control (Pomeranz et al., 1985). Moreover, during STAND LF_{SAP} exhibited a tendency towards higher values in POTS compared to CONTROL, thus corroborating the impression of (Marchi et al., 2013). This was confirmed by an analysis performed by directly comparing BASELINE and STAND. Indeed, a significant increase in LF_{SAP} could be detected in POTS when excluding the SB experimental condition.

STAND induced a decrease of μ_{MCBv} regardless of the pathology (Carey et al., 2001; Grubb et al., 1991; Wells et al., 2020; Zhang, Zuckerman, & Levine, 1998). A tendency toward a lower value of μ_{MCBv} was observed in the POTS group during STAND. This result is the likely consequence of the sympathetic activation, and it could not be attributed to modifications of $PaCO_2$ given that $\mu EtCO_2$ did not vary with STAND in both groups. Interestingly, in POTS, the variability of MCBv tendency to increase with STAND could be due to the greater contribution of MAP variability given by the stronger sympathetic activation (Gelpi et al., 2023).

Neither traditional non-causal nor directional causal methods could detect an impairment of the dCA response to orthostatic challenge in POTS. An increase in the information transfer from MAP to MCBv during an orthostatic challenge can be exploited to identify impairment in dCA (Bari et al., 2017). However, in the POTS group, regardless of the strategy adopted to compute information transfer (i.e., TE, CTE|RCM or CTE|$EtCO_2$), markers of directional association did not vary with STAND. These results were observed despite the sympathetic overactivation in POTS (Gelpi et al., 2023), thus suggesting the hyperadrenergic state cannot *per se* impair dCA. Moreover, the steadiness of the information transfer over the reverse pathway, namely from MAP to MCBv, confirms the preservation of the cerebrovascular control during STAND in POTS (Bari et al., 2017; Gelpi et al., 2023; Saleem et al., 2018), given that this pathway is responsible for continuous corrections of MAP when MCBv assumes inappropriate values (Cushing, 1902; McBryde et al., 2017).

5.7 SB effects on cerebrovascular information transfer in POTS

The vagal activation during SB is limited in the POTS group when compared to CONTROL. When breathing is performed at a slow pace, tidal volume tends to increase, leading to a more important stimulation of lung stretch receptors and to a more active gating of the vagal activity by the respiratory centres (Laborde et al., 2022). The result is an increase in respiratory sinus arrhythmia in healthy individuals. In the POTS protocol, subjects were requested to breathe at 8 breaths/min, slowing down their breathing compared to BASELINE (at around 14 breaths/min). The reduction of f_{RMC} compared to BASELINE confirmed that participants could perform the task in both CONTROL and POTS groups. Despite the subjects were performing the task for only 5 breaths, the expected rise of respiratory sinus arrhythmia was confirmed by the increase of HF_{HP} (Task Force of the European Society of Cardiology and the North American Society of Pacing and Electrophysiology, 1996) in the CONTROL group. Conversely, POTS exhibited a significantly lower value, thus suggesting a reduced vagal activation concomitant to the sympathetic activation typical of POTS (Furlan et al., 1998).

Remarkably, SB did not affect $PaCO_2$, as measured via $EtCO_2$ in both the CONTROL and POTS groups, as a likely consequence of the limited duration of the stimulus. Therefore, modifications in the $EtCO_2$ cannot explain the reduction of μ_{MCBv} during SB especially in the CONTROL subjects.

The information transfer indexes can detect variations in cerebrovascular control during SB, with differences between CONTROL and POTS. While transfer function-based and ARI markers did not vary, information transfer indexes strongly increased during SB especially in CONTROL individuals. This rise was evident over both the pressure-to-flow and flow-to-pressure pathways, suggesting that SB affects the closed-loop interaction between MAP and MCBv. Remarkably, traditional indexes could not differentiate between CONTROL and POTS during SB. Conversely, the information transfer indexes separate CONTROL subjects from POTS subjects. The lower values of all the indexes in POTS suggested a reduced ability to govern MCBv-MAP dynamic interactions as a likely consequence of their chronic state of sympathetic activation. This result suggests that the information transfer between the MCBv and MAP variability series might be favoured by a more active vagal control.

5.8 Directional cerebrovascular information transfer in STROKE

The STROKE population included in the thesis presented a deficit in cerebral perfusion. A reduced μ_{MCBv}, particularly evident in the AFFECTED hemisphere, was detected when compared to CONTROL subjects. After an ischemic stroke, the resulting cerebral oedema can increase ICP and decrease CPP, creating an additional barrier to the restoration of CBF (Fan et al., 2022; Panerai, 2008). The reduction of the CPP activates the flow-to-pressure pathway in the attempt to rise the CPP again.

A concomitant increase in AP was detected as well, with μ_{MAP} significantly higher in STROKE subjects than in CONTROL individuals. The acute elevation in AP, known as the acute hypertensive response, is commonly observed in the early period (for a few hours to a day) of ischemic stroke (Alqadri et al., 2013). In a portion of subjects, the hypertension is precedent to the ischemic event, being undiagnosed or inadequately treated (Alqadri et al., 2013). Indeed, hypertension is the most important risk factor for stroke: it induces endothelial dysfunction and increases shear stress and stiffness of the larger arteries that transmits pulsatile flow to the cerebral microcirculation (Cipolla et al., 2018). Irrespective of their prior hypertension, an abrupt rise in AP is a hallmark of ischemic stroke in ∼80% of patients (Britton et al., 1986). The rise could be the result of the Cushing response to hypoperfusion (Patarroyo & Anderson, 2012), or subjects with a history of chronic hypertension might have a higher limit of the autoregulatory range typically described by the Lassen's curve (Alqadri et al., 2013).

Despite the cerebral hypoperfusion and hypertension, STROKE subjects featured similar dCA when assessed with the traditional TFA and ARI indexes and this finding did not depend on the hemisphere. Remarkably, the AP rise identified in STROKE subjects was not large enough to overcome the autoregulatory limit of 150 mmHg. Thus, dCA impairment could not be detected since MAP variations were maintained within the traditional autoregulatory curve (Llwyd et al., 2019). Nevertheless, previous studies reported consistent findings concerning dCA impairment in the affected hemisphere associated with worse outcomes early after moderate-to-severe ischemic stroke (Elting et al., 2014; Nogueira et al., 2022). One reason for this inconsistency is that the STROKE population included in the thesis exhibited hypocapnia. Indeed, hypocapnia has a strong influence on improving dCA and could explain the lack of differences compared with the control group (Salinet et al., 2015). It could be hypothesized that the differences in TFA indexes and ARI could emerge if both groups had similar average values of $EtCO_2$.

Conversely, the information transfer indexes detected differences between STROKE and CONTROL individuals. Indeed, on the pressure-to-flow pathway, TE and CTE showed lower values in STROKE group regardless of the hemisphere. This result confirmed the previous studies using diverse methodologies to detect post-stroke dCA impairment (Elting et al., 2014; Nogueira et al., 2022). Considering the hypocapnia of the STROKE group, it could be

hypothesized that the decrease of TE in STROKE would be even more evident if CONTROL and STROKE groups were normalized to the same level of $EtCO_2$ (Salinet et al., 2015). Usually, an impairment of dCA takes the form of an increase of association between MAP and MCBv (Zhang et al., 2002) or the information transfer from MAP to MCBv (Bari et al., 2017). This result suggests that an impairment of dCA might be evident even when a decreased strength of the relationship from MAP to MCBv is detected. On the flow-to-pressure pathway, the information transfer increased on both hemispheres in STROKE subjects compared to CONTROL individuals. This increase suggests an activation of the Cushing reflex in response to the post-event hypoperfusion and this conclusion is corroborated by the hypertension. The absence of differences between AFFECTED and UNAFFECTED hemispheres suggests that the variation of cerebrovascular control in STROKE group is independent of the hemisphere, thus being uniform within the brain. The abovementioned conclusion did not depend on the type of information transfer index (i.e., TE or CTE), thus stressing the limed impact of $EtCO_2$ on dCA in presence of a very important influence on the static component of CA. The limited impact of $EtCO_2$ on the relationship from MAP to MCBv agrees with the finding reported in the POTS protocol when spontaneous breathing conditions were considered.

5.9 Limitations of the approach and experimental protocols

In this doctoral thesis, several limitations are commonly observed across the various protocols due to the need of using non-invasive measurements. Firstly, TCD was used to measure CBv, which is equivalent to CBF only if the vessel diameter does not vary. While previous studies observed only minor changes in MCA diameter (<4%) in response to AP variation or hypocapnia (Giller et al., 1993), more recent studies identified variations using high resolution magnetic resonance index (Al-Khazraji et al., 2019). In any of the protocols, MCA diameter was not assessed, limiting the strength of the results. Secondly, a direct measurement of sympathetic activity would directly assess the degree of activation of the adrenergic system (Pagani et al., 1997), confirming the findings extracted from the heart rate variability analysis and the involvement of autonomic nervous system in controlling dCA. Thirdly, the size of the groups is small, and this might have a direct impact on the statistical power of the studies. Unfortunately, the complexity of the protocols is the main factor limiting the size of the groups because all the signals must have been acquired simultaneously and must have comparable quality.

Moreover, in none of the protocols, the menstrual cycle was controlled nor recorded. For the STROKE protocol, the age of the subjects (above 60 years) suggested that the population included only post-menopausal women. For the HEALTHY and POTS protocols, the female subjects may have had a menstrual cycle, which might have compromised the results. Indeed, while the menstrual cycle has proven limited impact on CA, individual differences should be considered (Korad et al., 2022).

Some limitations were specific to the different experimental protocols. In the HEALTHY protocol, the CAP was not monitored. A variation in $PaCO_2$ combined with the sympathetic activation might explain the observed decline in MCBv during TILT (Cencetti et al., 1999). Indeed, hypocapnia could have induced vasoconstriction leading to a decrease of MCBv (Minhas et al., 2019). Moreover, low value of K^2 were detected at REST and TILT. The results regarding this protocol should be confirmed after applying a coherence threshold while monitoring $EtCO_2$. In the POTS protocol, the measurements at BASELINE were taken with participants in sitting position, thus leading to an orthostatic stress associated with the challenge that is of lower entity compared to a transition from a supine position to standing. Therefore, the preservation of cerebrovascular control observed in POTS might not be confirmed in the case of an orthostatic challenge of greater intensity. Moreover, the pharmacological therapy of

POTS might have played a role on the results since it reduced the degree of the sympathetic activation (Gelpi et al., 2023). Additionally, the SB required only 5 respiratory cycles implying a shorter time of analysis when compared to the other experimental conditions. In the STROKE protocol, the RCM was not monitored, and no orthostatic challenge was performed. Moreover, the subjects' heads were elevated by a pillow, known to reduce ICP and thus influence the dCA results (Lawley et al., 2017). Future studies should correct the protocol and investigate whether activation of the autonomic nervous system in STROKE subjects might limit the dCA impairment.

CHAPTER 6 - Conclusions

The aim of this doctoral dissertation is to study dCA in different scenarios of health and disease by employing a variety of methods of non-causal and causal analyses taken from the literature and optimized for the present application. The evaluation of cerebrovascular control is historically based on the computation of TFA and ARI indexes, while causal information transfer markers proposed in this thesis, namely TE and CTE, are much less exploited. The simultaneous computation of all these markers allows for the evaluation of different aspects of cerebrovascular control and a deeper assessment of the role played by causality. The methodologies were applied in different protocols carried out on healthy and pathological individuals. More specifically, the markers were computed in healthy subjects undergoing an orthostatic challenge, namely TILT and STAND, POTS subjects performing STAND and SB, and subjects in the acute phase of ischemic stroke. Experimental conditions and populations were specifically selected to test the hypothesis of the involvement of the autonomic nervous system in cerebrovascular regulation and the possibility of detecting its impairment.

The complexity of cerebrovascular interactions defies the methods used to assess dCA. Well established methods, such as TFA and ARI, are commonly used, despite the fact that no gold-standard has emerged. To overcome the traditional pressure-to-flow methodologies hypothesizing the open-loop relationship from MAP to MCBv, this thesis exploits a closed-loop approach that explicitly models bidirectional interactions. Indeed, from a physiological standpoint, it is well-known the presence of a pathway from MCBv to MAP that, for instance, is activated during a dramatic modification of ICP. Remarkably, the proposed analysis allows for conditioning out confounding factors known to have influences on the MAP-MCBv closed-loop relationship, such as the mechanical effect of respiration and $PaCO_2$. The main conclusions about the directional causal analysis are: i) information transfer between MAP and MCBv is significant along both the causal directions; ii) CTE appears to be particularly important in conditions empowering respiratory drive, such as during controlled breathing at slow breathing rate; iii) conditioning on RCM and $EtCO_2$ has different effects on the information transfer according to the experimental condition, direction of the interactions, and population.

The diverse approaches exploited in the thesis allowed for the evaluation of cerebrovascular regulation and its response to stimuli challenging homeostasis. Cerebral regulation has been shown to depend on neurogenic regulation. However, the contribution of the autonomic nervous system is still poorly characterized. The thesis investigates this by considering the basic pathway linking pressure to flow with the suitable changes of vascular resistance to keep MCBv constant, the presence of a feedback pathway capable of changing MAP in peculiar situations of MCBv and the effects of the respiratory system disturbing the link between MAP and MCBv. The main findings on the cerebrovascular interactions in healthy subject and pathological individuals are: i) in HEALTHY subjects, TILT reduced MCBv as a likely consequence of the sympathetic activation, but dCA was not affected; ii) STAND from sitting position did not affect significantly MCBv and dCA in both CONTROL and POTS subjects; iii) information transfer indexes could separate POTS individuals from CONTROL subjects during SB, suggesting that the impact of the autonomic nervous system on dCA is more evident under an experimental condition empowering vagal control; iv) none of the traditional non-causal indexes could separate CONTROL and POTS individuals during SB; v) despite the cerebral hypoperfusion and hypertension, STROKE exhibited similar dCA when assessed with the traditional TFA and ARI indexes; vi) in STROKE subjects the information transfer indexes detected a decrement of the strength along the pressure-to-flow relationship, suggesting an impairment of dCA, and an increment along the flow-to-pressure pathway, supporting the activation of the Cushing reflex; vii) in the STROKE protocol results held regardless of the

hemisphere, thus indicating that the physiological response to stroke involves the entire brain, and it is not specific to the ischemic area; viii) the impact of RCM and EtCO2 on the dCA was limited during spontaneous breathing.

The present thesis emphasizes the importance of investigating the closed-loop relationship between MAP and MCBv when assessing cerebrovascular control, and this directional analysis might be particularly insightful in pathological populations such as in STROKE subjects. Thus, future studies in the field of cerebrovascular physiology research should take into account also the influences of the flow-to-pressure pathway. The findings on healthy and pathological subjects suggest that the autonomic nervous system plays a role in cerebrovascular regulation, particularly in situations enhancing vagal control. Finally, conditioning on the respiratory signal is particularly important when the respiratory drive is empowered, such as during controlled breathing at slow breathing rates. Thus, monitoring the activation of the autonomic nervous system and the respiratory rate is fundamental in the assessment of dCA and cerebrovascular interactions, to avoid misinterpretations.

Bibliography

Aaslid, R., Lindegaard, K. F., Sorteberg, W., & Nornes, H. (1989). Cerebral autoregulation dynamics in humans. *Stroke*, *20*(1), 45–52. https://doi.org/10.1161/01.str.20.1.45 [doi]

Akaike, H. (1974). A new look at the statistical model identification. In - *IEEE Transactions on Automatic Control* (Vol. 19, Issue 6, pp. 716–723). https://doi.org/10.1109/TAC.1974.1100705

Al-Khazraji, B. K., Shoemaker, L. N., Gati, J. S., Szekeres, T., & Shoemaker, J. K. (2019). Reactivity of larger intracranial arteries using 7 T MRI in young adults. *Journal of Cerebral Blood Flow & Metabolism*, *39*(7), 1204–1214.

Alqadri, S. L., Sreenivasan, V., & Qureshi, A. I. (2013). Acute hypertensive response management in patients with acute stroke topical collection on stroke. *Current Cardiology Reports*, *15*(12). https://doi.org/10.1007/s11886-013-0426-7

Andrzejak, R. G., Kraskov, A., Stögbauer, H., Mormann, F., & Kreuz, T. (2003). Bivariate surrogate techniques: necessity, strengths, and caveats. *Physical Review. E, Statistical Physics, Plasmas, Fluids, and Related Interdisciplinary Topics*, *68*(6 Pt 2), 66202. https://doi.org/10.1103/physreve.68.066202

Barbic, F., Minonzio, M., Cairo, B., Shiffer, D., Zamuner, A. R., Cavalieri, S., Dipaola, F., Magnavita, N., Porta, A., & Furlan, R. (2020). Work Ability Assessment and Its Relationship with Cardiovascular Autonomic Profile in Postural Orthostatic Tachycardia Syndrome. *International Journal of Environmental Research and Public Health*, *17*(21), 7836. doi: 10.3390/ijerph17217836. https://doi.org/10.3390/ijerph17217836 [doi]

Bari, V., Barbarossa, L., Gelpi, F., Cairo, B., De Maria, B., Tonon, D., Rossato, G., Faes, L., Ranucci, M., Barbieri, R., & Porta, A. (2022). Exploring metrics for the characterization of the cerebral autoregulation during head-up tilt and propofol general anesthesia. *Autonomic Neuroscience: Basic and Clinical*, *242*. https://doi.org/10.1016/j.autneu.2022.103011

Bari, V., De Maria, B., Mazzucco, C. E., Rossato, G., Tonon, D., Nollo, G., Faes, L., & Porta, A. (2017). Cerebrovascular and cardiovascular variability interactions investigated through conditional joint transfer entropy in subjects prone to postural syncope. *Physiological Measurement*, *38*(5), 976–991. https://doi.org/10.1088/1361-6579/aa638c [doi]

Bari, V., Fantinato, A., Vaini, E., Gelpi, F., Cairo, B., De Maria, B., Pistuddi, V., Ranucci, M., & Porta, A. (2021). Impact of propofol general anesthesia on cardiovascular and cerebrovascular closed loop variability interactions. *Biomedical Signal Processing and Control*, *68*. https://doi.org/10.1016/j.bspc.2021.102735

Bari, V., Gelpi, F., Cairo, B., Anguissola, M., Pugliese, S., De Maria, B., Bertoldo, E. G., Fiolo, V., Callus, E., De Vincentiis, C., Volpe, M., Molfetta, R., Ranucci, M., & Porta, A. (2023). Characterization of cardiovascular and cerebrovascular controls via spectral causality analysis in patients undergoing surgical aortic valve replacement during a three-month follow-up. *Physiological Measurement*, *44*(9). https://doi.org/10.1088/1361-6579/acf992

Barnett, L., Barrett, A. B., & Seth, A. K. (2009). Granger causality and transfer entropy are equivalent for Gaussian variables. *Physical Review Letters*, *103*(23), 238701. https://doi.org/10.1103/PhysRevLett.103.238701 [doi]

Bendat, J. S., & Piersol, A. G. (1986). Decomposition of wave forces into linear and non-linear components. *Journal of Sound and Vibration*, *106*(3), 391–408. https://doi.org/10.1016/0022-460X(86)90186-0

Bor-Seng-Shu, E., Kita, W. S., Figueiredo, E. G., Paiva, W. S., Fonoff, E. T., Teixeira, M. J., & Panerai, R. B. (2012). Cerebral hemodynamics: concepts of clinical importance. *Arquivos de Neuro-Psiquiatria*, *70*, 357–365.

Brassard, P., Roy, M.-A., Burma, J. S., Labrecque, L., & Smirl, J. D. (2023). Quantification of dynamic cerebral autoregulation: welcome to the jungle! *Clinical Autonomic Research*, *33*(6), 791–810. https://doi.org/10.1007/s10286-023-00986-2

Bressler, S. L., & Seth, A. K. (2011). Wiener–Granger Causality: A well established methodology. *NeuroImage*, *58*(2), 323–329. https://doi.org/10.1016/J.NEUROIMAGE.2010.02.059

Britton, M., Carlsson, A., & De Faire, U. (1986). Blood pressure course in patients with acute stroke and matched controls. *Stroke*, *17*(5), 861–864.

Caicedo, A., Varon, C., Hunyadi, B., Papademetriou, M., Tachtsidis, I., & Van Huffel, S. (2016). Decomposition of near-infrared spectroscopy signals using oblique subspace projections: Applications in brain hemodynamic monitoring. *Frontiers in Physiology*, *7*(NOV). https://doi.org/10.3389/fphys.2016.00515

Carey, B. J., Manktelow, B. N., Panerai, R. B., & Potter, J. F. (2001). Cerebral autoregulatory responses to head-up tilt in normal subjects and patients with recurrent vasovagal syncope. *Circulation*, *104*(8), 898–902. https://doi.org/10.1161/hc3301.094908 [doi]

Cencetti, S., Lagi, A., Cipriani, M., Fattorini, L., Bandinelli, G., & Bernardi, L. (1999). Autonomic control of the cerebral circulation during normal and impaired peripheral circulatory control. *Heart (British Cardiac Society)*, *82*(3), 365–372. https://doi.org/10.1136/hrt.82.3.365 [doi]

Chacon, M., Nunez, N., Henriquez, C., & Panerai, R. B. (2008). Unconstrained parameter estimation for assessment of dynamic cerebral autoregulation. *Physiological Measurement*, *29*(10), 1179.

Charleston-Villalobos, S., Javorka, M., Faes, L., & Voss, A. (2023). Granger causality and information transfer in physiological systems: basic research and applications. *Frontiers in Network Physiology*, *3*.

Cipolla, M. J., Liebeskind, D. S., & Chan, S.-L. (2018). The importance of comorbidities in ischemic stroke: Impact of hypertension on the cerebral circulation. *Journal of Cerebral Blood Flow and Metabolism*, *38*(12), 2129–2149. https://doi.org/10.1177/0271678X18800589

Claassen, J. (2016). The plateau phase is a slippery slope: raising blood pressure may lower brain perfusion. *Journal of Physiology*, *594*(11).

Claassen, J. A. H. R., Thijssen, D. H. J., Panerai, R. B., & Faraci, F. M. (2021). Regulation of cerebral blood flowin humans: Physiology and clinical implications of autoregulation. *Physiological Reviews*, *101*(4), 1487–1559. https://doi.org/10.1152/physrev.00022.2020

Claassen, J. A., Meel-Van Den Abeelen, A. S., Simpson, D. M., Panerai, R. B., Alexander Caicedo Dorado, Mitsis, G. D., Brassard, P., Ainslie, P. N., Summers, P., Iwasaki, K., Ragauskas, A., Tzeng, Y. C., Müller, M., Wang, C. Y., Hu, H. H., Meel-Van Den Abeelen, A. S. S., Gommer, E., Karemaker, J. M., Aries, M., … Novak, V. (2015). Transfer function analysis of dynamic cerebral autoregulation: A white paper from the International Cerebral Autoregulation Research Network. In *Journal of Cerebral Blood Flow and Metabolism* (Vol. 36, Issue 4, pp. 665–680). SAGE Publications Ltd. https://doi.org/10.1177/0271678X15626425

Cushing, H. (1902). Some experimental and clinical observations concerning states of increased intracranial tension. *The American Journal of the Medical Sciences (1827-1924)*, *124*(3), 375.

Czosnyka, M., Smielewski, P., Kirkpatrick, P., Menon, D. K., & Pickard, J. D. (1996). Monitoring of cerebral autoregulation in head-injured patients. *Stroke*, *27*(10), 1829–1834. https://doi.org/10.1161/01.STR.27.10.1829

Dickinson, C. J. (1990). Reappraisal of the Cushing Reflex: The Most Powerful Neural Blood Pressure Stabilizing System. *Clinical Science*, *79*(6), 543–550. https://doi.org/10.1042/cs0790543

Diehl, R. R., Linden, D., Lücke, D., & Berlit, P. (1995). Phase relationship between cerebral blood flow velocity and blood pressure: a clinical test of autoregulation. *Stroke*, *26*(10), 1801–1804.

Eames, P. J., Potter, J. F., & Panerai, R. B. (2004). Influence of controlled breathing patterns on cerebrovascular autoregulation and cardiac baroreceptor sensitivity. *Clinical Science*, *106*(2), 155–162. https://doi.org/10.1042/CS20030194

Elstad, M., O'Callaghan, E. L., Smith, A. J., Ben-Tal, A., & Ramchandra, R. (2018). Cardiorespiratory interactions in humans and animals: Rhythms for life. *American Journal of Physiology - Heart and Circulatory Physiology*, *315*(1), H6–H17. https://doi.org/10.1152/ajpheart.00701.2017

Elting, J. W., Maurits, N. M., & Aries, M. J. H. (2014). Variability of the autoregulation index decreases after removing the effect of the very low frequency band. *Medical Engineering and Physics*, *36*(5), 601–606. https://doi.org/10.1016/j.medengphy.2013.10.009

Faes, L., Porta, A., & Nollo, G. (2015). Algorithms for the inference of causality in dynamic processes: Application to cardiovascular and cerebrovascular variability. *Proceedings of the Annual International Conference of the IEEE Engineering in Medicine and Biology Society, EMBS*, *2015-Novem*, 1789–1792. https://doi.org/10.1109/EMBC.2015.7318726

Faes, L., Porta, A., Rossato, G., Adami, A., Tonon, D., Corica, A., & Nollo, G. (2013). Investigating the mechanisms of cardiovascular and cerebrovascular regulation in orthostatic syncope through an information decomposition strategy. *Autonomic Neuroscience : Basic & Clinical*, *178*(1–2), 76–82. https://doi.org/S1566-0702(13)00045-3 [pii]

Fan, J.-L., Brassard, P., Rickards, C. A., Nogueira, R. C., Nasr, N., McBryde, F. D., Fisher, J. P., & Tzeng, Y.-C. (2022). Integrative cerebral blood flow regulation in ischemic stroke. *Journal of Cerebral Blood Flow and Metabolism*, *42*(3), 387–403. https://doi.org/10.1177/0271678X211032029

Faraci, F. M., Baumbach, G. L., & Heistad, D. D. (1989). Myogenic mechanisms in the cerebral circulation. *Journal of Hypertension*, *7*(SUPPL. 4).

Farquhar, W. B., Taylor, J. A., Darling, S. E., Chase, K. P., & Freeman, R. (2000). Abnormal baroreflex responses in patients with idiopathic orthostatic intolerance. *Circulation*, *102*(25), 3086–3091.

Furlan, R., Jacob, G., Snell, M., Robertson, D., Porta, A., Harris, P., & Mosqueda-Garcia, R. (1998). Chronic orthostatic intolerance: a disorder with discordant cardiac and vascular sympathetic control. *Circulation*, *98*(20), 2154–2159. https://doi.org/10.1161/01.cir.98.20.2154 [doi]

Gelpi, F., Bari, V., Cairo, B., De Maria, B., Tonon, D., Rossato, G., Faes, L., & Porta, A. (2022). Dynamic cerebrovascular autoregulation in patients prone to postural syncope: comparison of techniques assessing the autoregulation index from spontaneous variability series. *Autonomic Neuroscience*, *237*, 102920.

Gelpi, F., Bari, V., Cairo, B., De Maria, B., Wells, R., Baumert, M., & Porta, A. (2023). Evaluation of cardiovascular and cerebrovascular control mechanisms in postural orthostatic tachycardia syndrome via conditional transfer entropy: the impact of the respiratory signal type. *Physiological Measurement*, *44*(6). https://doi.org/10.1088/1361-6579/acdb47

Gierthmühlen, J., Allardt, A., Sawade, M., Baron, R., & Wasner, G. (2011). Dynamic cerebral autoregulation in stroke patients with a central sympathetic deficit. *Acta Neurologica Scandinavica*, *123*(5), 332–338. https://doi.org/10.1111/j.1600-0404.2010.01424.x

Giller, C. A., Bowman, G., Dyer, H., Mootz, L., & Krippner, W. (1993). Cerebral arterial diameters during changes in blood pressure and carbon dioxide during craniotomy. *Neurosurgery*, *32*(5), 737–742.

Gommer, E. D., Shijaku, E., Mess, W. H., & Reulen, J. P. (2010). Dynamic cerebral autoregulation: different signal processing methods without influence on results and reproducibility. *Medical & Biological Engineering & Computing*, *48*(12), 1243–1250. https://doi.org/10.1007/s11517-010-0706-y [doi]

Grady, P. A., & Blaumanis, O. R. (1988). Physiologic parameters of the cushing reflex. *Surgical Neurology*, *29*(6), 454–461. https://doi.org/https://doi.org/10.1016/0090-3019(88)90140-1

Granger, C. W. J. (1969). Investigating Causal Relations by Econometric Models and Cross-spectral Methods. *Econometrica*, *37*(3), 424–438. https://doi.org/10.2307/1912791

Grubb, B. P., Gerard, G., Roush, K., Temesy-Armos, P., Montford, P., Elliott, L., Hahn, H., & Brewster, P. (1991). Cerebral vasoconstriction during head-upright tilt-induced vasovagal syncope. A paradoxic and unexpected response. *Circulation*, *84*(3), 1157–1164. https://doi.org/10.1161/01.cir.84.3.1157 [doi]

Halsey Jr, J. H., & McFarland, S. (1974). Oxygen cycles and metabolic autoregulation. *Stroke*, *5*(2), 219–225.

Hamner, J. W., & Tan, C. O. (2014). Relative contributions of sympathetic, cholinergic, and myogenic mechanisms to cerebral autoregulation. *Stroke*, *45*(6), 1771–1777. https://doi.org/10.1161/STROKEAHA.114.005293 [doi]

Hamner, J. W., Tan, C. O., Lee, K., Cohen, M. A., & Taylor, J. A. (2010). Sympathetic control of the cerebral vasculature in humans. *Stroke*, *41*(1), 102–109. https://doi.org/10.1161/STROKEAHA.109.557132 [doi]

Holme, N. L. A., Zilakos, I., Elstad, M., & Skytioti, M. (2023). Cerebral blood flow response to cardiorespiratory oscillations in healthy humans. *Autonomic Neuroscience: Basic and Clinical*, *245*. https://doi.org/10.1016/j.autneu.2022.103069

Hyder, F., Shulman, R. G., & Rothman, D. L. (1998). A model for the regulation of cerebral oxygen delivery. *Journal of Applied Physiology*, *85*(2), 554–564.

Johnston, A. J., Steiner, L. A., Gupta, A. K., & Menon, D. K. (2003). Cerebral oxygen vasoreactivity and cerebral tissue oxygen reactivity. *British Journal of Anaesthesia*, *90*(6), 774–786.

Joshi, B., Brady, K., Lee, J., Easley, B., Panigrahi, R., Smielewski, P., Czosnyka, M., & Hogue Jr, C. W. (2010). Impaired autoregulation of cerebral blood flow during rewarming from hypothermic cardiopulmonary bypass and its potential association with stroke. *Anesthesia and Analgesia*, *110*(2), 321–328. https://doi.org/10.1213/ANE.0b013e3181c6fd12 [doi]

Kenny, R. A., Bayliss, J., Ingram, A., & Sutton, R. (1986). Head-up tilt: a useful test for investigating unexplained syncope. *The Lancet*, *327*(8494), 1352–1355.

Kety, S. S., & Schmidt, C. F. (1948). The effects of altered arterial tensions of carbon dioxide and oxygen on cerebral blood flow and cerebral oxygen consumption of normal young men. *The Journal of Clinical Investigation*, *27*(4), 484–492.

Korad, S., Mündel, T., Fan, J.-L., & Perry, B. G. (2022). Cerebral autoregulation across the menstrual cycle in eumenorrheic women. *Physiological Reports*, *10*(9). https://doi.org/10.14814/phy2.15287

Laborde, S., Allen, M. S., Borges, U., Dosseville, F., Hosang, T. J., Iskra, M., Mosley, E., Salvotti, C., Spolverato, L., Zammit, N., & Javelle, F. (2022). Effects of voluntary slow breathing on heart rate and heart rate variability: A systematic review and a meta-analysis. *Neuroscience & Biobehavioral Reviews*, *138*, 104711. https://doi.org/https://doi.org/10.1016/j.neubiorev.2022.104711

Lassen, N. A. (1959). Cerebral blood flow and oxygen consumption in man. *Physiological Reviews*, *39*(2), 183–238. https://doi.org/10.1152/physrev.1959.39.2.183 [doi]

Latka, M., Turalska, M., Glaubic-Latka, M., Kolodziej, W., Latka, D., & West, B. J. (2005). Phase dynamics in cerebral autoregulation. *American Journal of Physiology - Heart and Circulatory Physiology*, *289*(5 58-5). https://doi.org/10.1152/ajpheart.01307.2004

Lawley, J. S., Petersen, L. G., Howden, E. J., Sarma, S., Cornwell, W. K., Zhang, R., Whitworth, L. A., Williams, M. A., & Levine, B. D. (2017). Effect of gravity and microgravity on intracranial pressure. *The Journal of Physiology*, *595*(6), 2115–2127.

Liu, X., Czosnyka, M., Donnelly, J., Budohoski, K. P., Varsos, G. V., Nasr, N., Brady, K. M., Reinhard, M., Hutchinson, P. J., & Smielewski, P. (2015). Comparison of frequency and time domain methods of assessment of cerebral autoregulation in traumatic brain injury. *Journal of Cerebral Blood Flow and Metabolism*, *35*(2), 248–256. https://doi.org/10.1038/jcbfm.2014.192

Llwyd, O., Haunton, V., Salinet, A. S. M., Nath, M., Lam, M. Y., Saeed, N. P., Brodie, F., Robinson, T. G., & Panerai, R. B. (2019). Can we assess dynamic cerebral autoregulation in stroke patients with high rates of cardiac ectopicity? *Medical & Biological Engineering & Computing*, *57*, 2731–2739. https://doi.org/10.1007/s11517-019-02064-0/Published

Mahdi, A., Nikolic, D., Birch, A. A., Olufsen, M. S., Panerai, R. B., Simpson, D. M., & Payne, S. J. (2017). Increased blood pressure variability upon standing up improves reproducibility of cerebral autoregulation indices. *Medical Engineering and Physics*, *47*, 151–158. https://doi.org/10.1016/j.medengphy.2017.06.006

Marchi, A., Bari, V., De Maria, B., Esler, M., Lambert, E., Baumert, M., & Porta, A. (2016). Calibrated variability of muscle sympathetic nerve activity during graded head-up tilt in humans and its link with noradrenaline data and cardiovascular rhythms. *American Journal of Physiology-Regulatory, Integrative and Comparative Physiology*, *310*(11), R1134–R1143.

Marchi, A., Colombo, R., Guzzetti, S., Bari, V., Bassani, T., Raimondi, F., & Porta, A. (2013). Characterization of the cardiovascular control during modified head-up tilt test in healthy adult humans. *Autonomic Neuroscience : Basic & Clinical*, *179*(1–2), 166–169. https://doi.org/S1566-0702(13)00680-2 [pii]

McBryde, F. D., Malpas, S. C., & Paton, J. F. R. (2017). Intracranial mechanisms for preserving brain blood flow in health and disease. In *Acta Physiologica* (Vol. 219, Issue 1, pp. 274–287). Blackwell Publishing Ltd. https://doi.org/10.1111/apha.12706

Minhas, J. S., Haunton, V. J., Robinson, T. G., & Panerai, R. B. (2019). Determining differences between critical closing pressure and resistance-area product: responses of the healthy young and old to hypocapnia. *Pflugers Archiv European Journal of Physiology*, *471*(8), 1117–1126. https://doi.org/10.1007/s00424-019-02290-3

Minhas, J. S., Panerai, R. B., & Robinson, T. G. (2018). Modelling the cerebral haemodynamic response in the physiological range of PaCO2. *Physiological Measurement*, *39*(6), 065001.

Mitsis, G. D., Poulin, M. J., Robbins, P. A., & Marmarelis, V. Z. (2004). Nonlinear modeling of the dynamic effects of arterial pressure and CO2 variations on cerebral blood flow in healthy humans. *IEEE Transactions on Biomedical Engineering*, *51*(11), 1932–1943. https://doi.org/10.1109/TBME.2004.834272

Mokri, B. (2001). The Monro-Kellie hypothesis: Applications in CSF volume depletion. *Neurology*, *56*(12), 1746–1748. https://doi.org/10.1212/WNL.56.12.1746

Nogueira, R. C., Aries, M., Minhas, J. S., H Petersen, N., Xiong, L., Kainerstorfer, J. M., & Castro, P. (2022). Review of studies on dynamic cerebral autoregulation in the acute phase of stroke and the relationship with clinical outcome. *Journal of Cerebral Blood Flow and Metabolism*, *42*(3), 430–453. https://doi.org/10.1177/0271678X211045222

Obrist, W. D., Zhang, Z., & Yonas, H. (1998). Effect of xenon-induced flow activation on xenon-enhanced computed tomography cerebral blood flow calculations. *Journal of Cerebral Blood Flow & Metabolism*, *18*(11), 1192–1195.

Ogoh, S. (2019). Interaction between the respiratory system and cerebral blood flow regulation. *Journal of Applied Physiology*, *127*(5), 1197–1205.

Ogoh, S., Fadel, P. J., Zhang, R., Selmer, C., Jans, Ø., Secher, N. H., & Raven, P. B. (2005). Middle cerebral artery flow velocity and pulse pressure during dynamic exercise in humans. *American Journal of Physiology-Heart and Circulatory Physiology*, *288*(4), H1526–H1531.

Ogoh, S., & Tarumi, T. (2019). Cerebral blood flow regulation and cognitive function: a role of arterial baroreflex function. *The Journal of Physiological Sciences : JPS*, *69*(6), 813–823. https://doi.org/10.1007/s12576-019-00704-6 [doi]

Pagani, M., Montano, N., Porta, A., Malliani, A., Abboud, F. M., Birkett, C., & Somers, V. K. (1997). Relationship between spectral components of cardiovascular variabilities and direct measures of muscle sympathetic nerve activity in humans. *Circulation*, *95*(6), 1441–1448. https://doi.org/10.1161/01.CIR.95.6.1441

Panerai, R. B. (2008). Cerebral autoregulation: From models to clinical applications. In *Cardiovascular Engineering* (Vol. 8, Issue 1, pp. 42–59). https://doi.org/10.1007/s10558-007-9044-6

Panerai, R. B., Brassard, P., Burma, J. S., Castro, P., Claassen, J. A. H. R., van Lieshout, J. J., Liu, J., Lucas, S. J. E., Minhas, J. S., Mitsis, G. D., Nogueira, R. C., Ogoh, S., Payne, S. J., Rickards, C. A., Robertson, A. D., Rodrigues, G. D., Smirl, J. D., & Simpson, D. M. (2023). Transfer function analysis of dynamic cerebral autoregulation: A CARNet white paper 2022 update. In *Journal of Cerebral Blood Flow and Metabolism* (Vol. 43, Issue 1, pp. 3–25). SAGE Publications Ltd. https://doi.org/10.1177/0271678X221119760

Panerai, R. B., Dawson, S. L., Eames, P. J., & Potter, J. F. (2001). Cerebral blood flow velocity response to induced and spontaneous sudden changes in arterial blood pressure. *American Journal of Physiology.Heart and Circulatory Physiology*, *280*(5), H2162-74. https://doi.org/10.1152/ajpheart.2001.280.5.H2162 [doi]

Panerai, R. B., Dineen, N. E., Brodie, F. G., & Robinson, T. G. (2010). Spontaneous fluctuations in cerebral blood flow regulation: contribution of Pa CO 2. *J Appl Physiol*, *109*, 1860–1868. https://doi.org/10.1152/japplphysiol.00857.2010.-To

Panerai, R. B., Eames, P. J., & Potter, J. F. (2006). Multiple coherence of cerebral blood flow velocity in humans. *American Journal of Physiology.Heart and Circulatory Physiology*, *291*(1), H251-9. https://doi.org/01348.2005 [pii]

Panerai, R. B., White, R. P., Markus, H. S., & Evans, D. H. (1998). *Grading of Cerebral Dynamic Autoregulation From Spontaneous Fluctuations in Arterial Blood Pressure*. http://ahajournals.org

Patarroyo, S. X. F., & Anderson, C. (2012). Blood pressure lowering in acute phase of stroke: Latest evidence and clinical implications. *Therapeutic Advances in Chronic Disease*, *3*(4), 163–171. https://doi.org/10.1177/2040622312450183

Patel, N., Panerai, R. B., Haunton, V., Katsogridakis, E., Saeed, N. P., Salinet, A., Brodie, F., Syed, N., D'Sa, S., & Robinson, T. G. (2016). The Leicester cerebral haemodynamics database: normative values and the influence of age and sex. *Physiological Measurement*, *37*(9), 1485.

Paulson, O. B., & Knudsen, G. M. (2008). Comments on Point:Counterpoint: Sympathetic activity does/does not influence cerebral blood flow. Role of a rudimentary sympathetic nervous system on cerebral blood flow. *Journal*

of Applied Physiology (Bethesda, Md.: 1985), *105*(4), 1371–1372. https://doi.org/10.1152/japplphysiol.zdg-8199.pcpcomm.2008 [doi]

Paulson, O. B., Strandgaard, S., & Edvinsson, L. (1990). Cerebral autoregulation. *Cerebrovascular and Brain Metabolism Reviews*, *2*(2), 161–192.

Peng, T., Rowley, A. B., Ainslie, P. N., Poulin, M. J., & Payne, S. J. (2010). Wavelet phase synchronization analysis of cerebral blood flow autoregulation. *IEEE Transactions on Biomedical Engineering*, *57*(4), 960–968. https://doi.org/10.1109/TBME.2009.2024265

Pernice, R., Sparacino, L., Bari, V., Gelpi, F., Cairo, B., Mijatovic, G., Antonacci, Y., Tonon, D., Rossato, G., Javorka, M., Porta, A., & Faes, L. (2022). Spectral decomposition of cerebrovascular and cardiovascular interactions in patients prone to postural syncope and healthy controls. *Autonomic Neuroscience: Basic and Clinical*, *242*. https://doi.org/10.1016/j.autneu.2022.103021

Pomeranz, B., Macaulay, R. J., Caudill, M. A., Kutz, I., Adam, D., Gordon, D., Kilborn, K. M., Barger, A. C., Shannon, D. C., & Cohen, R. J. (1985). Assessment of autonomic function in humans by heart rate spectral analysis. *The American Journal of Physiology*, *248*(1 Pt 2), H151-3. https://doi.org/10.1152/ajpheart.1985.248.1.H151 [doi]

Porta, A., Bari, V., De Maria, B., Cairo, B., Vaini, E., Malacarne, M., Pagani, M., & Lucini, D. (2018). Peripheral resistance baroreflex during incremental bicycle ergometer exercise: Characterization and correlation with cardiac baroreflex. *Frontiers in Physiology*, *9*(JUN). https://doi.org/10.3389/fphys.2018.00688

Porta, A., Baselli, G., Rimoldi, O., Malliani, A., & Pagani, M. (2000). Assessing baroreflex gain from spontaneous variability in conscious dogs: Role of causality and respiration. *American Journal of Physiology - Heart and Circulatory Physiology*, *279*(48–5), H2558–H2567. https://doi.org/10.1152/ajpheart.2000.279.5.h2558

Porta, A., & Faes, L. (2013). Assessing causality in brain dynamics and cardiovascular control. In *Philosophical Transactions of the Royal Society A: Mathematical, Physical and Engineering Sciences* (Vol. 371, Issue 1997). Royal Society. https://doi.org/10.1098/rsta.2012.0517

Porta, A., & Faes, L. (2016). Wiener–Granger Causality in Network Physiology With Applications to Cardiovascular Control and Neuroscience. *Proceedings of the IEEE*, *104*(2), 282–309. https://doi.org/10.1109/JPROC.2015.2476824

Porta, A., Faes, L., Marchi, A., Bari, V., De Maria, B., Guzzetti, S., Colombo, R., & Raimondi, F. (2015). Disentangling cardiovascular control mechanisms during head-down tilt via joint transfer entropy and self-entropy decompositions. *Frontiers in Physiology*, *6*, 301. https://doi.org/10.3389/fphys.2015.00301 [doi]

Porta, A., Faes, L., Nollo, G., Bari, V., Marchi, A., De Maria, B., Takahashi, A., & Catai, A. (2015). Conditional Self-Entropy and Conditional Joint Transfer Entropy in Heart Period Variability during Graded Postural Challenge. *PloS One*, *10*(7), e0132851. https://doi.org/10.1371/journal.pone.0132851 [doi]

Porta, A., Furlan, R., Rimoldi, O., Pagani, M., Malliani, A., & Van De Borne, P. (2002). Quantifying the strength of the linear causal coupling in closed loop interacting cardiovascular variability signals. *Biological Cybernetics*, *86*(3), 241–251. https://doi.org/10.1007/s00422-001-0292-z

Porta, A., Gelpi, F., Bari, V., Cairo, B., De Maria, B., Tonon, D., Rossato, G., & Faes, L. (2023). Concomitant evaluation of cardiovascular and cerebrovascular controls via Geweke spectral causality to assess the propensity to postural syncope. *Medical and Biological Engineering and Computing*. https://doi.org/10.1007/s11517-023-02885-0

Porta, A., Gelpi, F., Bari, V., Cairo, B., De Maria, B., Tonon, D., Rossato, G., Ranucci, M., & Faes, L. (2021). Categorizing the role of respiration in cardiovascular and cerebrovascular variability interactions. *IEEE Transactions on Biomedical Engineering*, *69*(6), 2065–2076.

Porta, A., Gelpi, F., Bari, V., Cairo, B., De Maria, B., Tonon, D., Rossato, G., Ranucci, M., & Faes, L. (2022). Categorizing the Role of Respiration in Cardiovascular and Cerebrovascular Variability Interactions. *IEEE Transactions on Biomedical Engineering*, *69*(6). https://doi.org/10.1109/TBME.2021.3135313

Porta, A., Maestri, R., Bari, V., De Maria, B., Cairo, B., Vaini, E., La Rovere, M. T., & Pinna, G. D. (2018). Paced breathing increases the redundancy of cardiorespiratory control in healthy individuals and chronic heart failure patients. *Entropy*, *20*(12). https://doi.org/10.3390/e20120949

Quian Quiroga, R., Kraskov, A., Kreuz, T., & Grassberger, P. (2002). Performance of different synchronization measures in real data: A case study on electroencephalographic signals. *Physical Review E*, *65*(4), 41903. https://doi.org/10.1103/PhysRevE.65.041903

Rosner, J., Reddy, V., & Lui, F. (2023). *Neuroanatomy, Circle of Willis*. StatPearls Publishing, Treasure Island (FL). http://europepmc.org/books/NBK534861

Saleem, S., Sarafis, Z. K., Lee, A. H. X., Squair, J. W., F. Barak, O., Sober-Williams, E., Suraj, R., Coombs, G. B., Mijacika, T., & West, C. R. (2019). Spinal cord disruption is associated with a loss of cushing-like blood pressure interactions. *Journal of Neurotrauma*, *36*(9), 1487–1490.

Saleem, S., Teal, P. D., Howe, C. A., Tymko, M. M., Ainslie, P. N., & Tzeng, Y.-C. (2018). Is the Cushing mechanism a dynamic blood pressure-stabilizing system? Insights from Granger causality analysis of spontaneous blood pressure and cerebral blood flow. *Am J Physiol Regul Integr Comp Physiol*, *315*, 484–495. https://doi.org/10.1152/ajpregu.00032.2018.-Blood

Saleem, S., Teal, P. D., Kleijn, W. B., O'Donnell, T., Witter, T., & Tzeng, Y. C. (2015). Non-linear characterisation of cerebral pressure-flow dynamics in humans. *PLoS ONE*, *10*(9). https://doi.org/10.1371/journal.pone.0139470

Salinet, A. S. M., Robinson, T. G., & Panerai, R. B. (2015). Effects of cerebral ischemia on human neurovascular coupling, CO 2 reactivity, and dynamic cerebral autoregulation. *J Appl Physiol*, *118*, 170–177. https://doi.org/10.1152/japplphysiol.00620.2014.-Cerebral

Sanders, M. L., Elting, J. W. J., Panerai, R. B., Aries, M., Bor-Seng-Shu, E., Caicedo, A., Chacon, M., Gommer, E. D., Van Huffel, S., Jara, J. L., Kostoglou, K., Mahdi, A., Marmarelis, V. Z., Mitsis, G. D., Müller, M., Nikolic, D., Nogueira, R. C., Payne, S. J., Puppo, C., … Claassen, J. A. H. R. (2019). Dynamic cerebral autoregulation reproducibility is affected by physiological variability. *Frontiers in Physiology*, *10*(JUL). https://doi.org/10.3389/fphys.2019.00865

Schreiber, T. (2000). Measuring information transfer. *Physical Review Letters*, *85*(2), 461–464. https://doi.org/10.1103/PhysRevLett.85.461 [doi]

Simpson, D., & Claassen, J. (2018). CrossTalk opposing view: dynamic cerebral autoregulation should be quantified using induced (rather than spontaneous) blood pressure fluctuations. *Journal of Physiology*, *596*(1), 7–9. https://doi.org/10.1113/JP273900

Simpson, D. M., Panerai, R. B., Evans, D. H., & Naylor, A. R. (2001). A parametric approach to measuring cerebral blood flow autoregulation from spontaneous variations in blood pressure. *Annals of Biomedical Engineering*, *29*(1), 18–25. https://doi.org/10.1114/1.1335537 [doi]

Sorond, F. A., Serrador, J. M., Jones, R. N., Shaffer, M. L., & Lipsitz, L. A. (2009). The Sit-to-Stand Technique for the Measurement of Dynamic Cerebral Autoregulation. *Ultrasound in Medicine and Biology*, *35*(1), 21–29. https://doi.org/10.1016/j.ultrasmedbio.2008.08.001

Sparacino, L., Antonacci, Y., Barà, C., Valenti, A., Porta, A., & Faes, L. (2023). A method to assess Granger causality, isolation and autonomy in the time and frequency domains: theory and application to cerebrovascular variability. *IEEE Transactions on Biomedical Engineering*.

Taccone, F., Scolletta, S., Franchi, F., Donadello, K., & Oddo, M. (2013). Brain perfusion in sepsis. *Current Vascular Pharmacology*, *11*(2), 170–186.

Tarumi, T., Dunsky, D. I., Khan, M. A., Liu, J., Hill, C., Armstrong, K., Martin-Cook, K., Cullum, C. M., & Zhang, R. (2014). Dynamic cerebral autoregulation and tissue oxygenation in amnestic mild cognitive impairment. *Journal of Alzheimer's Disease : JAD*, *41*(3), 765–778. https://doi.org/10.3233/JAD-132018 [doi]

"Task Force of the European Society of Cardiology and the North American Society of Pacing and Electrophysiology." (1996). Heart rate variability. Standards of measurement, physiological interpretation, and clinical use. *European Heart Journal*, *17*(3), 354–381.

Tiecks, F. P., Lam, A. M., Aaslid, R., & Newell, D. W. (1995). Comparison of static and dynamic cerebral autoregulation measurements. *Stroke*, *26*(6), 1014–1019. https://doi.org/10.1161/01.str.26.6.1014 [doi]

Toska, K., & Eriksen, M. (1993). Respiration-synchronous fluctuations in stroke volume, heart rate and arterial pressure in humans. *The Journal of Physiology*, *472*, 501–512. https://doi.org/10.1113/jphysiol.1993.sp019958 [doi]

Vaini, E., Bari, V., Fantinato, A., Pistuddi, V., Cairo, B., De Maria, B., Ranucci, M., & Porta, A. (2019). Causality analysis reveals the link between cerebrovascular control and acute kidney dysfunction after coronary artery bypass grafting. *Physiological Measurement*, *40*(6), 064006-6579/ab21b1. https://doi.org/10.1088/1361-6579/ab21b1 [doi]

Vu, E. L., Brown, C. H., Brady, K. M., & Hogue, C. W. (2024). Monitoring of cerebral blood flow autoregulation: physiologic basis, measurement, and clinical implications. *British Journal of Anaesthesia*, *132*(6), 1260–1273. https://doi.org/10.1016/j.bja.2024.01.043

Watanabe, H., Washio, T., Saito, S., Hirasawa, A., Suzuki, R., Shibata, S., Brothers, R. M., & Ogoh, S. (2022). Validity of transcranial Doppler ultrasonography-determined dynamic cerebral autoregulation estimated using transfer function analysis. *Journal of Clinical Monitoring and Computing*, *36*(6), 1711–1721. https://doi.org/10.1007/s10877-022-00817-1

Wells, R., Malik, V., Brooks, A. G., Linz, D., Elliott, A. D., Sanders, P., Page, A., Baumert, M., & Lau, D. H. (2020). Cerebral Blood Flow and Cognitive Performance in Postural Tachycardia Syndrome: Insights from Sustained Cognitive Stress Test. *Journal of the American Heart Association*, *9*(24), e017861. https://doi.org/10.1161/JAHA.120.017861 [doi]

Willie, C. K., Tzeng, Y. C., Fisher, J. A., & Ainslie, P. N. (2014). Integrative regulation of human brain blood flow. In *Journal of Physiology* (Vol. 592, Issue 5, pp. 841–859). Blackwell Publishing Ltd. https://doi.org/10.1113/jphysiol.2013.268953

Yildiz, S., Thyagaraj, S., Jin, N., Zhong, X., Heidari Pahlavian, S., Martin, B. A., Loth, F., Oshinski, J., & Sabra, K. G. (2017). Quantifying the influence of respiration and cardiac pulsations on cerebrospinal fluid dynamics using real-time phase-contrast MRI. *Journal of Magnetic Resonance Imaging : JMRI*, *46*(2), 431–439. https://doi.org/10.1002/jmri.25591 [doi]

Zhang, R., Zuckerman, J. H., Giller, C. A., & Levine, B. D. (1998). Transfer function analysis of dynamic cerebral autoregulation in humans. *The American Journal of Physiology*, *274*(1 Pt 2), H233-41. https://doi.org/10.1152/ajpheart.1998.274.1.h233 [doi]

Zhang, R., Zuckerman, J. H., Iwasaki, K., Wilson, T. E., Crandall, C. G., & Levine, B. D. (2002). Autonomic neural control of dynamic cerebral autoregulation in humans. *Circulation*, *106*(14), 1814–1820. https://doi.org/10.1161/01.CIR.0000031798.07790.FE

Zhang, R., Zuckerman, J. H., & Levine, B. D. (1998). Deterioration of cerebral autoregulation during orthostatic stress: insights from the frequency domain. *Journal of Applied Physiology (Bethesda, Md.: 1985)*, *85*(3), 1113–1122. https://doi.org/10.1152/jappl.1998.85.3.1113 [doi]